Analysis of Bubble Size Distributions Using the McGill Bubble Size Analyser

Marta E. Bailey

Department of Mining, Metals and Materials Engineering

McGill University

Montreal, Canada

A thesis submitted to the Faculty of Graduate Studies and Research

in partial fulfillment of the requirements of the degree of

Master of Engineering

Your file Votre référence
ISBN: 0-494-06545-1
Our file Notre référence
ISBN: 0-494-06545-1

ABSTRACT

Among the apparently simplest methods to determine bubble size in flotation systems are photographic techniques, ranging from photography through transparent walls to imaging of extracted bubbles. All capture images, which to varying degrees include overlapping, touching or out of focus bubbles. As manual counting limits the total number of bubbles, image analysis software is used to automate the process. Accuracy is thus dependent on image treatment, including counting method and filters.

The McGill bubble size analysis method yields single plane, backlit images and utilises software that filters by shape factor. Proven effective for bubble size distributions ranging from approximately 0.5 to 3 mm, regular trends are observed when number (D_{10}) and Sauter (D_{32}) mean diameters are compared. When the method was extended to wide distributions typical of jetting spargers (e.g., 0.2 – 15 mm), no similar trends were evident. Revision of the analysis process for these two-phase systems included counting by number of holes, which reduced dependence on bubble shape. This allowed for inclusion of small and large bubbles, while excluding bubble clusters. A diameter assignment protocol reflecting individual bubble shape was also developed. Revised output distributions showed increased symmetry, and the D_{32} vs. D_{10} trend was recovered.

Impact of sample tube diameter on the output bubble size distributions, and types of bias introduced were also investigated. A means of selecting an appropriate sample tube diameter for a given bubble population is presented.

RESUME

Parmi les methods servant à la determination de la taille des bulles générées par flotation, les techniques photographiques sont les plus simples. Celles-çi varient de la photographie à travers murs transparents à l'imagerie des bulles isolées. Toutes ces techniques capturent des images qui, à différents degrees, incluent des bulles se chevauchant, se touchant ou floues. Puisque les methods manuelles de comptage limitent le nombre total de bulles comptées, un logiciel d'analyse d'images est utilisé pour l'automatisation du processus. La précision est donc dépendente du traitement des images, y compris de la méthode de comptage et des filtres.

La méthode pour l'analysis de la taille des bulles, conçue par McGill, donne des images à éclairage arrière à plan unique et utilise un logiciel qui filtre par facteurs de forme. Cette méthode est prouvée pour des distributions de tailles de bulles entre 0.5 et 3 mm, approximativement, et des tendances régulières sont obtenues lorsque les moyennes numériques (D_{10}) et Sauter (D_{32}) sont comparées. Ce n'est cependant pas le cas lorsque la méthode est appliquée à de larges distributions, typiques des barbotteurs à jets (ex., 0.2 – 15 mm). Une révision du processus d'analyse dans le cas de ces systèmes à deux phases a nécessité le comptage du nombre de trous, réduisant ainsi la dépendence à la forme des bulles. Ceci a permis l'inclusion des petites et grandes bulles, tout en excluant les amas. Un protocole pour l'attribution des diameters, tenant compte de la forme des bulles individuelles, a aussi été développé. Les distributions finales révisées indiquent que la symétrie a augmenté, et que la tendance entre D_{32} et D_{10} a été recouvrée.

L'impact du diamètre du tube d'échantillonage sur la distribution de la tailles des bulles finales, et les types de variations indroduites, sont aussi investigués. Une méthode de sélection du tube d'échantillonage pour une certaine population des bulles est également présentée.

ACKNOWLEDGEMENTS

I would like to thank the following for their contributions to my work and to the quality of my time spent at McGill University:

Prof. Jim Finch for helping to guide me through this seemingly ever changing project, and his constant support, enthusiasm and advise.

Dr. Cesar Gomez for his technical support and advise. Also the Flotation Group for their ideas, feedback and encouragement.

Jose Hernandez-Aguilar, Jorge Torrealba-Vargas, and Helin Girgin and for their patience, advise and most of all friendship.

Paul Voigt for his constant support, advise and enthusiasm. And also for his instrumental work in developing the bubble viewer manual.

Finally, my family for their constant encouragement.

TABLE OF CONTENTS

LIST OF FIGURES

LIST OF TABLES

LIST OF EQUATIONS

CHAPTER 1 – INTRODUCTION

1.1 BACKGROUND

Flotation is used worldwide as a relatively simple and robust method for separation of minerals and other solid and fluid particles. Based on exploitation of the hydrophobic character of some species, natural or induced by chemical additions, separation is achieved through particle attachment to air bubbles.

In an illustrative example, mineral particles are mixed with water to form a slurry and gas is introduced, dispersed into bubbles, which then attach to selected minerals carrying them to the froth layer, which overflows to yield the froth product. The non-float product is removed from the bottom of the cell. The chemistry of the system is generally controlled such that the valuable minerals are hydrophobic, the froth product becoming the 'concentrate' and the non-float product, the 'tailings'.

Whether a given mineral reports to the froth product is dependent on several factors. These include the degree of liberation (specifically the proportion of the particle surface that is mineral), the mixing of the system (the degree to which bubbles and particles are able to contact), and the probability of a particle attaching to a bubble and remaining attached until it is removed via the froth layer. This probability of recovery is governed by the probability of collision, attachment and detachment. For attachment, if the time required for the particle to attach is greater than the time spent in contact with the bubble, attachment will not occur; i.e., that particle remains in the slurry, being available for another collision/attachment event or being removed in the tailings.

Aside from the hydrophobic nature of the mineral particles, all other factors are dependent on bubble dispersion characteristics, making bubbles central to the process. Particular attention has been paid to their generation, behaviour in slurries and means to control the characteristics of the bubble population (or swarm). The hydrodynamics of cells are indicative of the suspension, mixing, and bubbling regime, all being important to the success of flotation, and thus ways to evaluate cell hydrodynamics, in particular gas dispersion properties, have been devised.

1.1.1 Hydrodynamic Variables

Several key hydrodynamic variables must be considered when evaluating gas dispersion. These variables include: superficial gas velocity (J_g [cm/s]), gas holdup (ε_g []) and bubble size (D_b [mm]). A combination of these variables may be used to estimate the bubble surface area flux (Sb [s^{-1}]) as defined in *Equation 1-1*, which is the amount of bubble surface area delivered per unit time per unit cell cross-section for solids collection, and can thus be correlated to the flotation rate constant (Gorain et al., 1998).

$$S_b = \frac{6J_g}{D_b}$$ *EQUATION 1-1*

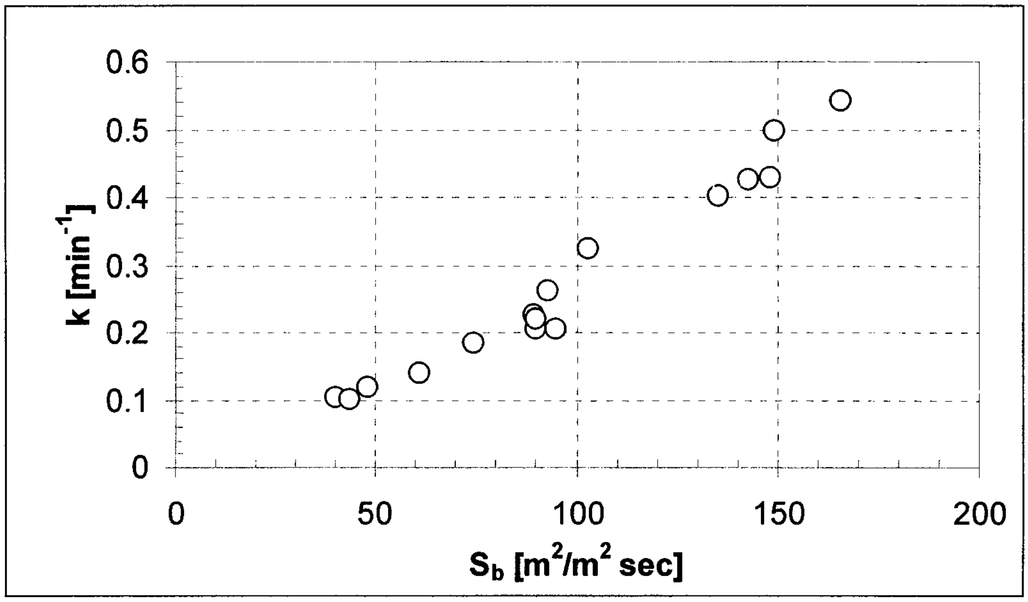

FIGURE 1-1: *K-SB RELATIONSHIP FOR CHILE-X IMPELLOR (GORAIN ET AL., 1997)*

Superficial gas velocity, (J_g, often shortened to 'gas rate') is the volumetric gas rate over a given area. It is a means for standardising gas flow measurements such that cells of different cross-sectional areas may be compared. Additionally, it allows for local measurement of the gas flow rate, permitting mapping of the gas dispersion.

Gas holdup is a dimensionless measure of the fraction of gas present in the system. The gas holdup can also be measured locally, and used for hydrodynamic characterisation. Until the upper operational limit of a cell, gas holdup and J_g follow an approximately linear trend, implying that increasing fractions of gas are held in the cell as gas rate increases. Gas rate and holdup can be used in combination to give an estimate of bubble size through the use of drift flux analysis (Xu et al., 1991). This relationship implies that for the same J_g, if one bubble generation device yields higher gas holdup than another, the gas is contained in smaller bubbles. The nature of the slurry (viscosity, density) may confound this interpretation.

Bubble size is the third hydrodynamic variable, and the most difficult to measure *in situ,* especially in the presence of solids. Measurement of bubble size bypasses the need for indirect calculation of mean bubble size through methods such as drift flux analysis, and extends the data by making available the bubble size distribution. These distributions have proved useful as they permit analysis of particle recovery on a bubble size-by-size basis (Gomez et al., 2003).

1.1.2 Importance of Bubble Size

Bubble size is of key importance to metallurgical performance. By virtue of the mechanics of particle attachment, bubbles must not be excessively large or small. When bubbles are too small, particles may have insufficient contact time to attach, or if attachment does occur, the bubble buoyancy may be too low for practical recovery. On the other hand, as bubble size increases the strength of the bubble streamlines increases, making collision between particles and bubbles more difficult.

Practical bubble size range for flotation has been stated as 0.5 to 2.0 mm (Gorain et al., 1995). In this range, particles are able to overcome the liquid streamlines around bubbles, have enough contact time to attach, and the resulting bubble/particle aggregate has enough buoyancy to disengage from the pulp.

As Jameson (1977) noted, bubble surface area flux, and therefore inversely bubble size, is proportional to the flotation rate constant (*Figure 1-1*, Gorain et al., 1997) implying that the rate of recovery is decreased as bubble size increases. The dependence of recovery on bubble size illustrates the industrial importance of its control.

1.2 BUBBLE SIZE MEASUREMENT

Sizing bubbles in both two and three-phase systems proves difficult in the best of cases. Bubbles may either be measured intrusively (i.e., probing and sampling) or unobtrusively. While intrusive measurement adds the potential for biasing, unobtrusive methods are limited, and bubble size may become a calculated value based on other measured variables. Examples of unobtrusive measurement are: X-ray (Rowe and Everett, 1972), pressure probes (Atkinson and Clark, 1988) and laser scattering (Sung and Burgess, 1987). It should be noted that each of these methods fails in the presence of solids. For flotation systems, therefore, intrusive methods dominate.

One commonly employed intrusive technique is the UCT (University of Cape Town) method which entails bubbles being drawn into a capillary and assuming the shape of a cylinder. The length and velocity of the cylinder is measured by optical means, and an equivalent output bubble diameter generated based on the total volume of gas collected (Tucker et al., 1994). Though finicky, this technique has been successfully applied in industrial studies, typically sampling up to ~3000 bubbles (Deglon et al., 2000). Some practical limitations with respect to accuracy have surfaced, including a tendency to underestimate true bubble size due to break-up if capillary size and suction rate are not carefully selected (Grau and Heiskanen, 2002; Hernandez-Aguilar et al., 2004).

The most common method of bubble size measurement is image analysis (Rodrigues and

Rubio, 2003). Though sometimes time consuming and requiring specialised equipment, image analysis methods are highly versatile and applicable in both two and three-phase systems. A more detailed description of visual bubble sizing techniques is given below.

1.2.1 Visual Bubble Sizing Techniques

The simplest means of visually imaging bubbles in two-phase applications is to photograph through the side of a transparent vessel, counting the bubbles seen at the wall. Lighting may be front, back, or stroboscopic. There are several limitations: Distortions occur with cylindrical-walled vessels (they can be mitigated by placing a transparent water-filled box around the point of interest); only bubbles near the wail are viewed; and the multiple planes of focus available complicate image processing. Regardless, variations on this technique have been applied widely (Unno and Inoue, 1980; Zhou et al., 1993; Yianatos et al., 2001; Polli et al., 2002; Schafer et al., 2002).

For extension to three-phase systems, one approach is to sample bubbles from the pulp and introduce into a water-filled area where they may be imaged. Techniques described in the literature include the installation of a vertical sampling tube directing bubbles to a transparent viewing chamber (Ahmed and Jameson, 1985; Malysa et al., 1999; Chen et al., 2001; Grau and Heiskanen, 2002). Alternatively, bubbles may be 'tapped' from the vessel at an angle up to 90° and imaged in the horizontal plane (de Rijk et al., 1994; Rodrigues and Rubio, 2003). Lighting may again be front, back or stroboscopic.

1.2.2 McGill Bubble Size Analyser

The McGill bubble size analyser (the “bubble viewer”, *Figure 1-2*) consists of a sampling tube attached to a viewing chamber with a window inclined 15° from vertical. (A brief guide to operation is provided in *Appendix A*.) To use, the sample tube is closed and the assembly filled with water of similar temperature and chemistry (in particular frother concentration) as present in the bulk (to preserve the bubble environment, primarily to prevent bubble coalescence). The sample tube is immersed to the desired location in the pulp (i.e., below the froth/pulp interface), and is opened. Bubbles rise up the sampling tube by natural buoyancy, and enter the viewing chamber where they spread into a single plane after contact with the inclined window. Due to diffused backlighting, bubbles cast shadows, which are digitally imaged as the bubbles slide up the window. The images (as seen in *Figure1-3*) show the bubbles as dark circles with a bright spot in the centre (for two-phase systems). In three-phase systems, the bright spot is often obscured due to solid loading so that bubbles appear as dark circles.

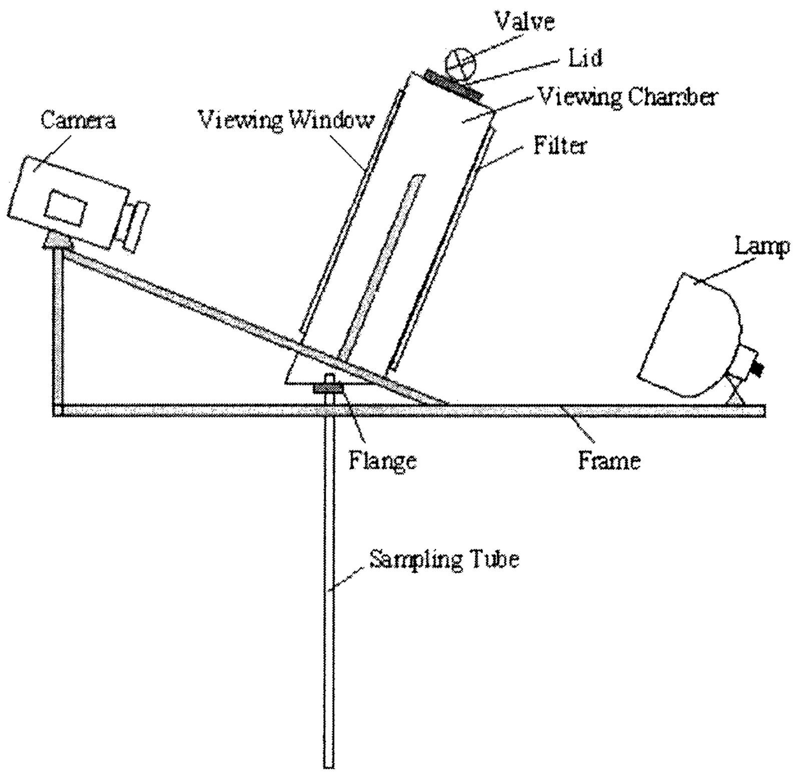

FIGURE 1-2: *SCHEMATIC REPRESENTATION OF MCGILL BUBBLE VIEWER.*

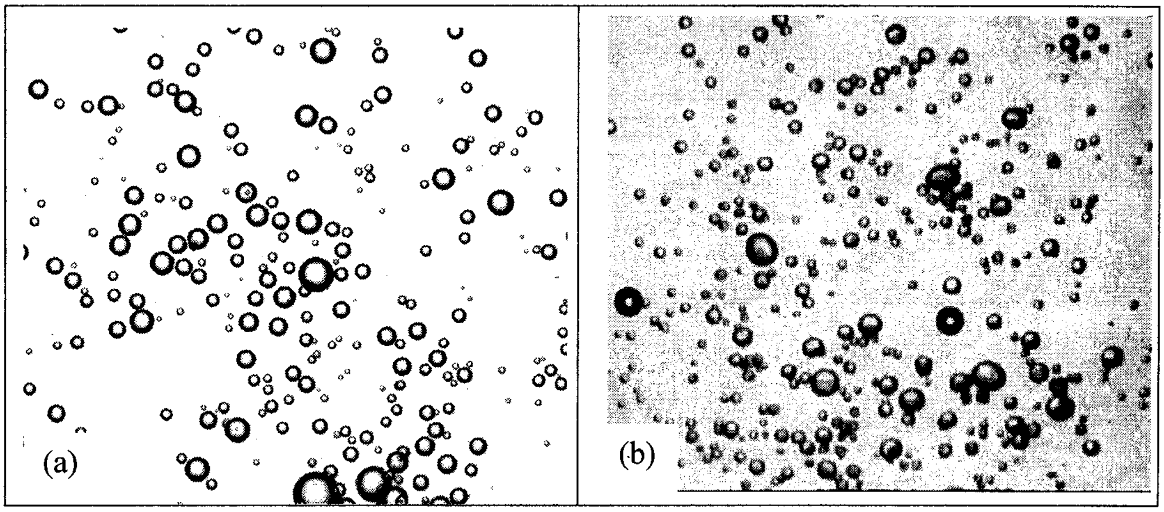

FIGURE 1-3: *SAMPLE BUBBLE IMAGES TAKEN USING THE MCGILL BUBBLE VIEWER (a) 2-PHASE; (b) 3-PHASE WITH TWO CALIBRATION DISKS (THICK BLACK RINGS).*

All data presented in this thesis was collected using a Canon GLSC-1 miniDV recorder, and images captured using ATI software. The sampling tube used had an inner diameter of 1.0 in. (2.54 cm, nominal), with an inline ball valve unless otherwise stated. Image analysis was done with Empix Northern Eclipse v6.0. Bubble size distributions, as presented in this thesis, are generated as histograms with logarithmic increments of $2\sqrt{2}$, and plotted as smoothed functions.

Several steps are taken to ensure image quality. Lighting must be applied evenly, and the use of an appropriate light diffuser is crucial. The intensity of light required varies by camera and may be controlled either by adjusting the distance between the light and the back window of the viewing chamber, or by regulating the intensity of the light. Care must also be taken to ensure that the camera lens, viewing chamber and window are free of debris, as these objects may cause difficulties during automated processing.

An acceptable two-phase image features even lighting with good contrast between background and bubbles. The bubbles should be closed circles. The magnification is a compromise between the smallest bubbles still featuring bright spots (i.e., being multiple pixels in diameter), and frames containing adequate numbers of bubbles for counting.

1.3 IMAGE PROCESSING

All visual bubble-sizing methods rely on image processing, which is (to varying extents) automated. Much of the process is generic.

First, images must be calibrated, i.e., the pixel size is associated with a tangible distance.

Typically this is done by using a distance marker, such as a calibrated disk or ruler, either at the beginning of or throughout an image sequence. Calibration should be made using relatively large distances, perhaps in the order of half the length of the field of view, to minimise error. Generally, calibration does not introduce significant error.

Images are greyscale, with bubbles being significantly darker than the background (with the obvious exception of negative image techniques, Polli et al., 2002). A greyscale threshold value must be selected to define the position of the bubble perimeter. Pixels with a greyscale value above the threshold are considered white for the purposes of image processing, while those with a value below are considered black.

The selection of the threshold is key, and, with the exception of some single bubble studies, is made by the operator due to the absence of standards. While the perimeter of a bubble is visually well defined at low magnification (e.g., *Figure 1-4*, left), increased magnification reveals a greyscale gradient both between the background and bubble perimeter, and between the bubble perimeter and the central bright spot.

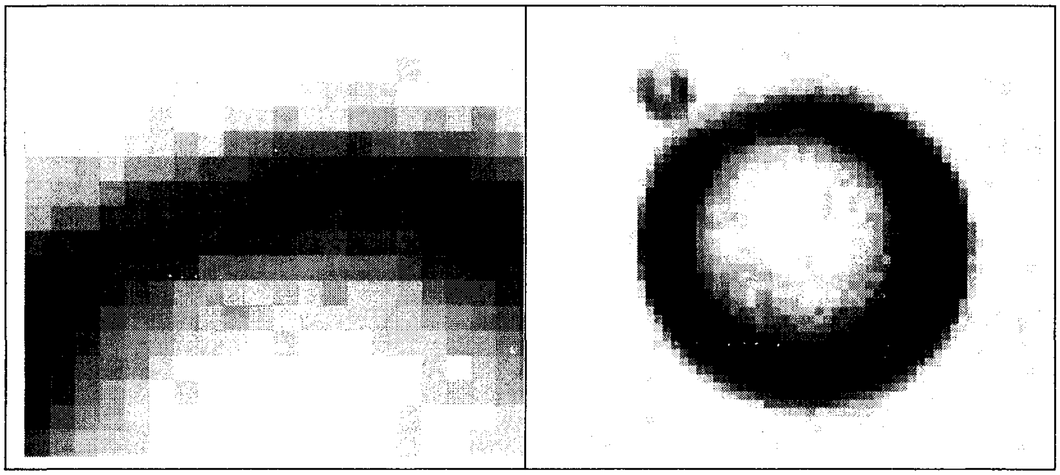

FIGURE 1-4: *BUBBLE PERIMETER AT TWO MAGNIFICATIONS SHOWING GREYSCALE GRADIENT.*

If the selected threshold value is too low, bubbles may not have complete perimeters, thus appearing as crescents, for which sizing fails. As small bubbles cast weaker shadows, the greyscale value of their perimeter is lighter than that of larger bubbles, thus making them particularly prone to under representation.

As the threshold value is increased, the bubble perimeter closes, giving a truer representation of bubble shape. Further increasing the threshold has the effect of increasing the bubble diameter, as successive layers of pixels in the greyscale gradient are considered black.

While some elegant techniques for threshold assignment have been developed for single bubble studies, yielding highly accurate bubble size representation (Leifer et al., 2003; Hernandez-Aguilar, 2004), these techniques are difficult to extend to bubble distributions, and fail in the presence of solids. Generally, the threshold is selected by ensuring the closure of the smallest bubbles, and accepting some minor over-sizing of bubbles in the larger size classes.

Besides threshold selection, the sizing techniques vary in other ways. The simplest employ manual measurement. In most cases, however, software is employed, the complexity of which ranges from analysis of user-selected objects, to automated filtering and object selection as in the case of the McGill technique. As automated object selection minimises processing time and gives a practical means of counting tens of thousands of bubbles increasing confidence in the derived size distribution, this type of software is increasingly common. Further review of the McGill bubble sizing technique and software is presented in relevant sections in the thesis.

1.4 METHODS OF BUBBLE GENERATION

The principle purpose of bubble generation systems in mineral flotation is to produce relatively small bubbles, 0.5 to 2 mm, at gas rates ranging from 0.5 to 2.0 cm/s (Dobby and Finch, 1991). Gas rate is limited at the lower end by sanding (solid particles settling out), and at the upper by cell boiling (large bubbles erupting through the froth). The operating gas rate range varies by cell type and bubble generation device.

Bubble generation devices may be broken into several categories, schematically represented in *Figure 1-5*. The four main ones are; sparging through porous media, jetting, and mechanical and static shear contacting (Dobby and Finch, 1991). For industrial applications, robust, low maintenance devices are required, leading to limited application of porous media due to plugging by solids. Particular attention will be paid to two devices successfully applied in industry, mechanical shear contacting and jetting.

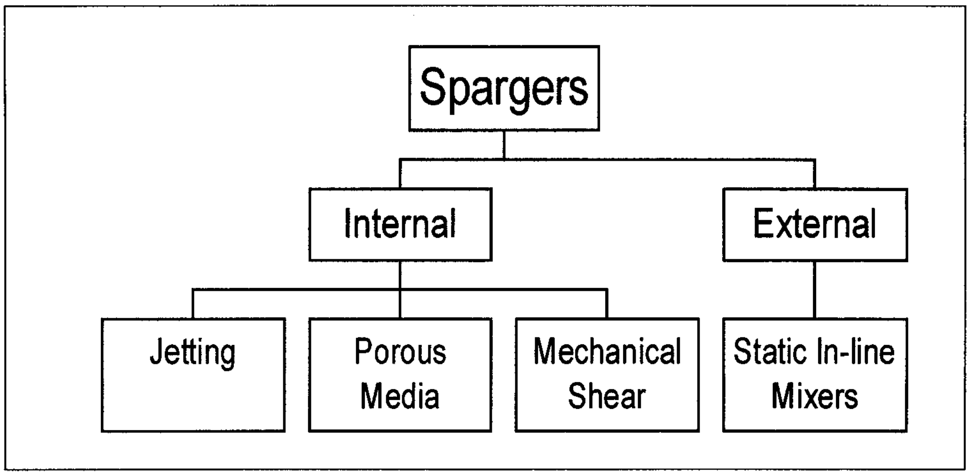

FIGURE 1-5: *OVERVIEW OF FOUR MAIN BUBBLE GENERATION DEVICES.*

While the method of bubble generation and gas rate have a significant impact on bubble size, chemical factors such as frother type and dosage also have a role. Effective control over the bubble generation system, air rate and chemistry are key to manipulating bubble size.

1.4.1 Mechanical Shear Contacting

Mechanical shear contacting is the predominant method of bubble generation in most machines used in mineral flotation – the so-called mechanical cells. While the impeller motion serves to suspend solids, it also generates and disperses bubbles. The rotation of the impeller creates high shear rates that disperse the air into discreet bubbles.

The key variables in the design and operation of mechanical shear contacting devices are impeller design (e.g., number of blades, length, and shape), rotation speed, air rate and physical properties of the slurry, all of which affect power draw (Bakker et al., 1994). Once the device is installed, only air rate, rotation speed and chemistry may be used to alter bubble size. The average bubble size and distribution width has been found to increase with increasing air rate and decreasing impeller speed (Gorain et al., 1995).

From experience with the McGill bubble viewer, size distributions produced by lab and industrial mechanical cells typically are log-normal in nature, and centre around 1.0 mm.

The response of the bubble size distribution to changing variables can be examined by plotting the Sauter (D_{32}) mean bubble size (*Equation 1*-3) against the number (D_{10}) mean bubble size *(Equation 1-2)*, as shown in *Figure 1-6* for both mechanical shear and porous spargers. The ratio of the number and Sauter means is an indication of distribution width, and the relation to a unimodal distribution (a line intercepting at zero, with a slope of unity), makes for simple visual comparison between data sets. For the case of increasing gas rate (constant impeller speed), the data form a trend, which progressively veers away from the unimodal distribution line, indicating not only that the mean sizes are increasing, but also that the distribution is becoming wider. This trend with varying gas rate is typical.

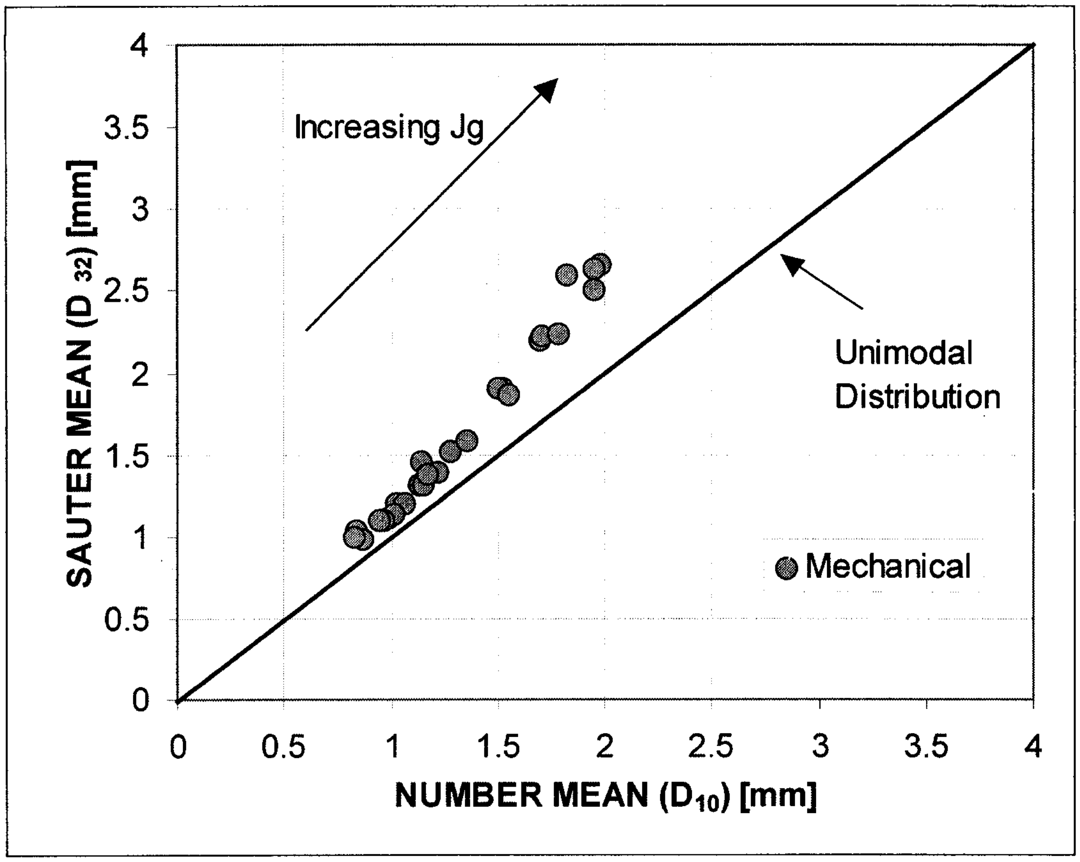

FIGURE 1-6: *VARIATION OF NUMBER AND SAUTER MEAN DIAMETERS WITH GAS RATE. BUBBLES PRODUCED MECHANICALLY.*

$$D_{10} = \frac{\sum n_i D_i}{\sum n_i} \qquad \textit{EQUATION 1-2}$$

$$D_{32} = \frac{\sum n_i D_i^3}{\sum n_i D_i^2} \qquad \textit{EQUATION 1-3}$$

1.4.2 Jetting Spargers

In the selection of internal bubble generation devices for industrial flotation columns, jetting spargers are often favoured as they promise freedom from plugging and generally have low maintenance. Jetting spargers produce bubbles through the injection of high velocity gas through a small diameter orifice (as small as 1.0 mm (Finch, 1995), and generally not exceeding 5.0 mm). Bubbles are likely produced through a combination of shear and turbulence along the surface of the jet. Maximum bubble size is controlled by the hydrodynamics of the system, such that bubbles above this diameter are unable to withstand the shear forces and are broken (Varley, 1995).

The formation of small bubbles is believed to occur by shearing action around the periphery of the jet, while the larger bubbles result from turbulent break up at the end of the jet. It is thus expected that increasing jet length will increase the production of small bubbles due to increased surface area for shear, thus decreasing the overall number mean.

To increase jet length, the momentum of the jet must be increased, conveniently summarised by the Reynolds number which is used to correlate jet studies (Krevelen, 1950; Leibson, 1956; Zhang et al., 2001). Reviewing the terms of the Reynolds number, means of increasing jet momentum are evident.

$$\mathrm{Re} = \frac{F_{inertia}}{F_{viscous}} = \frac{Dv\rho}{\mu}$$

EQUATION 1-4

One way is to increase the gas density (ρ), either by increasing gas pressure, or through the injection of water (in the order of ~1v/v%), both of which have been shown to decrease the average bubble size produced (Finch, 1995; Lin, 1999).

Alternatively, the velocity (υ) of the jet may be increased, either by decreasing the orifice diameter, or increasing the volumetric flow of gas. Leibson (1956) explored this and found that for the same gas rate, bubble size decreased with decreasing jet orifice diameter. (The connection of increasing flow rate to increase momentum and decrease bubble size was not shown in that work because pressure decreased with increasing gas rate, thus counteracting the momentum effect.)

In my case, initial two-phase bubble size measurements were conducted with a jetting sparger, the SlamJet by CPT, in a pilot column (4 m in height, 0.5 m diameter, 1965 cm^2), and showed uncharacteristic behaviour when the number and Sauter means were compared under various conditions (*Figure 1-7*). Upon inspection, an extremely wide bubble size distribution, ranging from 0.3 to 15 mm was evident. Sample images are provided in *Figure 1-8*. As can be seen in *Figure 1-9*, the jetting sparger produces (fractionally) significantly more small bubbles than a typical mechanical system, but volumetrically most is held in large bubbles. This wide bubble size distribution, and the scatter shown on the number/Sauter mean plot suggested the need for revision of the McGill bubble size analysis technique, until now only used for bubbles in the range of approximately 0.5 to 3.0 mm.

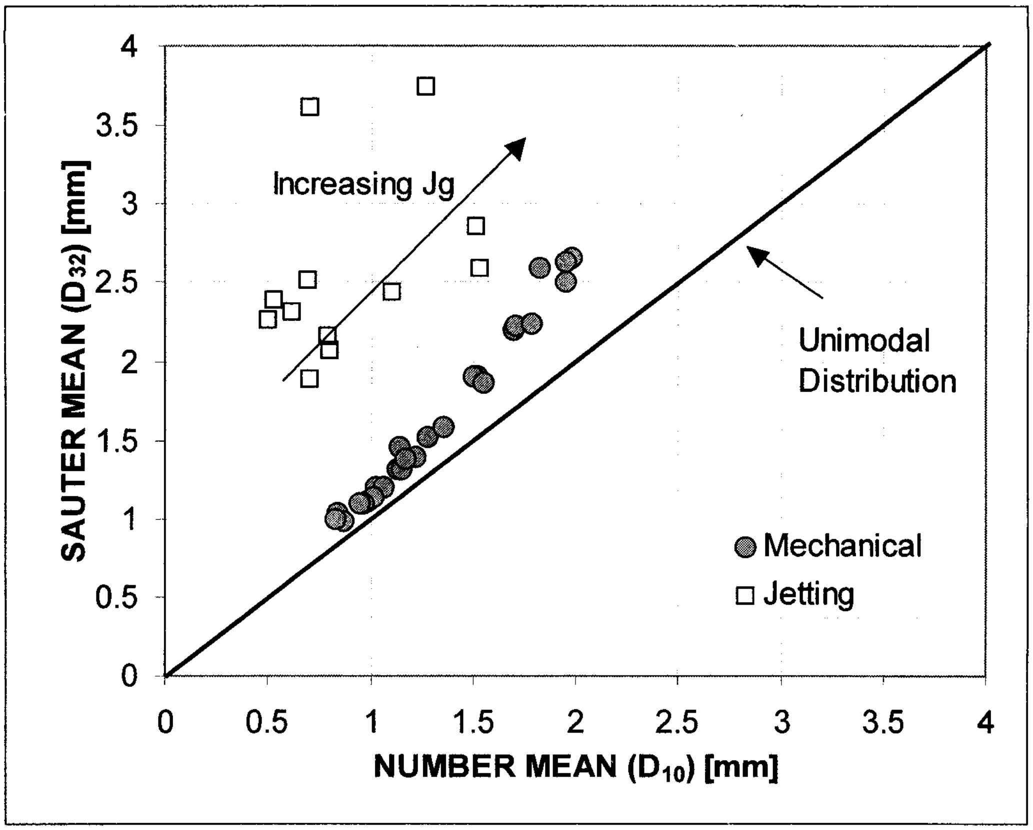

FIGURE 1-7: *VARIATION OF NUMBER AND SAUTER MEAN DIAMETERS WITH GAS RATE. BUBBLES PRODUCED MECHANICALLY AND WITH JETTING SPARGER.*

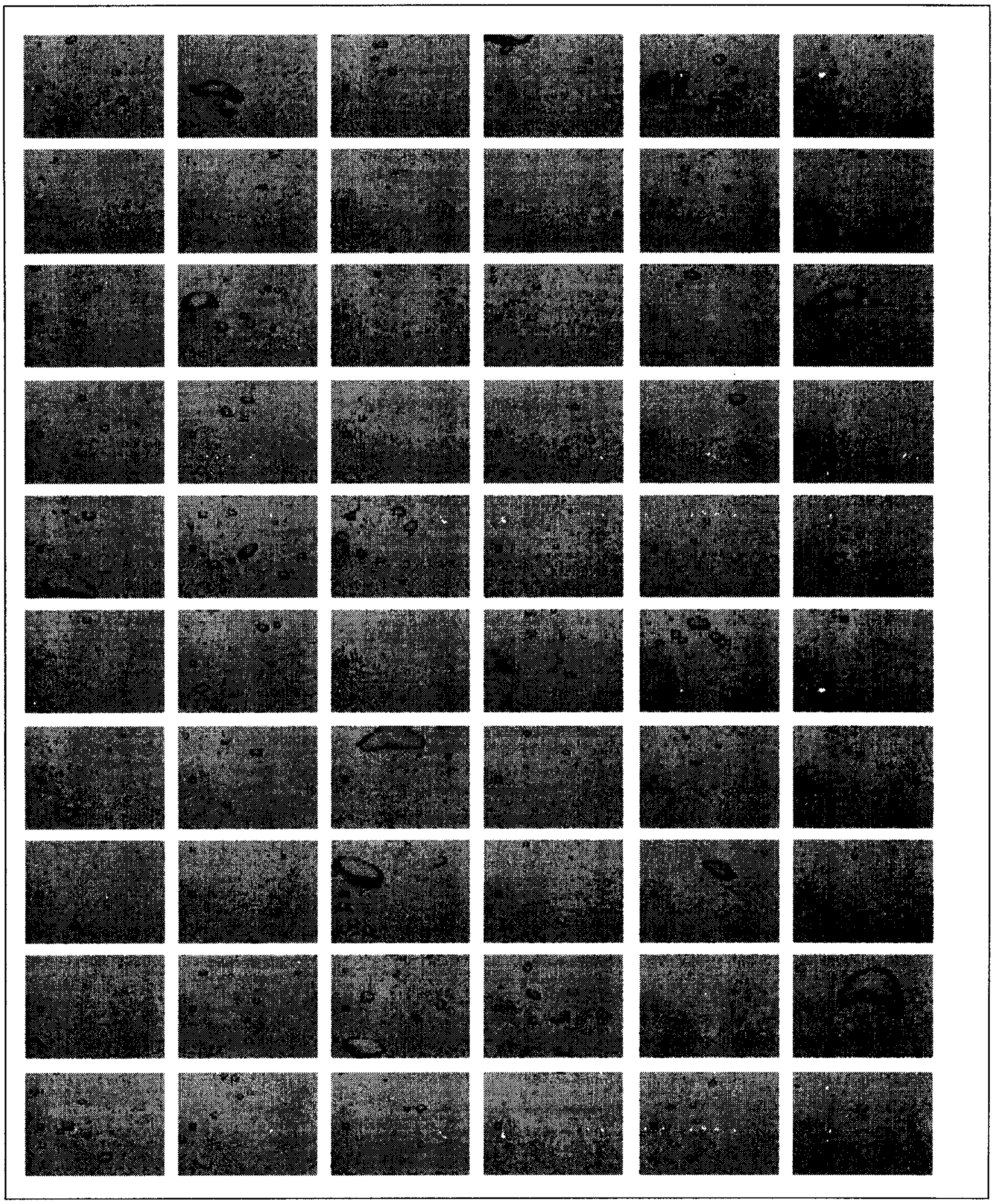

FIGURE 1-8: *SAMPLE IMAGES OF BUBBLES PRODUCED BY A JETTING SPARGER. NOTE THE PERIODIC APPEARANCE OF LARGE BUBBLES.*

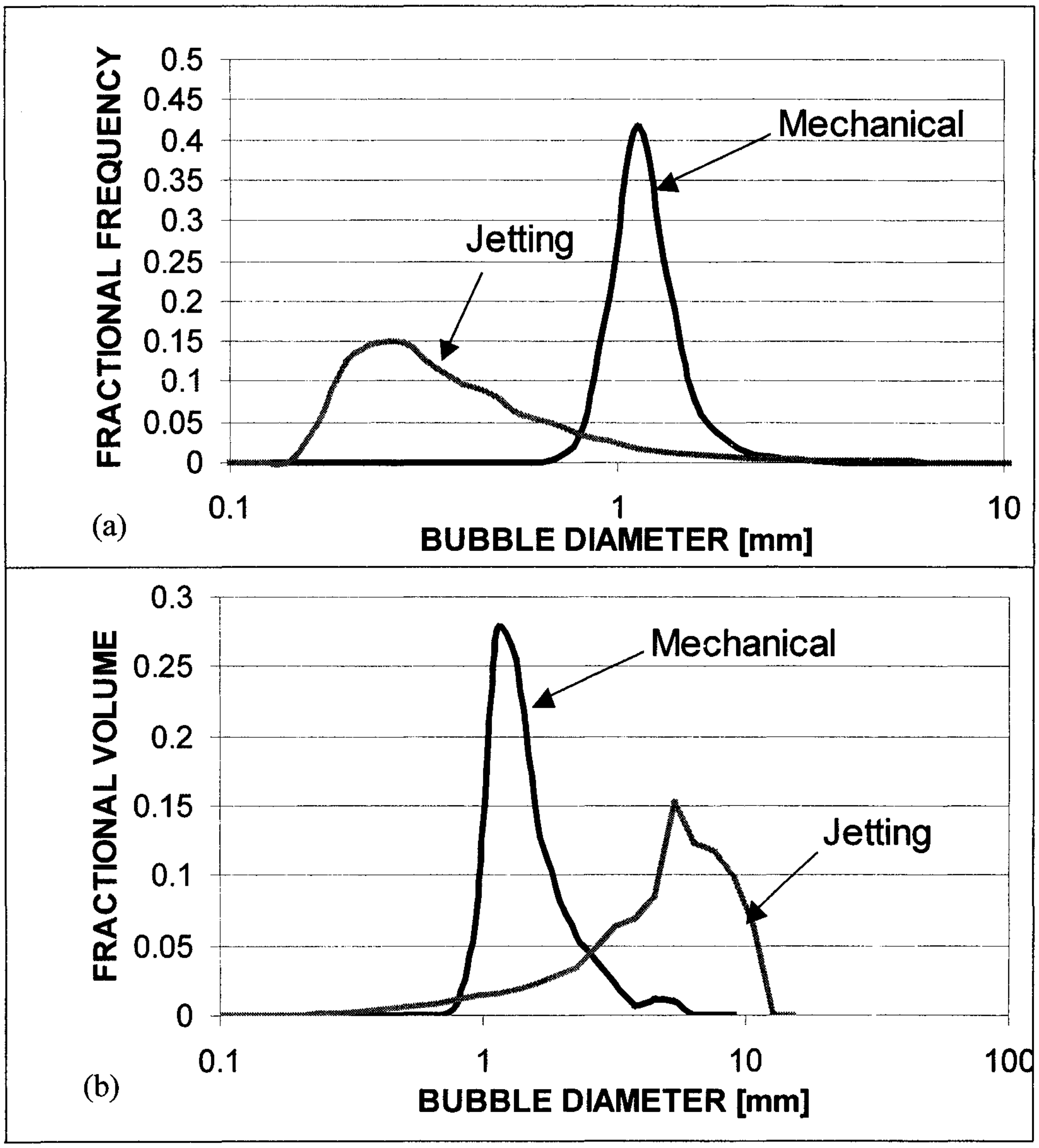

FIGURE 1-9: *(a) TYPICAL NUMBER FREQUENCY AND (b) TYPICAL VOLUME FREQUENCY DISTRIBUTIONS FOR JETTING AND MECHANICAL BUBBLE SIZE DISTRIBUTIONS*

1.5 RESEARCH OBJECTIVES

The focus of the thesis is to adapt the McGill bubble sizing technique to wide distributions. The bulk of the work was done in two-phase using laboratory and pilot-scale columns, with exceptions where noted.

The specific objectives are:

1. To develop an alternative automated image analysis process, improving representation of wide bubble size distributions.

2. To develop a method of diameter assignment for large non-spherical bubbles based on individual bubble characteristics to improve bubble size representation.

3. To provide a procedure for the selection of an appropriate sampling tube diameter based on the bubble population present for improved sampling accuracy.

1.6 THESIS OUTLINE

Chapter 1 provides a general overview of the importance of bubble size in flotation, including the need for direct measurement of bubble size. Various measurement methods are outlined, with particular focus on visual techniques. An overview of a general image processing procedure for visual bubble sizing is also given. Some industrially important methods of bubble generation are outlined, with particular focus on jetting systems for the development of the research objectives.

Following the introduction and problem definition provided in Chapter 1, the thesis is subdivided into four main sections, each comprising a chapter.

Chapter 2 describes the development of an alternative, automated bubble image analysis method. A comparison with the current technique used at McGill is given.

Chapter 3 illustrates a manipulation method of the minimum diameter criterion to estimate a representative bubble size distribution for instances where non-bubble artefacts are present.

A method of assigning a single diameter to each bubble based on shape characteristics for accurate representation of bubble volume is given in Chapter 4.

Chapter 5 introduces a method for selection of sampling tube diameter, with a discussion on the potential biasing of output bubble size data due to improper selection.

Conclusions and recommendations for future work are given in Chapter 6.

Appendix A presents a brief manual for the operation of the McGill bubble viewer for lab and industrial applications. The Visual Basic source code for the alternative image analysis method is given in Appendix B.

CHAPTER 2 - ALTERNATIVE IMAGE ANALYSIS METHOD

2.1 INTRODUCTION - OVERVIEW OF CURRENT TECHNIQUE

Images obtained using the McGill bubble viewer must undergo analysis before quantitative measurements can be extracted. The current analysis process consists of a series of steps, most decided by operator judgement, thus leading to potential problems in data continuity between operators. As a basis for comparison of current and proposed techniques, the analysis process is briefly reviewed.

The first hurdle for image analysis is the quality of the image itself. As different aspects influencing image quality vary, namely background greyscale, contrast, light distribution, multiple 'bright spots' in bubbles, and the presence of foreign objects (i.e., mineral particles, paper fragments, debris in water) each specific case requires slightly different treatment. It is largely due to these issues that a standardised process has not yet been established; there are simply too many special cases. A general analysis process is described.

Following the calibration, and threshold setting as described in Chapter 1, a region of interest (ROI) is set. This region is established such that any image flaws, e.g., smudges, dirt, or dark areas, are eliminated. Any objects counted that are not bubbles, including any objects used for calibration, can skew results, as groupings of dark pixels are counted regardless of whether they are bubbles or flaws. Lack of care in setting the ROI can lead to a lack of consistency between data sets.

Once the operator selects the calibration, threshold and ROI, a custom written Empix programme, 'Bubbles', is applied to count and size the objects. 'Bubbles' scans the rows of pixels and counts every object in the image, and then applies two operator-set filters in an attempt to avoid counting non-bubble objects.

The first filter is diameter. The operator defines a minimum and maximum diameter; any object with a diameter outside the specified range is not counted. Typically, diameters counted are between 0.2 and 20 mm, though values vary with magnification. Ultimately the minimum diameter should be based on the calibration, assuming a minimum number of pixels (for example, three) that together constitute a bubble. Clearly, this system is prone to small dark spots in the image being counted, as they need only be several pixels in diameter to be deemed an object.

The second filter is shape factor. Eclipse defines the shape factor as *Equation 2-1*.

$$ShapeFactor = \frac{4\pi(Area)}{(Perimeter)^2} \qquad \text{EQUATION 2-1}$$

For an object that is a perfect circle, the shape factor would equal unity, while a straight line would have a value approaching zero. However, since the images are digital each object consists of pixels, and as a result, even a 'perfect' circle has a shape factor below one. Typically, circular objects have shape factors above 0.85, an example being the calibration disk.

The standard minimum value for the shape factor filter is 0.7. This setting is intended to exclude non-spherical objects (typically single bubbles are approximately spherical until they exceed 3 mm in diameter), and also exclude groups of overlapping or touching objects. The remaining objects are relatively spherical and are assumed to be single bubbles contained within the ROI.

With these input criteria, the images to be analysed are selected and 'Bubbles' filters through the objects. The final output is in the form of an MS Excel spreadsheet which contains a variety of descriptors for each object, including one measured and two calculated diameters, the shape factor, maximum and minimum radii and the object area. These results may be used to generate bubble size distributions, and a variety of mean bubble sizes, among other metrics.

2.2 SHAPE FACTOR

As selection of the minimum diameter filter can be established through careful choice of threshold and ROI, and objects considered too small to be bubbles can be filtered after the analysis process, only the shape factor criterion is examined in depth here.

Ideally, if all bubbles were circular in shape and no undesirable objects were contained in the ROI, filtering by shape factor would prove an excellent separation process to discern single bubbles (with very high shape factors) from clusters of bubbles (with significantly lower shape factors). However, as will be discussed, a simple set minimum value, above which all objects are counted, is not adequate to discriminate between single bubbles and clusters of bubbles.

2.2.1 Sensitivity to Object Size

Considering *Equation 2-1* and that objects consist of pixels, one key concern is revealed: the effect of additional single pixels on shape factor is more significant for small objects than it is for large ones. Let's take as an example the case of a square object, which by calculation has a shape factor of 0.79. Now, if this square consisted of nine pixels, to which one extra pixel was added, the shape factor would be reduced to 0.64. However, a 49-pixel object, with one additional pixel would only have its shape factor reduced to 0.70. This difference due to absolute size is clearly significant when a minimum shape factor is set. A small object, which deviates slightly from a regular shape, is less likely to be counted than a large object with a similar absolute deviation. Therefore, the sensitivity of the shape factor to changes in object shape decreases with increasing object size.

2.2.2 Sensitivity to Threshold

An incorrect threshold setting can affect the final results in several ways. The most apparent is that if an object is not closed (the threshold setting is too low), that object, taking the shape of a crescent, will have a low shape factor and hence would not be counted. This is a significant problem for image sets with little contrast, as the threshold setting which allows all bubbles to close often will also induce flaws to be counted as well. In this case, careful selection of the ROI is particularly crucial.

Another side effect of increasing threshold values may also play an important role in determining which objects are counted when combined with the considerations in Section 2.2.1. Increasing the threshold setting typically has the effect of adding pixels to the perimeter of an object, as it is not simply black on a white background. A gradient from dark grey to the background greyscale is present, and is generally not uniform around the perimeter of the object. As a result, by increasing the threshold value increasing amounts of this perimeter area are counted as part of the object. As is demonstrated in *Figure 2-1*, altering the threshold on a single object (in this case, a 0.3 mm and a 1.05 mm bubble, both with high shape factors) has a marked effect on shape factor.

Initially, the objects have very low shape factors, as they do not close (not shown). Once closed, the threshold value fluctuates as pixels are added at various points around the perimeter. In the case of these very high shape factor bubbles, this fluctuation would not be significant enough to reduce the shape factor below 0.7; however, it can be expected that for a bubble with a lower shape factor, in the order of 0.7, changes in threshold could lead to a bubble not being counted. It is noted from *Figure 2-1*, that the magnitude of fluctuation is larger for the smaller bubble, leading to the conclusion that the sensitivity of shape factor to threshold setting increases as object size decreases. This conclusion is justified through arguments presented in Section 2.2.1.

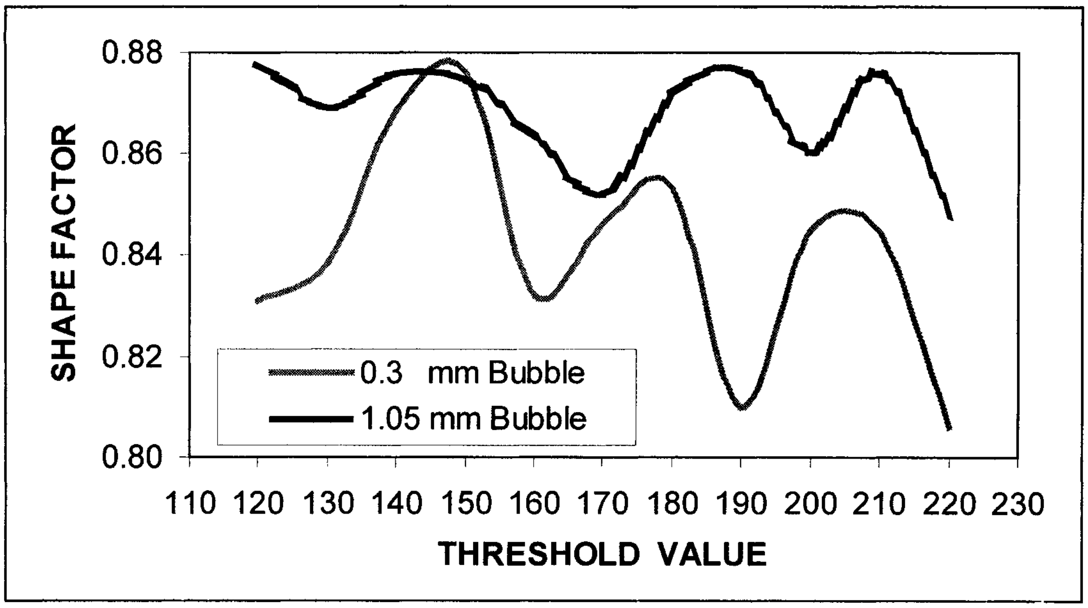

FIGURE 2-1: *EFFECT OF VARYING THRESHOLD ON SHAPE FACTOR*

At the other end are large objects. For the purpose of this discussion, an object above approximately 3 mm diameter will be considered large. Once a bubble exceeds this diameter, it becomes increasingly elliptical, i.e., its shape factor is reduced. As a further complication, the shape of the bubble fluctuates as it moves, so the shape factor for the same object is constantly changing. Generally, large bubbles are not counted, as their shape factors are too low to meet the standard shape factor criterion.

2.2.3 Effect of Shape Factor Selection on Distribution

Currently, the standard minimum shape factor setting is 0.7. However, there is room for operator judgement in what the appropriate setting is for a particular case.

It can be anticipated that by increasing the minimum shape factor setting, increasingly circular objects would be counted, at the extreme, excluding anything short of a perfect circle. Hence, the distribution would be expected to shift to finer sizes and become narrower, as proportionately more small bubbles would be counted.

As the minimum shape factor setting is decreased, increasingly imperfect circular objects would be counted. While this includes larger bubbles, such as those appearing as ellipses, it would also include an increasing number of bubble clusters.

In order to demonstrate the effect of the shape factor criterion, a set of sample images was processed using various minimum shape factor values, varying from 0.2 to 0.8 in increments of 0.1. The test set of images was taken using a laboratory scale self-aspirating 5.5 L mechanical cell, with impeller speed of 1400 rpm and 5 ppm DowFroth 250C frother. The diameter filter was set as 0.1 to 20 mm. The bubble size is relatively fine with a narrow range. This should be considered a conservative case, as deviations from the typical distribution are rare for bubbles generated under these conditions.

The resulting distributions are plotted in *Figure 2-2*, showing an obvious shift in the width of the distribution, favouring wider distributions at lower shape factors. The effect of varying shape factor is also apparent in the various means, number of objects counted, and maximum and minimum diameters, as outlined in *Table 2-1*. Clearly, the selection of the shape factor is not a trivial matter. It is assumed that as the shape factor is decreased, increasing numbers of bubble clusters are counted, and that for the most part the increasing maximum bubble size may be attributed to the counting of bubble clusters.

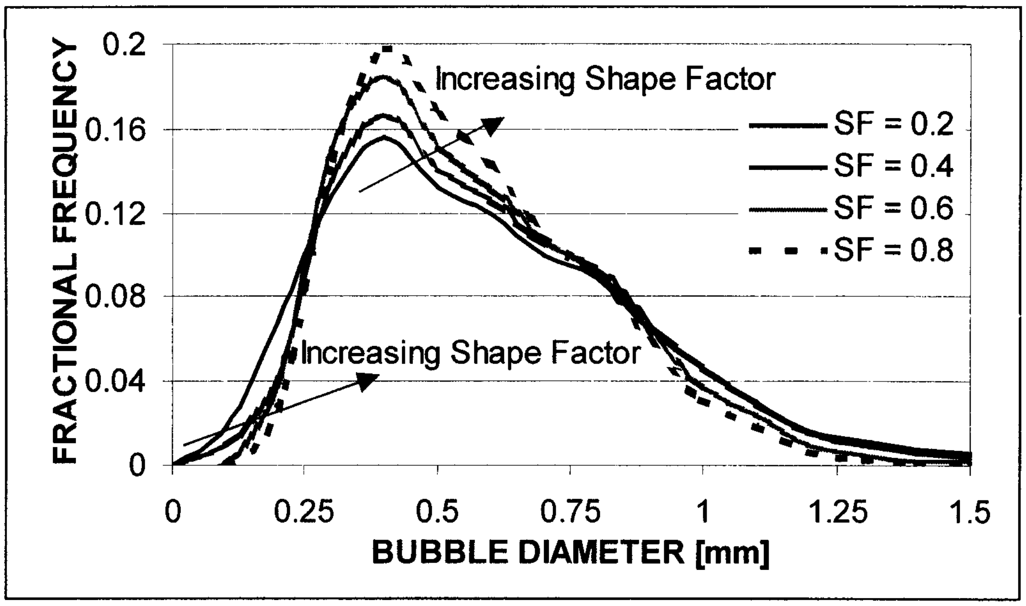

FIGURE 2-2: *VARIATION OF BUBBLE SIZE DISTRIBUTION WITH CHANGING SHAPE FACTOR.*

TABLE 2-1: *SUMMARY OF VARIATIONS IN BUBBLE POPULATION BY VARYING SHAPE FACTOR.*

Shape Factor	Sauter Mean Diameter [mm]	Maximum Diameter [mm]	Minimum Diameter [mm]	Number Counted
0.2	0.88	3.11	0.06	12 491
0.3	0.86	3.11	0.06	12 227
0.4	0.83	3.11	0.06	11 707
0.5	0.79	2.28	0.06	11 214
0.6	0.76	2.28	0.07	10 464
0.7	0.72	1.92	0.09	9 992
0.8	0.71	1.78	0.09	9 222

With shifting distributions based on shape factor selection, the true distribution is not clear. As the shape factor setting changes, so do the number of true objects discounted and false objects counted, making it difficult to determine a true mean value and distribution using a shape factor criterion, as there is no absolute standard for comparison.

Clearly, in practical systems it is very rare that a shape factor value can be set such that all single bubbles are counted, while all clusters are ignored. It was due to the potential biasing of the output distribution that an alternative method of analysing bubble images was devised.

2.3 PROPOSED FILTERING ALTERNATIVE

An alternative method of processing and interpreting the bubble size data generated by Eclipse was devised for two-phase systems, to reduce the dependence on shape factor. The programme takes advantage of the 'Fill Holes' option in 'Bubbles'.

An explanation of the process and logic used is outlined below. A macro, Holesv8, was written in MS Visual Basic to be used with the MS Excel output from Eclipse and is provided in *Appendix B*.

To use Holesv8, a set of images must be processed twice. Each processed set should have the diameter filter set as 0 to 20 mm and the shape factor filter as 0 to 1.2. The difference between the two processing runs lies with the 'Fill Holes' option, which is used in one case and not the other (selecting and then unselecting 'Fill Holes' will deactivate the option). The parallel sets of data should then be made into one file, with the 'Fill Holes' set being pasted beside the other set, leaving one blank column between them. Nothing else in either file should be altered. Holesv8 may then be executed. The result will be the original file in its original format, and a new file, saved in a location specified by the programme, with the file name as the experiment name as specified in cell A2 of the original file. The new file will contain the Eclipse output data for each object passing the programme filters, as well as a plot of the normalised number frequency.

Before using this programme for the first time, the path for saving file 'temp.xls' as defined in the first block of code should be changed such that the file will save to an appropriate location on the user's system.

After copying the original file into a temporary file, Holesv8 must align the data sets. It is not uncommon for bubbles to have extra objects inside them, for example, other bubbles, or more commonly, dark patches caused by light refraction. In the case where the holes are not filled, each of these internal objects is counted as an object. In rare cases, the data set with filled holes will also contain an extra object, the origin of which is currently unknown. This occurs in less than one percent of images and so is not considered a pressing issue.

To align the data sets such that corresponding objects occupy the same row, a set of true or false test equations is applied. The first test determines if the number of holes present in the objects is equal. The second test determines if the diameters of the objects are equal. The diameter (the longest chord across the centre of mass) changes in some cases between data sets with holes filled and holes not filled, as the centre of mass can change based on uneven thickness of the object's perimeter.

It was noted that in cases where both these statements are either true or false, or the number of holes is equal while the diameters are not, the same objects have been counted, meaning that the objects are corresponding. However, if the number of holes was equal, while the diameters were not, the objects were not corresponding. This is because the extra objects tend to have no holes. Since objects with no holes always have the same diameter, this false reading reveals that the objects do not correspond. The programme then scans down several rows and tries to match other rows of objects to determine which data set contains the unmatched object. Once the false object is deleted the scan continues.

Occasionally, the scan fails to detect a false object. This case occurs when the internal object has at least one hole. In this case, the picture labels cease to match and all test statements become false. If this occurs, the programme should be stopped and the faulty image deleted. This occurs in very few images, less than one image per hundred and the deletion process is not time consuming. The data from that image should be deleted from the original data and the programme restarted.

Once all false objects have been deleted, the first of the filters takes place. This filter removes all objects that do not a) contain exactly one hole and have a volume equivalent diameter larger than 0.2 mm, or b) have more than one hole, have a volume equivalent diameter larger than 0.2 mm, and have a shape factor greater than 0.8. The result of this filter is that all objects containing no holes are removed. As most bubbles (in air-water systems) contain bright spots, and hence holes, this was not seen to be an issue. By setting the minimum number of holes to one, small dark spots in the background can be eliminated. The minimum diameter of 0.2 mm was selected as it is rare, given the current bubble viewer set-up and magnification used, that a bubble less than this size could be accurately measured. In addition, for small objects, the calculated volume equivalent diameter is sometimes calculated as zero, clearly not possible. This filter removes any objects with 'zero' diameter. However, this value can easily be changed in the programme for special situations, for example for images with high magnification the value may be reduced to 0.1 or 0.05.

The second part of the filter was employed because if an object has even one blank pixel in addition to the typical bright spot, it would be counted as having more than one hole, and would be discounted. However, the majority of these bubbles are real, and often have high shape factors. It was noted that by using a minimum shape factor of 0.8, bubble clusters could be avoided much more effectively than with the minimum of 0.7. A point of future improvement would be to change the definition of a hole in the Eclipse software, such that a hole was only counted if it was above perhaps three pixels in size.

At this point, only one type of undesirable bubble still remained, a bubble with one small, unclosed bubble attached to it. Though this case sounds obscure, they were always present, sometimes accounting for up to 5% of the objects counted.

In order to remove these bubbles, a further filter was added. For this, a column was added to the right hand side of the remaining data. This column appears labelled in the final results as 'Ratio', and calculates the ratio of the area of the object as measured by Eclipse, and the area of a circle having the radius of the object's maximum radius. It was noted that the undesirable objects had a ratio of under 0.5 with rare exceptions, while desirable objects had ratios usually well over 0.7. Through the filter, any object with a ratio of less than 0.5 is removed.

This methodology is sound as the maximum radius is the longest distance between the centre of mass and the furthest pixel of the object's perimeter, which in the case of this type of bubble is significantly further than the true radius of the single bubble. Hence, the projected area as calculated is large, giving a small ratio. For desirable bubbles, this ratio will be much higher, as the maximum radius is not as extreme. A sample image containing over 300 objects, approximately 20 of which were this special case, was used to test this filter. One undesirable bubble passed the filter, and one desirable bubble was removed. Though imperfect, a marked improvement on the objects retained was noted.

Finally, all passing data is copied to a new file, named and saved as the input experiment name. All data from the set without filled holes is deleted and a normalised frequency distribution is plotted. At this point, the programme ends. The original file may be closed and kept for future reference. The new file should be saved to the desired location.

2.3.1 Comparison of Current Technique and Alternative

The validity of the alternative method was assessed in two ways. First, through processing a set of images using both techniques, and second by processing a series of single images and examining the differences in objects counted. From the first method, a quantitative comparison was achieved, while by the latter, a qualitative idea of which bubbles were and were not being counted was established. The conclusions of both methods are outlined.

2.3.1.1 Image Set Comparison

Two sets of images were selected to quantitatively compare results obtained by each method. One 'typical' set of images was selected; in this case a mechanical cell with frother. The second set, was 'atypical', produced by a jetting sparger in the presence of frother, having a wide size distribution and a significant population of irregularly shaped bubbles. The generated results are compared in *Table 2-2* on the basis of number and Sauter means, as well as number of objects counted. Additionally, normalized frequency plots were compared.

TABLE 2-2: *COMPARISON OF STANDARD AND HOLESV8 METHODS, TYPICAL AND ATYPICAL CASES.*

Parameter	Typical		Atypical	
	Standard	**Holesv8**	**Standard**	**Holesv8**
D_{10} (mm)	0.51	0.50	0.80	0.75
D_{32} (mm)	0.72	0.71	2.13	1.62
Number	9 992	9 539	34 793	17 692

As shown, fewer objects are counted using the alternative method when compared to the standard analysis method. This is attributed to fewer false objects being counted. It is also likely that some true objects are also being discounted. However as shown (*Figures 2-3 and 2-4*), the distributions are smooth and unimodal. These types of distributions, from experience, are those anticipated, supporting the technique. Both calculated means yield higher values for the standard method in all cases. In the case of the Sauter mean diameter, the variation is indicative of a higher portion of large objects being counted, as large objects have a stronger influence on the Sauter mean than smaller objects.

However, these counted objects are not necessarily single bubbles, as can clearly be seen in *Figures 2-5 and 2-6* (Section 2.3.1.2).

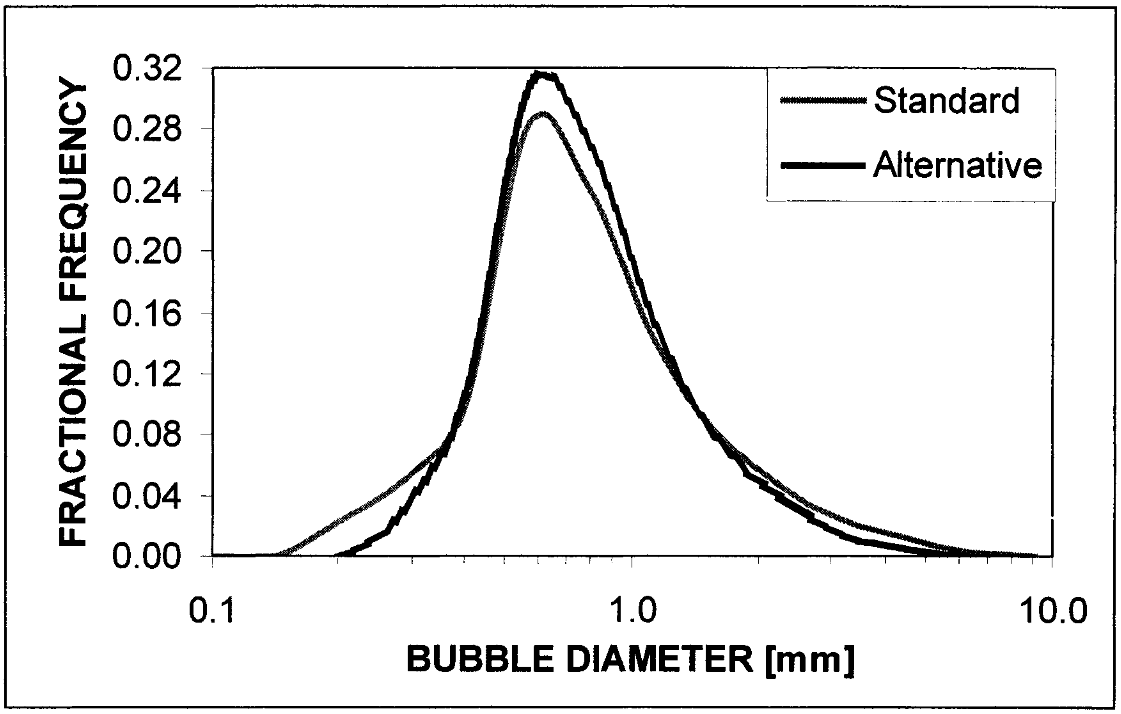

FIGURE 2-3: *NORMALISED DISTRIBUTIONS OF AN ATYPICAL DATA SET PROCESSED WITH STANDARD AND HOLESV8 METHODS.*

In the case of the atypical distribution (*Figure 2-3*), several points may be noted. Firstly, the standard method clearly counts more small objects than Holesv8. It is likely that these small objects (deforming the distribution below 0.5 mm) are patches of dark pixels or small objects without holes, which are discounted by the alternative method. The peak of the distribution occurs at the same point, and the distributions follow much the same curve after this point. Some deviation is noted, as the Holesv8 results appear to have a slightly higher fraction of large bubbles. Generally, the application of Holesv8 smoothed the distribution curve, despite counting fewer objects. Based on image-by-image comparisons (Section 2.3.1.2), it appears that the distribution obtained using Holesv8 is a closer depiction of reality than the standard method.

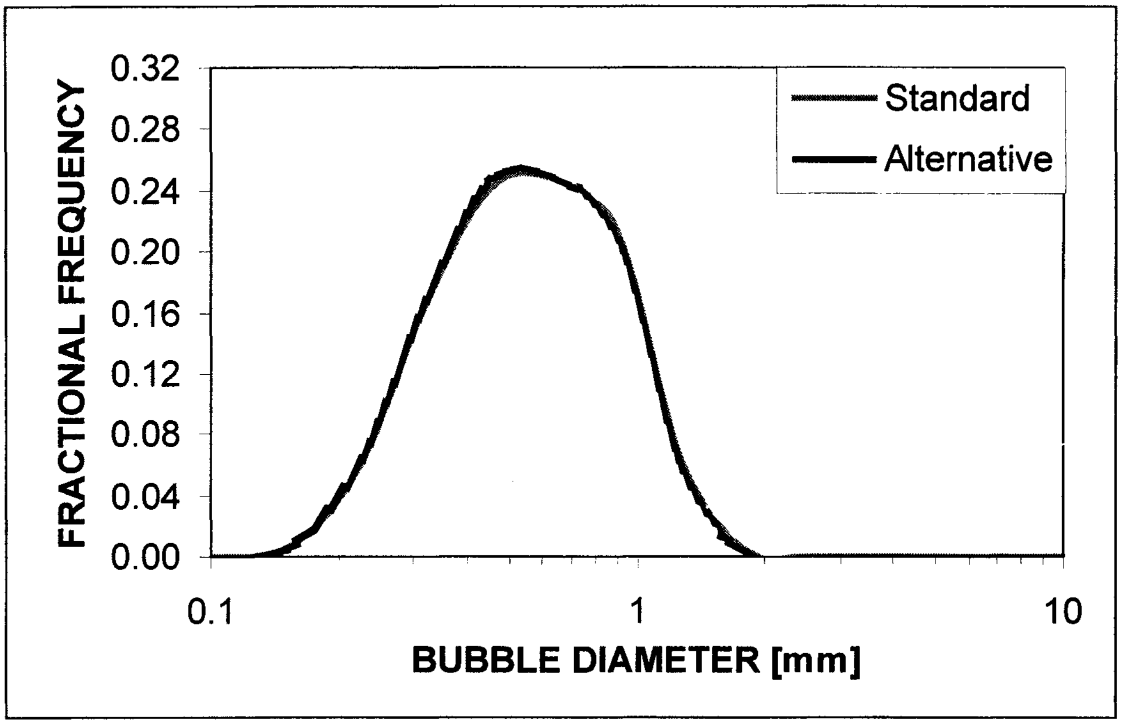

FIGURE 2-4: *NORMALISED DISTRIBUTIONS OF A TYPICAL DATA SET PROCESSED WITH STANDARD AND HOLESV8 METHODS.*

When Holesv8 was applied to a typical set of objects (*Figure 2-4*): the differences both in mean values and distributions are reduced, indicating that little gain in accuracy is made. It can be noted in the distribution that above 0.8 mm, the Holesv8 distribution lies very slightly below the standard distribution, indicating that somewhat fewer large bubbles are counted. This is concurrent with fewer large objects, such as bubble clusters being counted. As the distributions are in such good agreement, the calculated mean values are also in excellent agreement.

2.3.1.2 Single Image Comparisons

To carry out this comparison, individual images were processed using both techniques. The image as seen in Eclipse was captured and objects counted by only one of the processes were identified. As a gold standard for comparison, the same images were visually analysed to select single bubbles. Again, a comparison was made; objects counted by Holesv8 that according to the gold standard should not have been counted are illustrated. Two comparisons are given, the first an image with an atypical (wide and irregular) size distribution (*Figures 2-5, 2-6*), and the second with a typical distribution (*Figure 2-7*). The images shown were taken from the image sets discussed in Section 2.3.1.1, and are considered to be representative of the overall set.

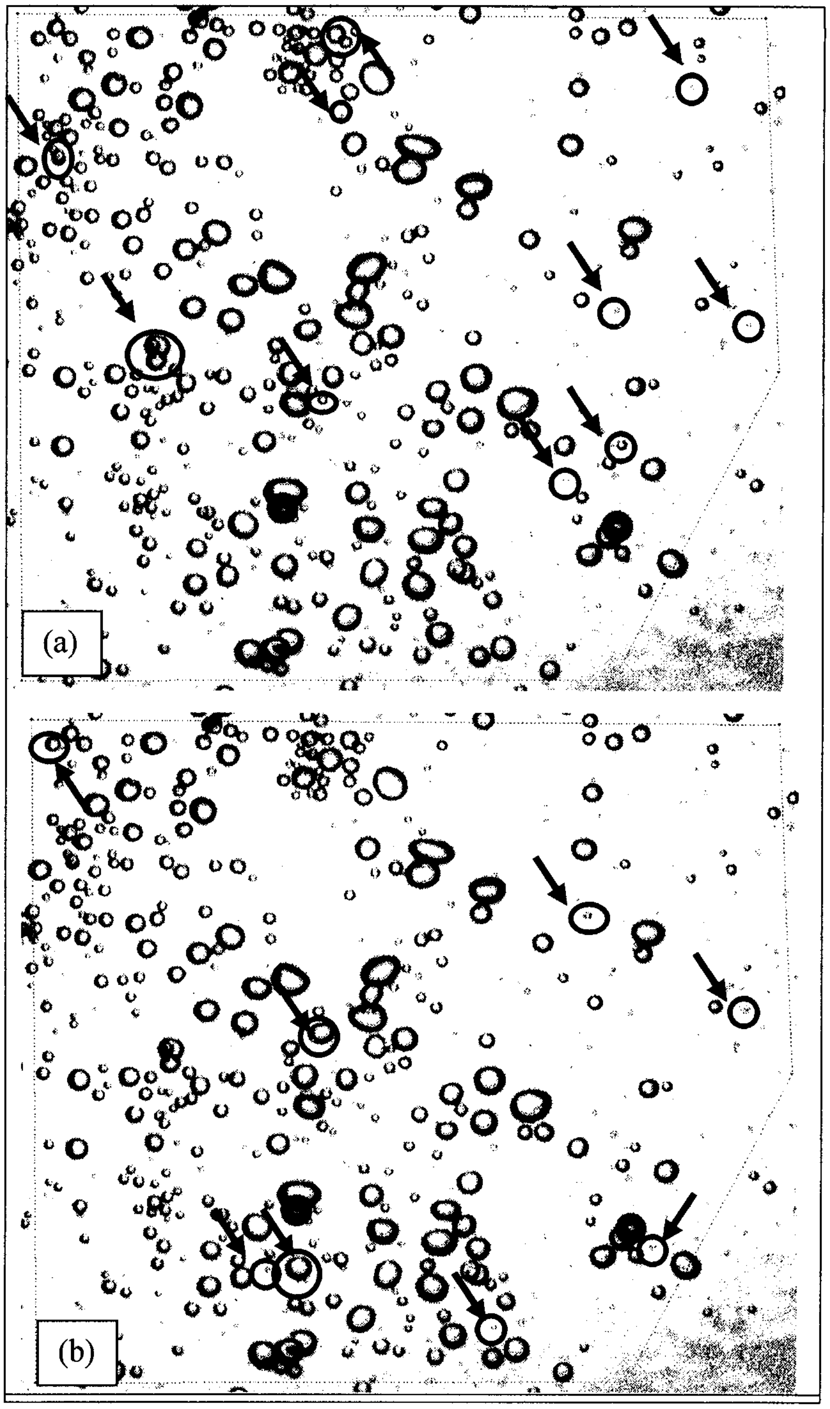

FIGURE 2-5: *IMAGE COMPARISON; (a) OBJECTS COUNTED USING STANDARD METHOD BUT NOT BY HOLESV8; (b) OBJECTS COUNTED BY HOLESV8 BUT NOT BY STANDARD METHOD*

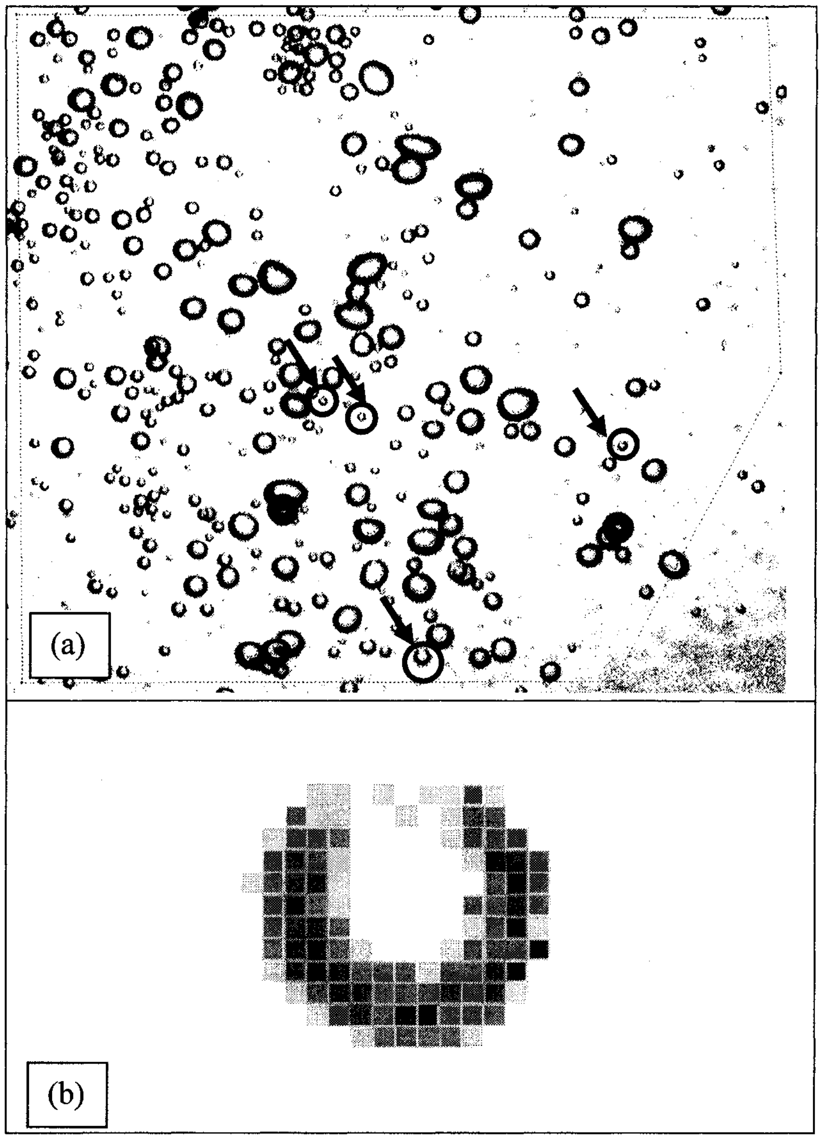

FIGURE 2-6: *IMAGE COMPARISON; (a) OBJECTS INCLUDED BY VISUAL ANALYSIS BUT NOT BY HOLESV8; (b) ONE OF THE OBJECTS COUNTED VISUALLY.*

In the first case (*Figure 2-5*), it is clear that neither method is ideal. While the standard method counts some bubble clusters and background objects not counted by Holesv8, some background objects are counted by Holesv8 and not by the standard method. However, the number of false objects is clearly reduced through use of the proposed alternative. It is also clear that some true objects, particularly irregularly shaped ones, are counted in the alternative method, which would otherwise be ignored under the standard method. When compared with the visual method (*Figure 2-6*), Holesv8 does not count some seemingly spherical objects. However, upon further magnification, a flaw in the visual technique is exposed. While the objects appear closed, a pixel-by-pixel examination shows that some of the objects are not in fact closed, leading to these objects being counted by the visual technique. While neither method is perfect, Holesv8 appears the better of the two options, and in some cases is superior to the visual method.

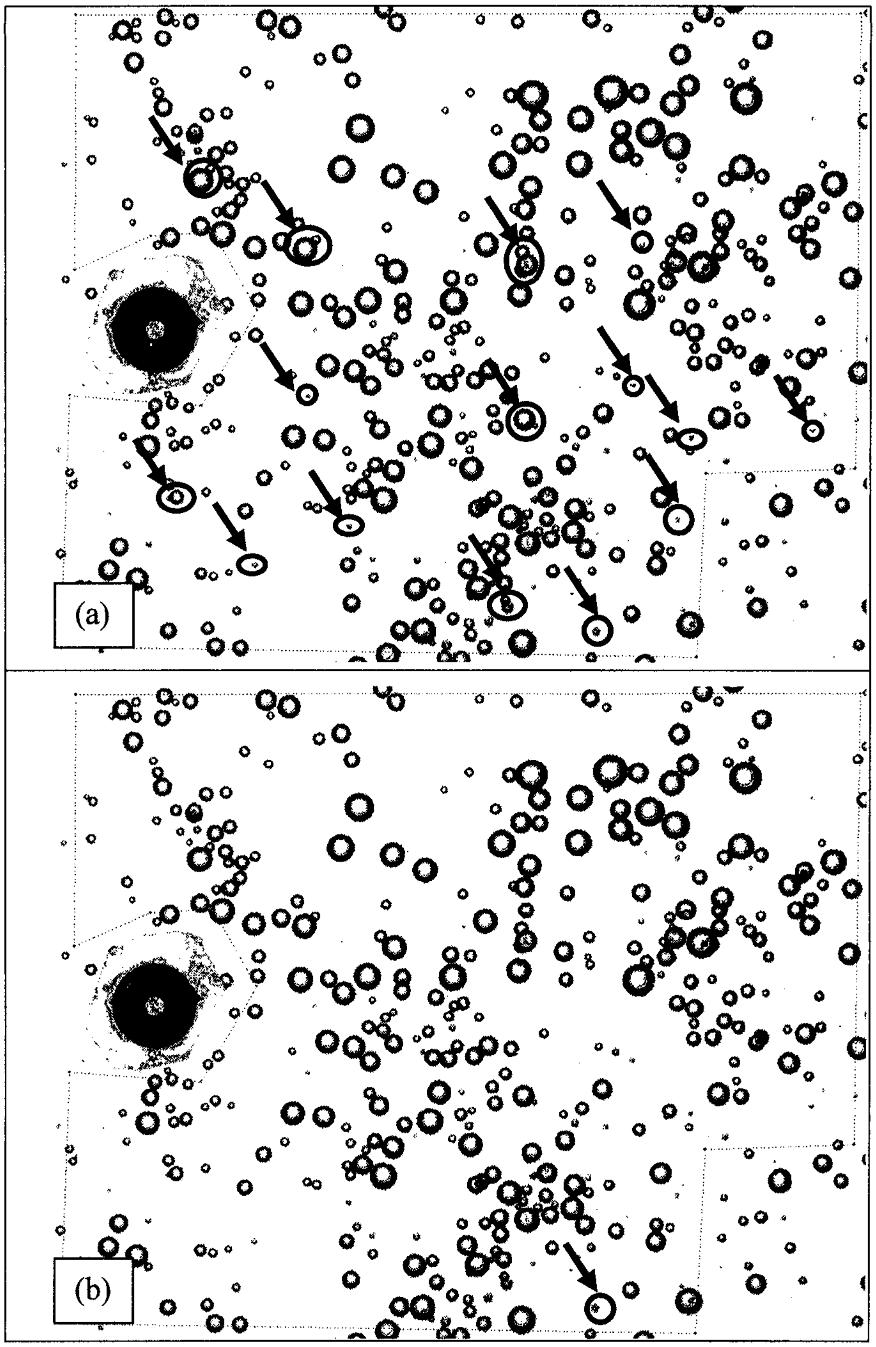

FIGURE 2-7: *IMAGE COMPARISON; (a) OBJECTS COUNTED USING STANDARD METHOD BUT NOT BY HOLESV8; (b) OBJECTS INCLUDED BY VISUAL ANALYSIS BUT NOT BY HOLESV8. IN THIS CASE, HOLESV8 DID NOT COUNT ANY OBJECTS NOT COUNTED BY THE STANDARD METHOD.*

In the second case (*Figure 2-7*), an image of spherical bubbles produced by a mechanical cell, there is a clear improvement when Holesv8 is applied as opposed to the standard method. While Holesv8 did not count any additional objects, it did discount clusters of bubbles otherwise counted as single bubbles by the standard method. In all, 195 objects were counted by the standard method, while seven of these were discounted by the alternative, or nearly 4%. In this case, only one object visually selected was not counted by Holesv8.

Generally, it was observed that while some false objects are counted using the proposed technique, they are far fewer in number than those counted under the current method. While overall difference to the numerical averages and extreme values is not large in many cases, it becomes clear that the proposed method achieves greater data confidence, as fewer undesirable objects are analysed. With regularly shaped bubbles, the benefits of using Holesv8 can be inconsequential for the output distribution; however, its impact on the output increases as the bubbles become more irregularly shaped and wider in distribution.

2.3.2 Limitations and Future Considerations for Alternative

The proposed method, though believed to be an improvement over the standard method, is not without limitations.

Firstly, there is one of time. For a data set initially containing approximately 50 000 objects, the programme on an average computer may take in the order of 25 minutes to run, the time increasing as bubbles become more irregular, due to the increased number of false objects removed during scanning. However, smaller total bubble numbers are usually adequate to obtain a representative distribution, i.e., there is a trade-off. Additionally, as computers used for image analysis typically have large RAM, CPU and BUS capacity, it could be expected that this programme could run significantly faster on an image processing computer.

Limitations also exist during the process of aligning the image objects from the two data sets. In some cases, where the extra object contains a hole, the programme is unable to detect the presence of a false object. As code to scan for alignment is already present (for cases where the number of holes match, while the diameters do not), alteration of the programme to also scan each row in which neither the number of holes nor diameters are equal would not be difficult. However, it is possible that the resulting additional runtime would out-weigh the benefits. Simple deletion of the problem image and restart of the programme is at present the simplest solution.

Under the current version of Eclipse and 'Bubbles' available, a hole is considered to be one or more white pixels surrounded by black pixels. However, particularly for large bubbles, there is a gradient from light to dark grey both on the perimeter of the bubble, and between the outline and bright spot inside each bubble. Therefore it is not uncommon to have small holes present in the black outline. Holesv8 is unable to account for bubbles of low shape factor with small holes present. Several solutions to this problem may be investigated. These include altering the Eclipse code such that only holes consisting of greater than a defined number of pixels are counted, while still filling all blank pixels for the 'Fill Holes' option. Alternatively, another method distinguishing between bubbles and clusters could be developed. If this problem could be avoided, then the shape factor filter in Holesv8 could be removed, allowing for more true bubbles to be counted, and removing all dependence on the shape factor criterion as a filtering technique.

The final filtering stage, based on an area ratio, also causes a small number of true bubbles to be discounted, while counting a small number of undesirable bubbles. This could be avoided by further refining the final filter stage of Holesv8. Given the current 'Bubbles' output, it is not thought that a better filter criterion is present in the Eclipse output data.

The method is currently limited to two-phase applications. Bubbles in three-phase images do not generally have a bright spot, or hole, due to solid coating. Future considerations include an alternative filter, which would allow for objects containing no holes to be counted, while still excluding false objects such as areas of dark background.

Finally, as can be seen in the sample images (*Figures 2-5, 2-6 and 2-7*), in almost any given image, there will be bubbles that touch and are therefore discounted. As a result, these bubbles are not taken into account in the final distribution. This affects large bubbles, which tend to have small bubbles touching their downstream side due to wake effects, as well as small bubbles which tend to be numerous, thus increasing the probability of their touching. It is not uncommon, in images of only small bubbles to observe networks, none of which contribute to the overall output distribution, yet account for a significant proportion of the bubble population. By taking large bubble populations, biasing is reduced, but practical considerations must be taken into account: if an average image in a set contained few bubbles, in order to count even 20 000 bubbles well over 500 images may be required, thus unduly increasing processing time. An alternative may be to investigate a cluster separation process.

Separation processes, commonly used in particle size analysis software, can operate in a variety of ways, thus careful examination of the technique must be made before it can be applied to this situation. One key difference between particle and bubble separation is simply that particles are solid and contact over only small areas, while bubbles being fluid deform and attach over large areas.

One separation process removes layers of pixels from the perimeter of the object until the objects separate. In the case of bubbles the final size may be significantly smaller than it is in reality. A bubble with a large overlap (e.g., a small bubble partially covered by a larger bubble) may have its entire perimeter removed before separating. Even using programmes that restore the removed pixels before processing, bubbles with significant overlap could still be discounted.

Eclipse offers a separation process. This is based on drawing lines between holes, and artificially separating the objects, yielding bubbles with some flat sides. The first pitfall of this method is simply that flat-sided bubbles are clearly not representative of reality (although may be more realistic than either failing to consider them, or removing layers of pixels until they separate). Additionally, a shape factor based filter cannot be used, as flat-sided bubbles would likely be discounted. A second problem is that even one white pixel surrounded by black pixels is considered as a hole. This implies that one small hole would be counted as a separate object. This has not been tested as an in depth description of the methodology of the process is not available. Finally, a method of tracing the programme such that an object number comparison could be made has not been found. Though some promise is seen in the Eclipse process, confirmation of the separation procedure and examination of the manner in which it handles special cases has not yet been made.

2.4 CONCLUSIONS

An alternative method, in the form of an MS Visual Basic programme, Holesv8, has been proposed as a replacement for the current standard analysis method employed in Eclipse using the 'Bubbles' application.

Holesv8 relies less on the shape factor criterion for distinguishing between single bubbles and undesirable objects. This is viewed as an improvement over the current standard technique, as shape factor is more sensitive to variations in small objects as opposed to larger ones. In addition, some clusters of bubbles still have relatively high shape factors, and under the current method are interpreted as single bubbles, thus skewing the output distribution. In cases where large bubbles are present as single bubbles, but have relatively low shape factors, Holesv8 accepts these bubbles that would otherwise be discounted under the standard method. Generally, less skewing of the bubble size distribution is anticipated by reducing the dependence on shape factor as a filtering criterion.

A comparison between the standard method and Holesv8 was conducted, both numerically by comparing mean values and distributions, and qualitatively through comparison of images. It is concluded that Holesv8 has little effect on mean values and distributions for regular bubble populations; however, clusters are discounted giving greater data integrity. The impact of Holesv8 on irregular populations is much more significant, as an increased number of true, single bubbles are counted, while clusters are discounted. The overall effect is a decrease in calculated averages, and a smoothing of the numerical distribution.

Holesv8 is proposed as an improvement on the standard analysis method, as it limits the dependence on a single filtering criterion and instead distinguishes between undesirable objects and single bubbles through tests involving the characteristics of each object. In the case of irregular bubble populations, a notable improvement in distribution representation was realised.

CHAPTER 3 – DIAMETER FILTER MANIPULATION TO ESTIMATE TRUE BUBBLE SIZE DISTRIBUTION

3.1 INTRODUCTION

During three-phase operation of the bubble viewer, solids are carried into the viewing chamber by two mechanisms, attachment and entrainment. Attached solids are released when bubbles reach the air/water interface at the top of the viewing chamber and burst, beginning to cloud the chamber. Entrainment in the bubble wake is generally less of a problem, these particles being eliminated while moving up the tube against a net downward flow. Generally, the only compensation needed to account for solids is a varying threshold, reflecting the gradual darkening of images. The accumulation of solids will limit the time for image collection.

One three-phase application encountered provided a particular problem, namely pulp and paper de-inking by flotation, where the paper fibres entered the sampling chamber, apparently by entrainment. The solids (paper fibres) were significantly larger than typical mineral particles and did not cloud the system as before, rather the light intensity within the viewing chamber remained good even over runs exceeding four minutes. Paper fragments appeared in images as grey objects, in the order of 0.3 mm in diameter (within one order of magnitude of the bubble diameter). As a result, using the standard processing procedure, a bimodal distribution was obtained, with the finer peak being attributed to paper fragments. To process, the diameter filter was exploited to reveal an estimate of the true distribution. A comparison of the bubble size distribution along two banks of flotation de-inking Voith cells is then presented.

3.2 EXPERIMENTAL WORK

On February 5 and 6, 2003 measurement of air dispersion properties along two banks of the de-inking flotation circuit at the Gatineau Mill of Bowater Incorporated was carried out. The applicable section of the flow sheet, along with the local nomenclature, is outlined in *Figure 3-1*. The two banks of seven Voith cells run in parallel, with the first five cells of each bank as primary cells. The accepts are removed after the fifth cell, while the rejects continue on to the last two cells which function as secondary cells. The accepts of the seventh cell are removed, while the rejects are recycled to the first cell. Five of the seven cells (C2, C4, C5, C6 and C7) were sampled on each bank, with parallel cells being measured consecutively. The two remaining primary cells were inaccessible. The self-aerating Voith Sulzer EcoCell, as employed at Gatineau Mill is shown in *Figure 3*-2 (Finch and Hardie, 1999).

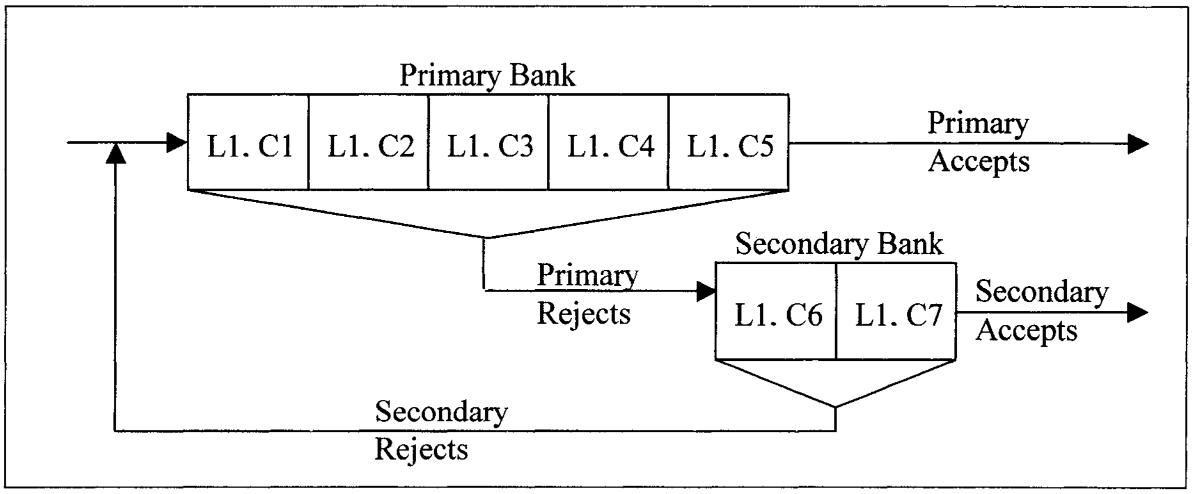

FIGURE 3-1: *BASIC FLOW SHEET AND NUMBERING SYSTEM. LINE 2 IS IDENTICAL AND RUNS IN PARALLEL.*

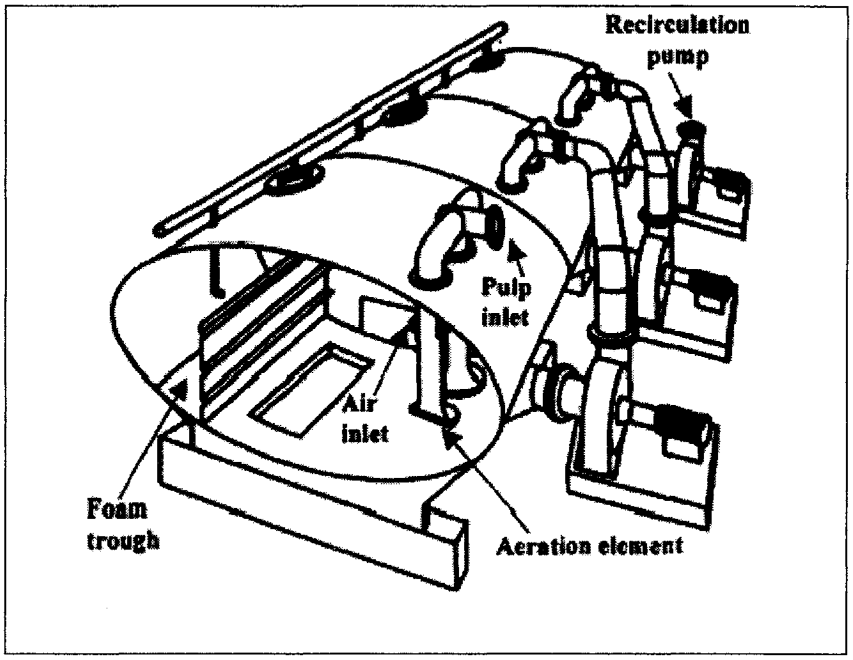

FIGURE 3-2: *SCHEMATIC OF VOITH SULZER ECOCELL*

The oval cross-section of the Voith cells required the bubble viewer to be tilted sideways at an angle of approximately 10° (the incline of the viewing chamber window remained 15°). Since bubbles no longer moved up the centre of the viewing window, the position of the camera was adjusted, and angled such that bubbles moved vertically through the captured images.

By nature of the de-inking process, the pulp temperature is elevated (approximately 60°C), so the assembly was filled with clear tap water of similar temperature.

The bubble viewer was configured with a telescopic sampling tube, with nominal diameter 0.5 in. (1.27 cm). The sampling depth was 60 cm below the froth surface.

3.3 ANALYSIS OF BUBBLE/FIBRE SYSTEM

The images obtained posed a challenge not previously encountered using the bubble viewer in mineral processing plants. Due to the low specific gravity of paper fibres, fragments are prone to entrainment in the wake of the rising bubbles and became evident in the viewing chamber. In other applications, the downward water flow essentially eliminated entrained particles. A sample image is provided in *Figure 3-3*. Ideally, the fibres would be excluded during the image processing, however this was not possible, as fibres were found to have similar greyscale and shape factor values as bubbles. Noting the difference in diameter that generally existed between fibres and bubbles, a minimum diameter criterion was explored to discriminate between the two objects.

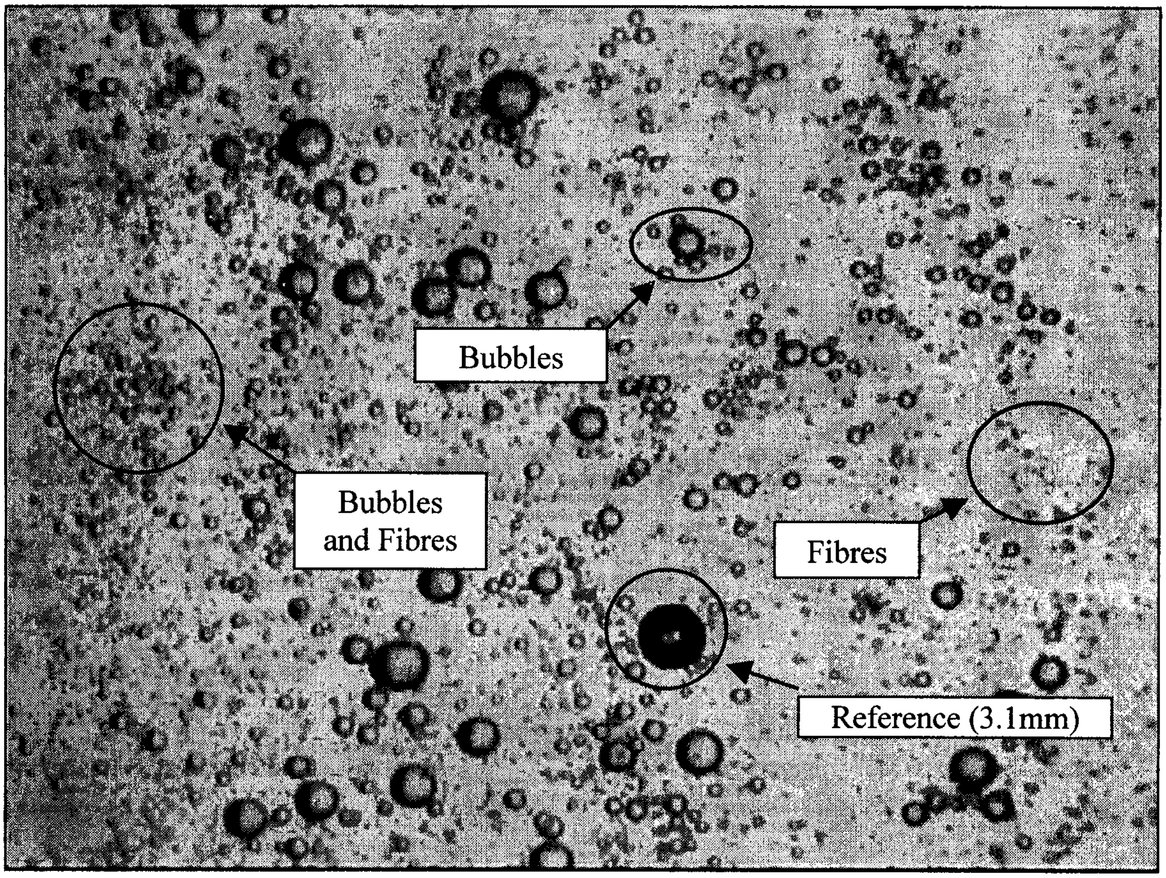

FIGURE 3-3: *SAMPLE IMAGE (LINE 2, CELL 5).*

In order to establish the appropriate minimum diameter, each image was processed initially with a minimum diameter of 0.2 mm, smaller than any bubbles evident in the images. Next, using MS Excel functions, the minimum diameter accepted in the data set was increased in increments of 0.1 mm to a maximum of 0.7 mm. The resulting frequency plot, as in *Figure 3-4*, shows the change in the 'bubble size' distribution as fewer fibres are counted (i.e., with increasing minimum diameter criterion).

An estimate of the true bubble size distribution was that associated with the lowest minimum diameter (D_{min}) value to yield a single peak, log-normal distribution typical of most bubble populations encountered to date. In the sample case (*Figure 3-4*), this corresponds to a D_{min} of 0.6 mm. Each data set was analysed and the appropriate D_{min} selected in the same manner.

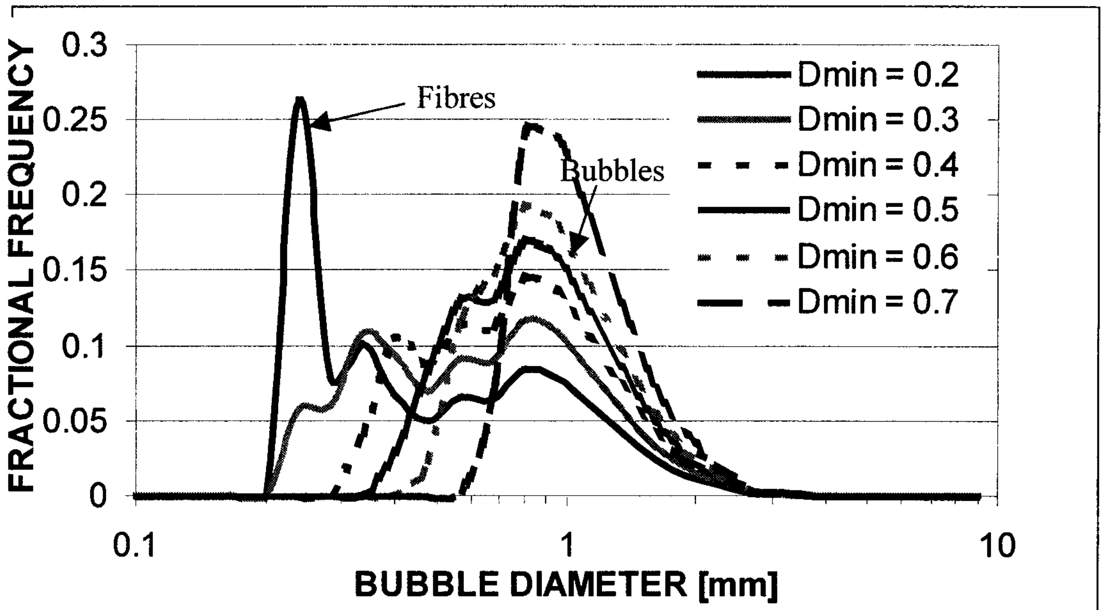

FIGURE 3-4: *EFFECT OF INCREASING MINIMUM DIAMETER ON BUBBLE SIZE DISTRIBUTION (LINE2, CELL5).*

It is likely in this exercise that some of the smallest bubbles are not counted, while some of the larger fibre fragments report as bubbles. However, in the absence of any other practical separation technique and since this one yields 'typical' distributions without distortion, the results are considered representative of the actual bubble population present.

Figure 3-4 suggests that by increasing the minimum diameter, the distribution becomes progressively coarser. This is a numerical artefact. As the minimum diameter is increased, fewer small objects are counted, while the same number of larger objects is counted. As a result, fractionally, the larger objects constitute a progressively larger portion of the overall bubble population.

3.4 COMPARISON OF BANKS BY BUBBLE SIZE

The mean bubble diameter results are summarized in *Table 3-1* with nomenclature as in *Figure 3-1*. *Table 3-1* illustrates that while the two banks operate in parallel on the same (split) feed, significant variation in bubble size cell to cell and between the lines occurs. *Figure 3-5* shows the Sauter mean diameter along each bank (Cell 2 to 4 is an interpolation). Though the mean values differ between the lines, both follow a similar profile. Generally, Line 1 had larger bubble sizes at the front of the line compared to Line 2.

TABLE 3-1: *SUMMARY OF NUMBER (D_{10}) AND SAUTER (D_{32}) MEAN BUBBLE DIAMETERS.*

Cell (Line, Cell)	D_{10} [mm]	D_{32} [mm]
L1, C2	1.11	1.45
L2, C2	0.99	1.28
L1, C4	1.29	1.78
L2, C4	1.10	1.51
L1, C5	0.98	1.26
L2, C5	0.85	1.20
L1, C6	0.79	1.24
L2, C6	1.17	1.50
L1, C7	0.81	0.93
L2, C7	0.85	0.95

To check if this result is affected by the choice of D_{min}, *Figure 3-6* shows that the same trend is obtained using fixed D_{min} values of either 0.5 or 0.7 mm respectively; i.e., the choice is not critical.

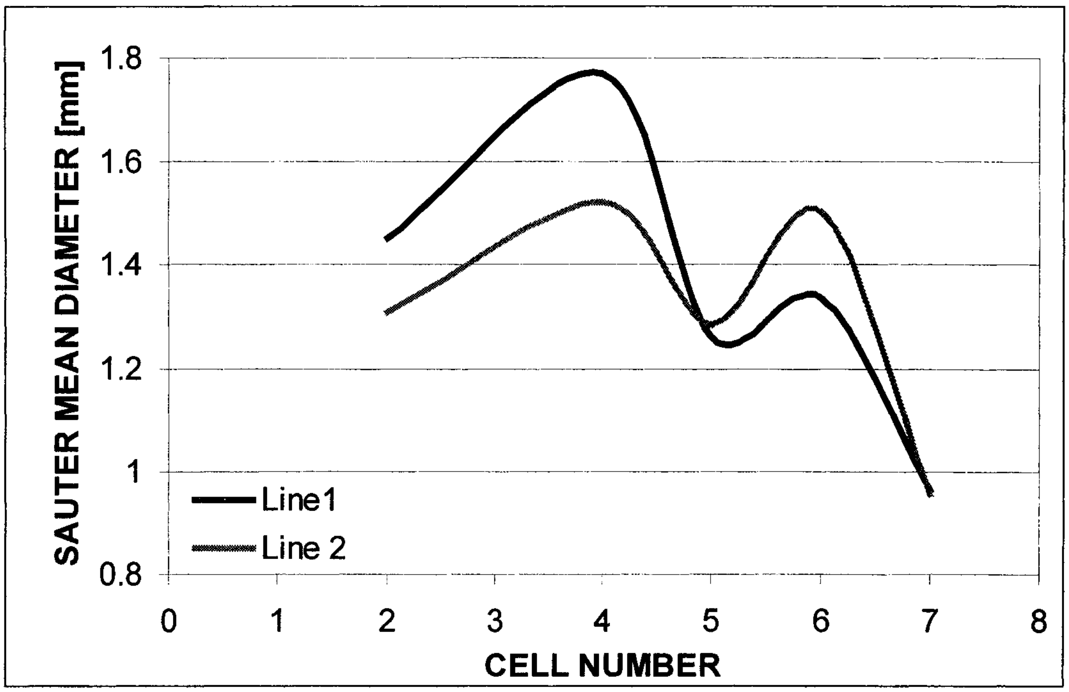

FIGURE 3-5: *COMPARISON OF SAUTER MEAN BUBBLE SIZE ALONG THE TWO PARALLEL BANKS.*

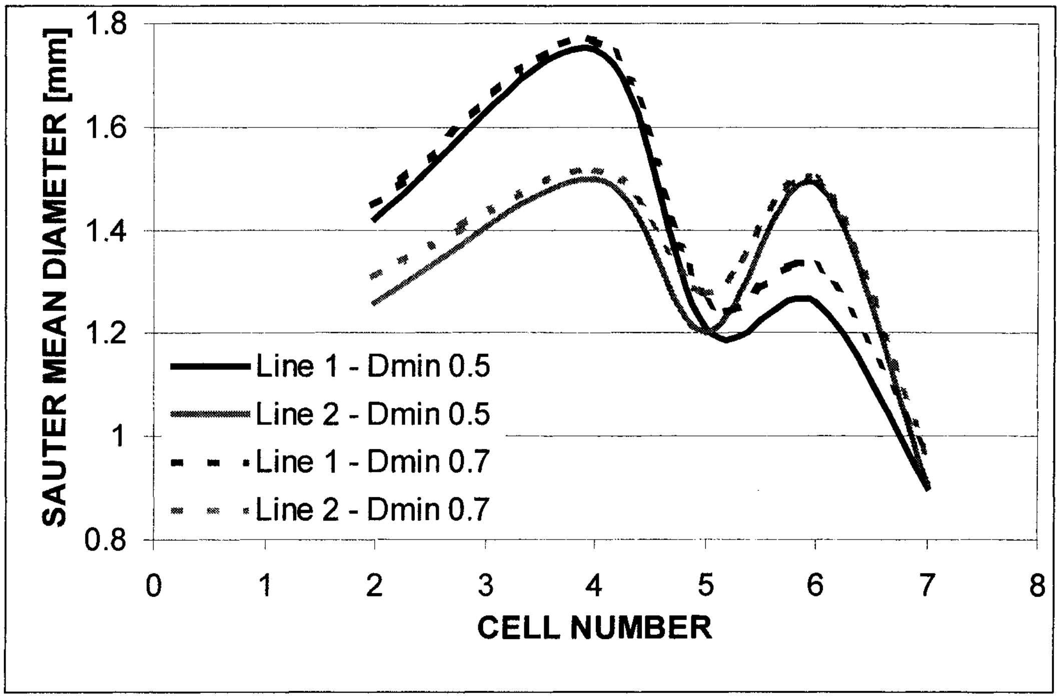

FIGURE 3-6: *COMPARISON OF SAUTER MEAN BUBBLE SIZE ALONG LINE 1 FOR MINIMUM DIAMETERS 0.5 AND 0.7 mm.*

3.5 DISCUSSION

While there are differences in mean bubble size, the characteristics of the size distributions remain consistent. This is illustrated when the number and Sauter mean diameters are plotted against each other (*Figure 3-7*); points that lie along a common trend line are indicative of similarly shaped distributions, as is the case here. While points lying together are generally not from parallel cells, this grouping shows that, all else being equal, cells producing similar bubble sizes also produce similar distribution shapes. No significant deviation from this trend was noted. This implies that the differences observed between cells and between lines are not related to the method of bubble generation (i.e., the differences are not related to uneven wear or other equipment issues present in one line). If this interpretation is correct, and the bubble sizing issue is fairly resolved, we have a tool to probe the origin of the differences. Anecdotally, the lines are considered to behave differently; perhaps bubble size is the origin.

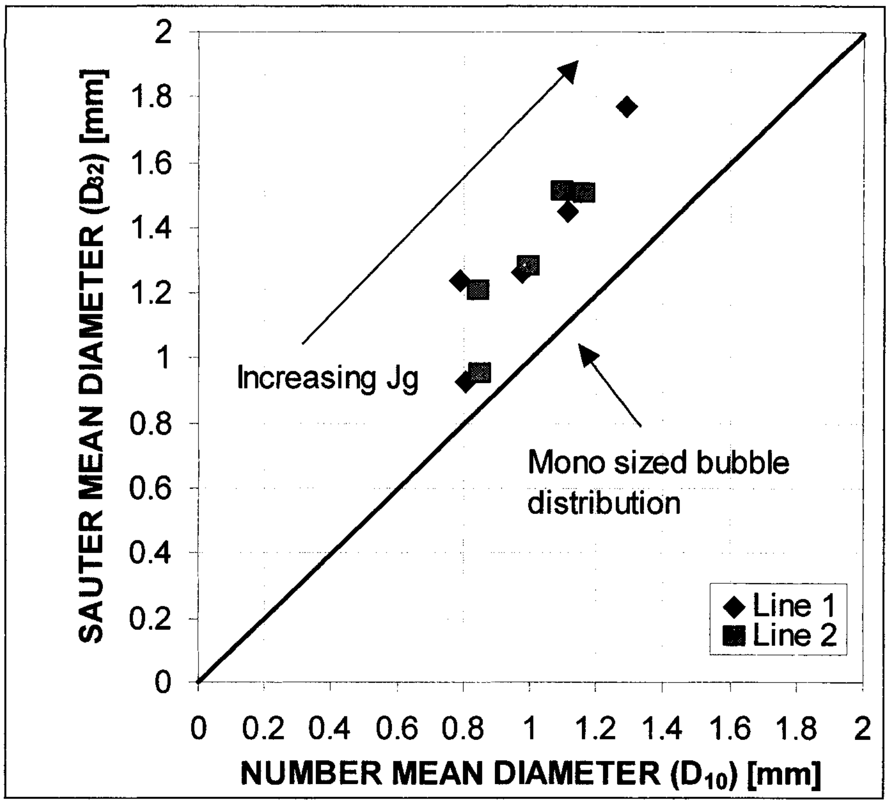

FIGURE 3-7: *SAUTER MEAN DIAMETER VERSUS NUMBER MEAN DIAMETER.*

While selecting a single D_{min} for comparison yielded similar trends with only slight deviation in values, selecting a D_{min} for each data set (i.e., a variable minimum diameter) is considered a more robust method of comparison. If significant variation was noted in the size or proportion of fibres and bubbles, selection of a fixed D_{min} could lead to misrepresentation, either by discounting an increased proportion of bubbles (as would be in the case where bubbles were particularly fine), or including an increased proportion of fibres (as would be the case if the fibres were coarse). The extreme would be setting D_{min} to zero, in which case all bubbles and fibres would be counted, and the mean values would vary with the concentration of fibres in each image. This skewing of the distribution, and hence the mean values could lead to unfair comparisons.

3.6 CONCLUSIONS

The McGill bubble viewer was successfully employed on two banks of Voith cells at Bowater's Gatineau de-inking plant. A processing technique to compensate for the presence of fibre fragments in the viewing chamber was developed, producing distributions considered representative of the true bubble population.

Comparison of the banks revealed similar shaped bubble size distributions in each cell, with one line producing larger bubbles than the other line towards the front with the trend reversing towards the rear.

CHAPTER 4 - DIAMETER ASSIGNMENT PROTOCOL

4.1 INTRODUCTION

The final hurdle for bubble sizing using any visual technique is the representation of bubbles by a single diameter. Beyond ~3 mm, bubbles cease to be spherical, introducing the need for equivalent diameters which attempt to represent a non-spherical object by a single number. These equivalent diameters may be formed using selected metrics from image analysis. As a complication, image analysis techniques present only two dimensions such that the bubble shape in the third dimension must be assumed.

Beyond spherical, bubbles assume a variety of shapes, the simplest being the ellipsoid. However, as these large bubbles move, their shape constantly changes due to pressure fluctuations. *Figure 4-1* illustrates this, presenting subsequent frames for a bubble ~5 mm in diameter as it moves up the viewing window. Depending on the frame selected, different equivalent diameter values would be assigned, implying changing bubble volume, which is clearly not the case. As image selection is a random process, the selected diameter should represent a statistical compromise. Naturally some bubbles will be underestimated, while others are overestimated. Ideally, this variation in size estimation will average out over a large number of bubbles, resulting in a representative distribution. As typical samples are in excess of 10 000 bubbles, and often in excess of 50 000, this compensation likely occurs.

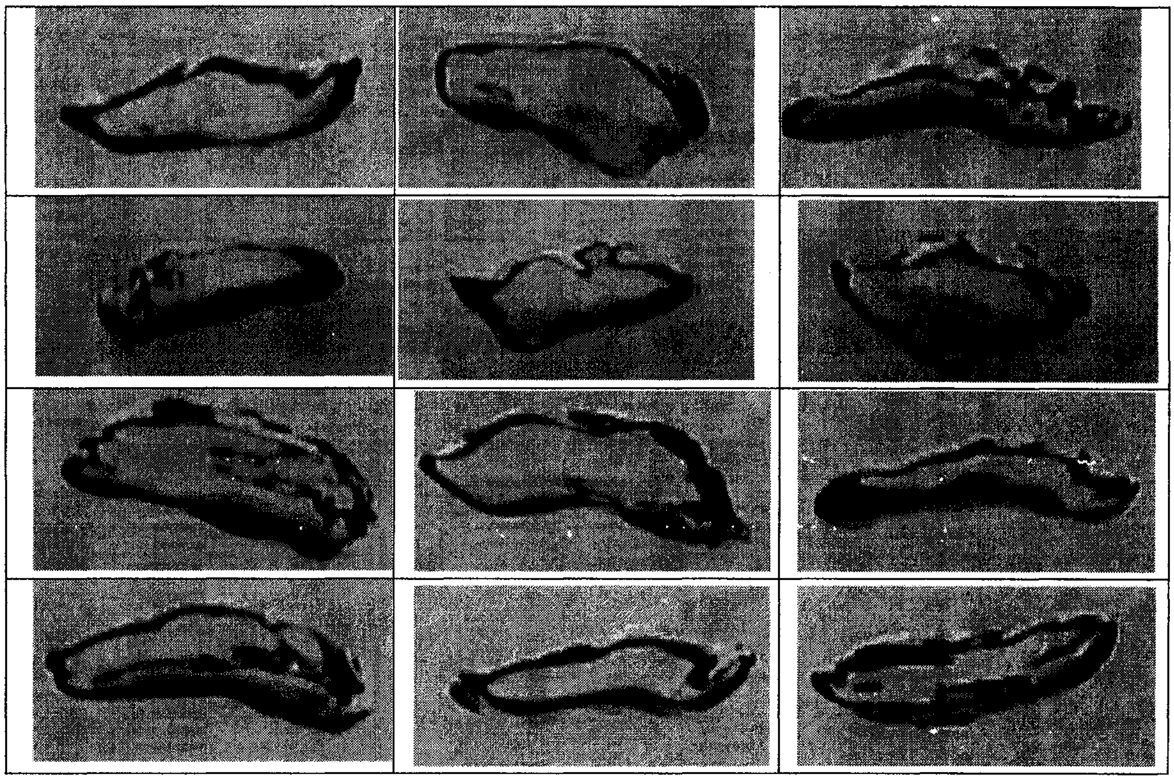

FIGURE 4-1: *FRAME-BY-FRAME IMAGES OF ~5mm BUBBLE SHOWING SHAPE VARIATION.*

4.1.1 Available Equivalent Diameters

Along with metrics such as area, maximum and minimum radii, three diameters are output by Empix Northern Eclipse v6.0. The calculation of each is outlined with a schematic.

Diameter is the simplest output, and the only one to be directly measured. Diameter represents the longest chord across an object through its centre of mass. For a perfect circle, Diameter represents the true diameter of the object. As objects become progressively less spherical, Diameter becomes less representative of the true bubble size.

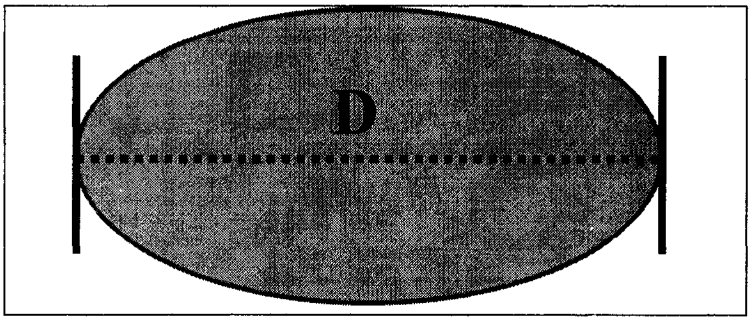

FIGURE 4-2: *SCHEMATIC REPRESENTATION OF DIAMETER.*

Equivalent Circle Diameter (ECD) is the diameter of a circle having the same area as the object. Eclipse counts the total number of pixels in the objects, assigning the equivalent area, and then calculates the diameter of a circle with this area. For relatively spherical bubbles, this is considered the most accurate diameter, and is blanket assigned to most data sets consisting predominantly of bubbles less than 3 mm.

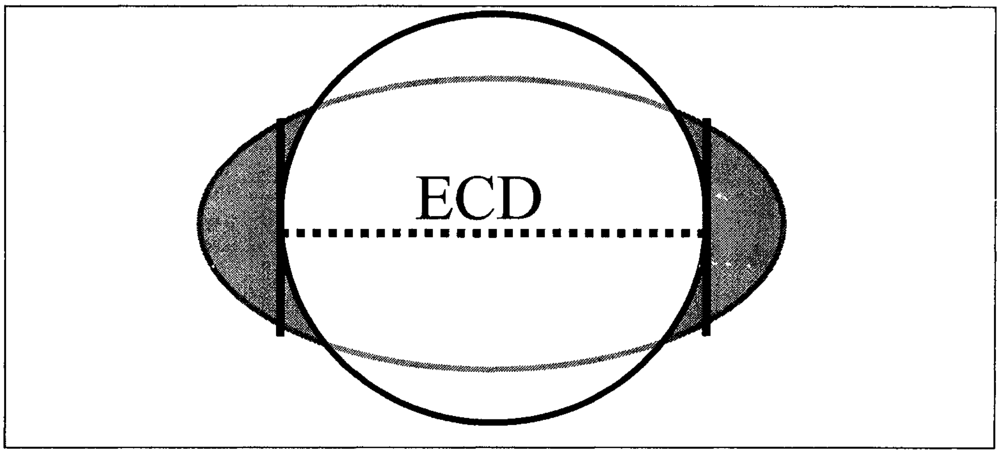

FIGURE 4-3: *SCHEMATIC REPRESENTATION OF EQUIVALENT CIRCLE DIAMETER (ECD).*

Equivalent Volume Diameter (EVD) is considered the most applicable to non-spherical bubbles. The maximum (a) and minimum (b) radii from the centre of mass are taken and an ellipsoid constructed, assuming symmetry about the minor (b) axis. The diameter of a sphere having the same volume as the ellipsoid is then calculated.

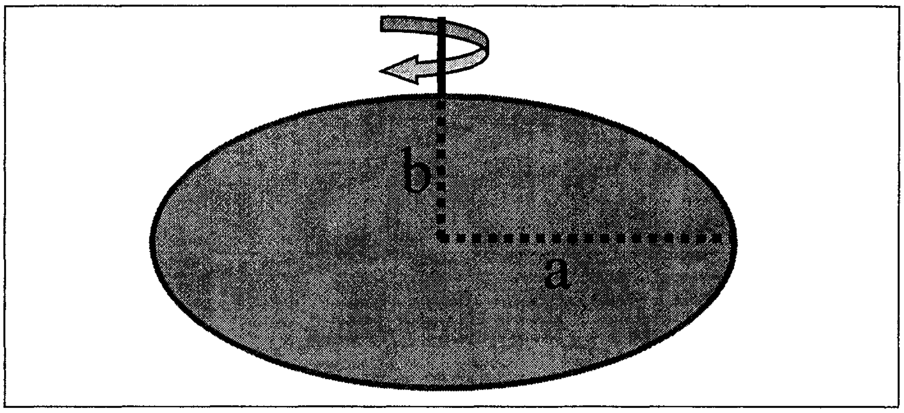

FIGURE 4-4: *SCHEMATIC REPRESENTATION OF EQUIVALENT VOLUME DIAMETER (EVD).*

Other equivalent diameters may be calculated based on other metrics, however these have not been used, as bubble dimension assignment throughout the literature is largely restricted to one of these three diameters.

The current method entails the selection of a single equivalent diameter (most commonly ECD) for the data set. Distributions may then be produced, typically against number or volume. To calculate a distribution by volume, the selected diameter is assumed to be the diameter of a sphere, thus assigning a bubble volume.

As wide size distributions contain a variety of bubble shapes, ranging from spherical to irregular, it was thought that a method of diameter assignment based on individual bubble characteristics would increase the accuracy of the overall process.

4.2 EXPERIMENTAL APPARATUS AND METHODS

In order to evaluate the accuracy of an assigned diameter, comparison to a standard must be made. In the case of bubble measurement the only absolute standard is bubble volume, being the only true indication of bubble size that may be directly measured. The volume predicted for a sphere based on the assigned diameter may thus be compared to the true volume and an indication of error obtained. Two size classes of bubbles, small (~3 mm) and large (>3 mm) were generated, and a diameter assignment protocol developed.

4.2.1 Small Single Bubble Generation and Measurement

Generation of single bubbles, ~3 mm in diameter, was achieved using pressure difference to drive a small volume of gas, producing bubbles from a capillary. The set up, outlined in *Figure 4-5*, comprises two tanks and a column housing the capillary for bubble generation. The upper tank is filled to a given level with water, which drives some water into the lower tank through a tube, thus compressing the air, which travels to the bubble-generating capillary. The difference in water level between the two tanks controls airflow to the column: The greater the difference the greater the bubble frequency. With each generated bubble, an equivalent volume of air is displaced from the lower tank, and replaced with an equal volume of water from the upper tank, thus reducing the height difference and the airflow. Experiments were, therefore, conducted over relatively short time periods to ensure that the head change was negligible. A typical experiment took 5 minutes giving a displacement of approximately 8 cm^3 of water, or 1 mm of water in a 4 in. (10.16 cm, nominal) column. This was considered acceptable as no appreciable variation in bubble size or frequency was noted.

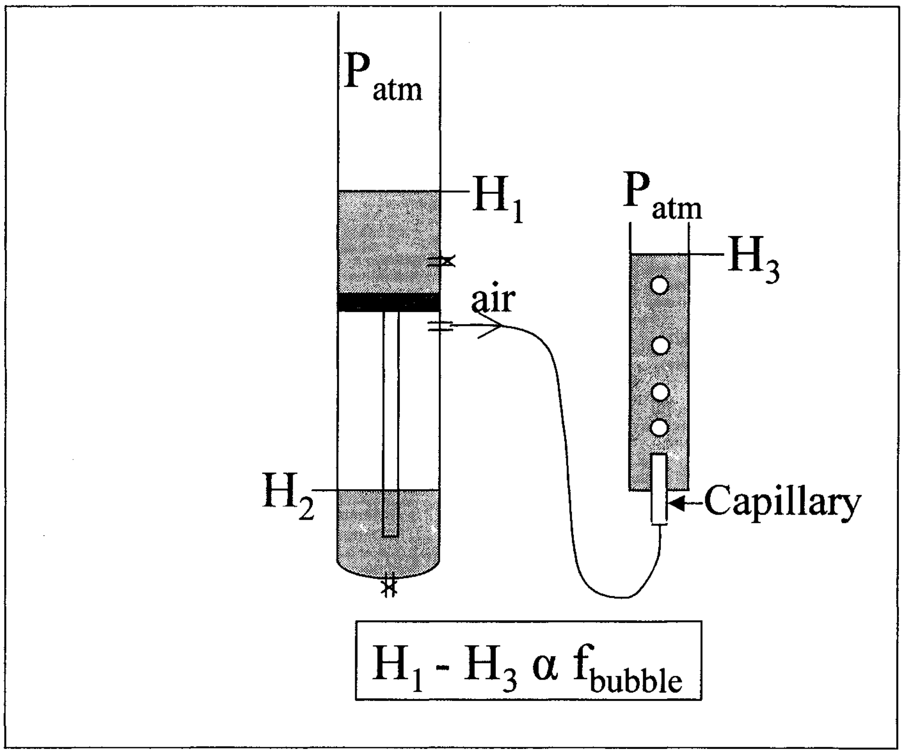

FIGURE 4-5: *EXPERIMENTAL SET UP FOR SINGLE BUBBLE GENERATION.*

Bubbles were generated through a 0.5 mm (nominal) glass or plastic capillary without frother, yielding reasonably spherical bubbles of approximately 3 mm.

To measure bubble volume, an inverted burette with a belled tip was used to capture the bubbles. The burette was filled with water and placed over the bubble stream. The number of bubbles required to displace 0.5 cm^3 was counted three times at the same height above the column. This number was recorded. The bubble viewer was then employed to image the same stream of bubbles for several minutes. To conclude, the burette volume measurement was again taken three times. If the average of the three runs varied by more than two bubbles from the first run, the experiment was discarded as bubble volume had significantly changed.

4.2.2 Large Bubble Generation and Measurement

Capillaries were again used, but for the selected orifice sizes, 2.5 and 3.5 mm, the pressure drop achieved with the two-tank set up proved inadequate. Instead, a flow meter was employed and air directly fed to the capillaries at a rate of 0.06 L/min, the lowest flow rate possible with a 0-5 L/min flow meter.

Single bubbles could not be produced, as fine control over the gas rate was not achievable. Instead, several bubbles (a 'cluster') of various sizes (typically non-spherical) were periodically produced from the capillary, making independent measurement by burette impossible. To measure the total volume of bubbles in this case, the bubble viewer was arranged so that bubbles from each cluster entered the sampling tube. The camera field of view was set such that all bubbles passed through it. At the same time the water level in the viewing chamber was measured. At the end of the trial, the sampling tube was sealed, all bubbles allowed to clear the viewing chamber, and the water level measured again to give the total volume of bubbles collected. During capture from the miniDV tape every bubble was imaged exactly once using manual capture coupled with slow motion video. It was established that every bubble was counted during processing, thus allowing a comparison of the true total volume with the calculated volume based on assigned diameters.

4.3 PROPOSED ASSIGNMENT METHOD

For the purpose of diameter assignment the sphericity of each bubble was assessed and an appropriate diameter assigned. Initially only the 'small bubbles' were used, as the volume error associated with each individual bubble could be calculated from the true bubble volume. The diameter (Diameter, ECD or EVD) giving a predicted volume closest to the true bubble volume was assigned, thus minimising error. It was noted that the error associated with ECD and EVD assignments were comparable, thus only Diameter and EVD were assigned for simplicity.

Several means of assessing a bubble's sphericity apart from the shape factor were devised. The favoured indication, being the most sensitive, was the area ratio. This ratio was given by dividing the output area by the area of a circle with the radius of the maximum radius as measured by Eclipse. Thus for a perfect circle, the ratio is unity and decreases with decreasing sphericity. In some cases, values greater than unity are also possible. As the area entails the square of the maximum radius, the variation as bubbles depart from sphericity is magnified.

$$AreaRatio = \frac{(Area)}{\pi(MaxRadius)^2} \qquad \textit{Equation 4-1}$$

Upon assessment of the 'large bubble' sets, it was noted that when the ECD was equal to or greater than the EVD, the object was generally circular, and error was minimised by assigning Diameter. When EVD was greater than ECD, the object was generally non-spherical, and assignment of EVD minimised error.

Figure 4-6 illustrates the observation that the difference between ECD and EVD is indicative of object sphericity, thus suporting the proposed assignment method. Two peaks are noted, showing that objects assigned Diameter generally have a high area ratio, i.e., are spherical, while bubbles assigned EVD have low area ratio, i.e., are non-spherical. The overlap of the distributions is attributed to including the small bubble (~3 mm) data for which assignment is less discriminatory. This assignment method is considered robust as it relies solely on output values relative to each other, as opposed to specific cut-off values that may vary between data sets.

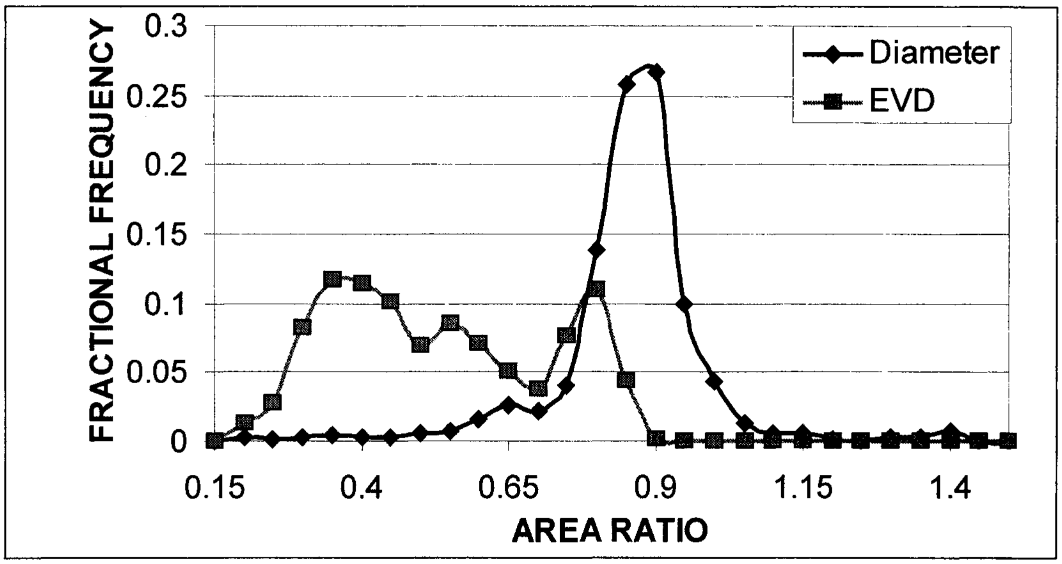

FIGURE 4-6: *DISTRIBUTION OF AREA RATIO FOR BUBBLES ASSIGNED DIAMETER OR EVD.*

4.4 RESULTS AND COMPARISON

The diameter assignment method (summarised below) was applied to both the small and large bubble sets, and the error relative to the total measured (i.e., true) volume assessed. Volume is considered a sensitive test, as it relies on the cube of the assigned diameter, magnifying the error.

IF ECD ≥ EVD assign Diameter

ELSE assign EVD

The error obtained by assigning only one diameter (Diameter, ECD or EVD) to every bubble regardless of its characteristics was compared to that of the proposed assignment method. A summary of the results is presented in *Tables 4-1* and *4-2*, for the small bubble and large bubble data sets, respectively.

TABLE 4-1: *SUMMARY OF DIAMETER ASSIGNMENT RESULTS FOR RELATIVELY SMALL AND SPHERICAL BUBBLES. (% ERROR IS TAKEN FROM THE TRUE VOLUME)*

Experiment		**% Error**
Set 1	*Current*	- 22.3 ± 0.3
	Proposed	+ **3.1** ± 0.4
Set 2	*Current*	- 19.9 ± 0.4
	Proposed	+ **2.4** ± 0.5
Set 3	*Current*	- 26.8 ± 0.3
	Proposed	- **4.8** ± 0.4
Set 4	*Current*	- 24.8 ± 0.3
	Proposed	- **2.4** ± 0.4

It can be seen that the error associated with small, relatively spherical bubbles is reduced. Generally the reduction was from the order of 20% volume under estimation with the assignment of strictly ECD as in the current technique, to less than 5% error by the proposed assignment method. The error is also now more random (showing both positive and negative values), compared to the current method which always yields an underestimation of the true volume.

TABLE 4-2: *SUMMARY OF DIAMETER ASSIGNMENT RESULTS FOR WIDE BUBBLE SIZE DISTRIBUTIONS. (% ERROR IS TAKEN FROM THE TRUE VOLUME)*

Experiment		**% Error**
Set 1 (3.5mm capillary)	*Current*	- 40.8 ± 0.3
	Only EVD	- 14.3 ± 0.4
	Proposed	**- 0.1** ± 0.5
Set 2 (2.5mm capillary)	*Current*	- 32.3 ± 0.3
	Only EVD	- 1.2 ± 0.5
	Proposed	**+ 2.6** ± 0.5
Set 3 (2.5 mm capillary)	*Current*	- 27.8 ± 0.4
	Only EVD	+ 4.5 ± 0.5
	Proposed	**+ 4.9** ± 0.5

In the case of the large bubble sets, the results show more scatter in the error, particularly the error associated with assigning only EVD. This scatter reflects the irregular nature of the distributions produced. Set 1, showing high error associated with EVD includes significant numbers of small, spherical bubbles, which are better represented by Diameter. In contrast the two sets with low error associated with EVD contained predominantly irregular bubbles, which are considered best represented by EVD, which evidently is the case. The proposed method is a compromise, assigning diameters based on individual bubble characteristics, and gives consistently low error for all three sets.

4.5 CONCLUSIONS

A diameter assignment protocol based on individual bubble characteristics, easily automated using MS Excel functions, has been presented. To assess the effectiveness, the calculated volume of a spherical bubble having the assigned diameter was compared to the true volume. The volumetric comparison, involving the cube of the assigned diameter, provides a sensitive test. Generally, assignment of exclusively ECD or EVD led to underestimation, with the proposed assignment method markedly reducing this error and making it random.

The error associated with assigning only one diameter showed significant scatter for large bubble sets, reflecting the distribution of bubble shapes present. The diameter assignment method, allowing for a representative diameter to be selected based on bubble characteristics, reduced the error, indicating more accurate representation.

Generally, the proposed diameter assignment method, while adding seconds to processing time, yields improved bubble size results over the current technique, for both spherical and non-spherical bubbles.

CHAPTER 5 – IMPACT OF SAMPLE TUBE DIAMETER ON BUBBLE SIZE DISTRIBUTION

5.1 INTRODUCTION

As with the other McGill sensors for gas rate and gas holdup, the bubble viewer is based on bubbles entering a tube by natural buoyancy, in this case moving on into a viewing chamber where they are imaged. Since the bubble viewer is a closed system, a volume of water equal to the volume of air entering the tube must be displaced. This may be referred to in terms of a net superficial velocity, J_L [cm/s]. It should also be noted that while J_L is the downward water flow averaged over the tube area, local liquid velocities (U_L, [cm/s]) may be significantly higher. As a bubble moves up the tube, it displaces an equal volume of liquid, which has a higher local value than the average J_L.

This argument gives rise to sampling concerns; downward liquid velocities at the base of the tube may be great enough to prevent bubbles under a certain size from entering the tube, thus biasing the sample. Increasing the sample tube diameter is a logical response to combat this effect, as the high local U_L will affect a smaller portion of the tube cross-sectional area, leaving a greater fraction for bubbles to enter unimpeded. This logic is outlined in *Figure 5-1*. Extending the concept, the only instance in which U_L values could not prevent small bubbles from entering would be when the sampling tube diameter approached that of the vessel - clearly unrealistic. A compromise is, therefore, required to obtain a bubble sample with minimal bias while keeping the set up compact enough to be practical.

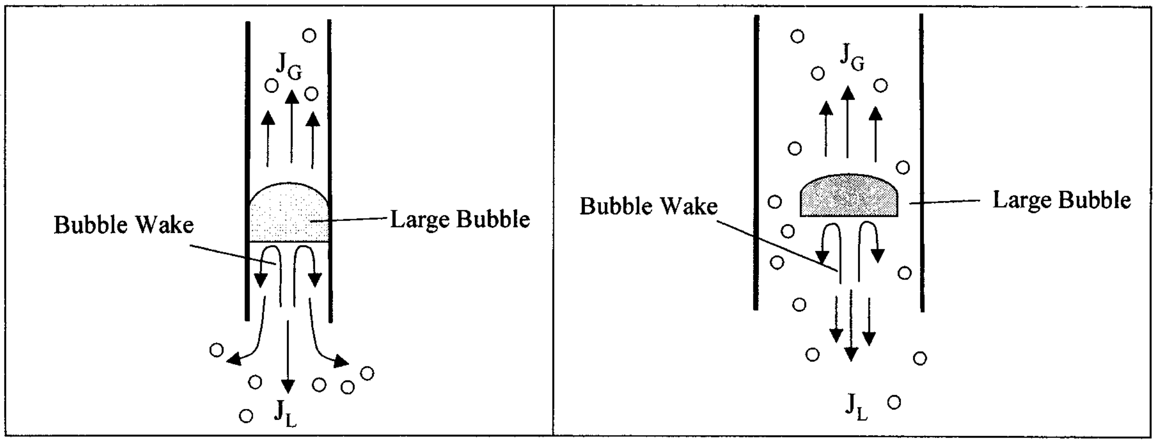

FIGURE 5-1: *SCHEMATIC OF THE EFFECT OF LOCAL J_L VALUES AT THE SAMPLE TUBE ENTRANCE.*

Under current operation, the bubble viewer is equipped with a sampling tube selected by the operator. Typically for laboratory applications, the distance between the bubble viewer and the desired sampling location is small (less than 1 m), so a single tube, generally of 1.0 in. (2.54 cm, nominal) inner diameter, is used. For industrial applications, greater distances are often encountered, occasionally greater than 2 m. For flexibility, a telescopic tube is employed, with a minimum nominal diameter of 0.5 in. (1.27 cm). The maximum sampling tube diameter possible with the current bubble viewer configuration is 1.0 in..

Practically, the minimum sample tube diameter drawing a representative bubble sample is the target. Increasing tube diameter increases the volume of air entering the viewing chamber, and thus the rate at which air accumulates and the water level drops, limiting the duration of the test. Additionally when solids are present, increased tube diameter increases the rate of solids accumulation in the viewing chamber, reducing the duration of adequate lighting for imaging. Evidently, a compromise is required.

5.2 EXPERIMENTAL WORK

Two sets of experiments were used to assess the potential effect of sample tube diameter on the output bubble size distribution, both conducted in two-phase systems.

As wide bubble size distributions are particularly prone to biasing (with large bubbles producing high local U_L values, which may exclude the smallest bubbles), the first set of experiments was carried out in a pilot scale column with 120 L/min gas rate and 20 ppm MIBC, using a jetting sparger (which gives wide distributions) equipped with a 2.5 mm nozzle. Two sample tube diameters were used, 0.5 in. (nominal) typically employed in industrial surveys, and 1.0 in. (nominal), the maximum diameter currently used in some laboratory studies. Both were 1 m in length. Sampling location (depth and radial position) was constant; the tests were taken sequentially with approximately 10 minutes elapsing from the commencement of sampling with one tube diameter to the conclusion of sampling with the second.

The second set of experiments was carried out in a 2 m, 4 in. (10.16 cm, nominal) diameter column filled with water and containing approximately 20 ppm MIBC. A 5 μm porous disk, with a gas flow rate of 3 L/min, was used to produce the bubbles. This set up gives a narrower bubble size distribution than the jetting spargers. With constant sampling depth and location, four trials were sequentially completed using 0.25, 0.5, 0.75 and 1.0 in. (0.64, 1.27, 1.91, 2.54 cm, nominal) sampling tubes. Total experimental time was approximately 30 minutes.

5.3 RESULTS

5.3.1 Jetting Sparger Trials – Wide Size Distribution

The distributions obtained from the jetting sparger (*Figure 5-2*) show two features related to biasing: The additional bubbles of 0.4 - 0.6 mm diameter detected with the 1.0 in. tube and the additional ca. 0.3 mm bubbles detected with the 0.5 in. tube.

Sampling a greater fraction of small bubbles with the 1.0 in. sampling tube was anticipated from the argument that these bubbles are preferentially rejected by the high local U_L values at the tube entrance. This interpretation is partially upheld, but is evident only for bubbles 0.4 - 0.6 mm. Apparently another mechanism is present, accounting for the additional 0.3 mm bubbles recorded by the 0.5 in. tube.

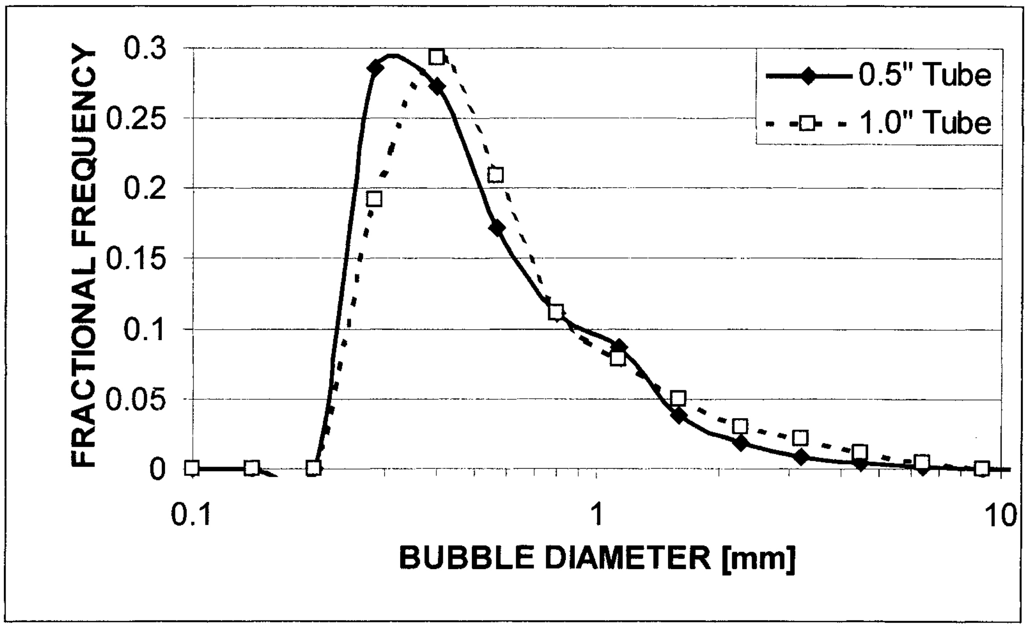

FIGURE 5-2: *COMPARISON OF DISTRIBUTIONS OBTAINED FROM A JETTING SPARGER WITH 0.5 in. AND 1.0 in. (NOMINAL) SAMPLING TUBES.*

Upon inspection of the bubbles entering the viewing chamber, an explanation was forthcoming. The largest bubbles were sufficient to cover the 0.5 in. tube cross-section, observed as slugs in the tube. When the digital video was reviewed, the large bubbles could be seen moving through the field of view, carrying small bubbles in their wake. After the large bubble had passed, these small bubbles continued to be observed, indicative of their slow rise velocity once released from the wake. As image capturing is a random sampling process with one image taken approximately each second, small bubbles are disproportionately imaged due to the increased time required to clear the field of view. This slug/wake effect is believed responsible for the unexpected additional fine bubbles sampled with the small tube.

5.3.2 Porous Sparger Trials – Narrow Size Distribution

Distributions obtained using the four sampling tube diameters are shown in *Figure 5-3*. In this case the number mean bubble diameter was approximately 2 mm. The distributions changed both in mean size and shape between the 0.25 in. and 0.5 in. sampling tubes, indicating a change in sample. Irregular bubble flow through the tube was noted with the 0.25 in. tube, demonstrating that diameter was too small to consistently sample bubbles, presumably with bubbles not only being excluded because of the impact of U_L on small bubbles, but also being excluded by virtue of being too large to enter. The distribution shape remained consistent for the 0.5, 0.75 and 1.0 in. tubes, but shifted to a progressively coarser mean size with increasing tube diameter. This progression indicates the inclusion of progressively larger bubbles, the proportion of which outweighs any additional small bubbles entering the tube because of the lesser impact of local U_L values.

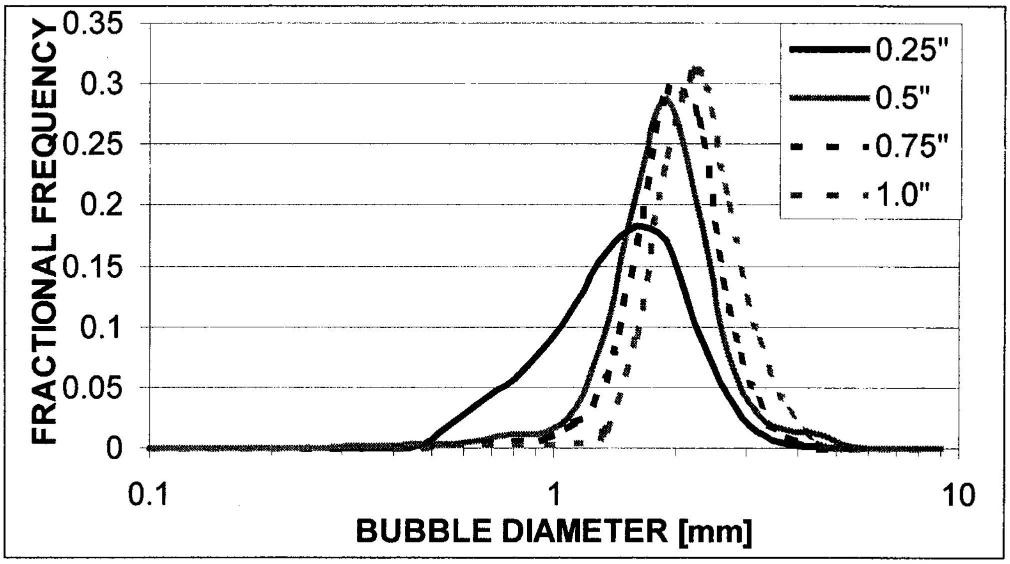

FIGURE 5-3: *COMPARISON OF DISTRIBUTIONS OBTAINED FROM A POROUS SPARGER WITH 0.25, 0.75, 0.5 AND 1.0 in. (NOMINAL) SAMPLING TUBES.*

5.4 DISCUSSION

Both sets of results support one key finding; sample tube diameter does affect the bubble size distribution obtained. Three issues are addressed, namely: Biasing in favour of small bubbles (sampling by entrainment in the wake of large bubbles), biasing against small bubbles (exclusion due to U_L), and biasing against large bubbles.

5.4.1 Biasing Towards Small Bubbles

The instance of biasing towards small bubbles has only been noted in cases where the larger bubbles move as slugs through the sampling tube. Under free fluid flow, bubbles (or particles) that are entrained do not necessarily remain entrained; instead there is a constant exchange of bubbles between the wake and bulk. However, when a bubble moves through the sampling tube as a slug, fluid flow is constrained, and fine bubbles remain trapped in the wake. Upon exiting the sampling tube into the viewing chamber, free fluid flow is re-established, thus some fine bubbles leave the wake, explaining the prolonged period of fine bubbles appearing in the field of view.

If increasing tube diameter is not an option, means of avoiding this situation are limited. If random image sampling is maintained, these fine bubbles will always be disproportionately counted, yielding a distribution biased towards the finest bubbles. A sampling tube sufficiently large such that no slugs occur should limit the effect, reducing the periodic arrival of large numbers of fine bubbles. This may be verified visually in two-phase systems, but in the presence of solids the sampling tube is often rendered opaque, or is difficult to see due to flotation cell geometry, making detection of slugs in the sampling tube difficult. In the viewing chamber, slugging in the tube may be detected by observing the out-flow of bubbles. If the flow is consistent, no slugs are present. However, if the flow is cyclic with the periodic introduction of one large bubble, or many moderately sized bubbles, followed by very fine bubbles, slugs are present in the tube and a larger diameter should be employed. It should be noted that if a telescopic tube were employed, this evidence for slugs in the tube and viewing chamber may be lost (slugs in the smallest tube at the bottom may be lost in the larger diameter tubes above).

5.4.2 Biasing Against Small Bubbles

Biasing against small bubbles is attributed to the downward displacement of water as bubbles enter the sampling tube. If the local downward velocity is greater than the rise velocity of a given bubble, that bubble will not enter the sampling tube. Since small bubbles have lower rise velocities, they are prone to exclusion.

This problem is most acute with wide distributions. The effect may be reduced by increasing sampling tube diameter and reducing the fraction of tube area affected. The maximum convenient sampling tube diameter should be selected.

5.4.3 Biasing Against Large Bubbles

As noted in discussing *Figure 5-3*, increasing sampling tube diameter can also increase the proportion of large bubbles entering the tube; that is, bubbles may be excluded from the sampling tube because they are too large to enter.

In principle, biasing against large bubbles can be limited by finding the tube diameter beyond which no further change in the distribution is present. In practise, the largest convenient tube size will have to suffice. The appropriate size of tube does not appear to have been reached in *Figure 5-3*.

5.5 CONCLUSIONS

The maximum possible sample tube diameter should be employed to limit biasing against both small and large bubbles, consistent with practicality. In the current configuration, a 1.0 in. (nominal) sampling tube is "convenient". This tube may not eliminate sampling issues, as shown in *Figure 5-3*, however it is considered the best compromise. Further work should be conducted to investigate the magnitude of bias incurred with the 1.0 in. tube.

Ideally, the sampling tube giving an unbiased sample should be used. To select the appropriate sampling tube, scoping tests should be conducted with incremental tube diameters. The minimum tube diameter with no slug flow and beyond which the distribution does not change is the target. Again, practical considerations will have to factor in the selection.

CHAPTER 6 – CONCLUSIONS & RECOMMENDATIONS

6.1 CONCLUSIONS

The conclusions drawn from this work, subdivided by chapter, are as follows:

6.1.1 Alternative Image Analysis Technique

1. Both small and large bubbles are prone to exclusion when filtered by shape factor. Care should be taken when selecting any image analysis technique to ensure that automated filters distinguish objects in a manner representative of the true system.
2. The alternative filtering method, discriminating objects based on the number of holes present (two-phase images only), reduces data scatter for wide bubble size distributions.
3. Application of the alternative filtering technique smoothes wide bubble size distributions, giving results closer to expected based on previous experience. There is negligible impact on narrow (the more common) distributions.
4. Image comparisons showed that the alternative filter counts fewer bubble clusters, more small bubbles, and slightly more large, irregular bubbles than the standard technique.
5. Visual object selection offers a standard for comparison on an image-by-image basis.

6.1.2 Diameter Filter Manipulation

6. For three-phase applications with less than an order of magnitude size difference between bubbles and solids, the minimum diameter filter can be used to distinguish between bubbles and other objects.

7. The minimum diameter yielding a unimodal, log-normal distribution should be selected to ensure standardised comparisons between cells. This minimum diameter gives a compromise between excluding non-bubble objects, and including small bubbles.

6.1.3 Diameter Assignment Method

8. As with the standard technique, uniformly applying ECD to all bubbles, regardless of shape, gives a consistent under representation of the true volume.

9. By assigning a bubble diameter based on bubble shape characteristics, volumetric error is reduced and randomised indicating improved representation.

10. For a given bubble, the difference between ECD and EVD can be used as an independent indication of sphericity.

11. The error associated with only assigning EVD proved irregular, ranging between 15% under representation to 5% over representation. This variation is likely due to the presence of spherical bubbles (which are best represented by Diameter), with a higher proportion of spherical bubbles yielding greater under representation. Populations with predominantly non-spherical bubbles (best represented by EVD) thus are more accurately represented when only EVD is

applied.

6.1.4 Impact of Sample Tube Diameter

12. The diameter of the sampling tube affects bubble sampling, introducing bias, predominantly against small bubbles due to high downward liquid velocities. Large bubbles may also be unable to enter the sampling tube, and thus also be excluded.

13. When slug flow occurs in the sampling tube, extremely small bubbles (~ 0.3 mm) can be entrained in the wakes of large bubbles, and contribute disproportionately to the final distribution.

14. When beginning experiments with an unknown bubble population, initial tests with varying sample tube diameter should be carried out. Ideally, the minimum tube diameter beyond which no distribution change is observed should be selected. Practical consideration may preclude this; the compromise to date is a 1.0 in. tube.

15. The telescopic tube commonly used for industrial trials, while not showing evidence of slug flow, employs a 0.5 in. sampling tube, and thus introduces the prospect of sample bias.

6.2 RECOMMENDATIONS

6.2.1 Alternative Image Analysis Technique

1. Extension of the alternative image analysis technique to three-phase systems. An alternative method of distinguishing between single bubbles, background and bubble clusters should be developed, independent of shape factor and number of holes present. Indications of bubble shape based on centre of mass and minimum and maximum radii and orientation may be exploited for this purpose.

2. For two-phase applications, the proposed alternative method should be extended such that all dependence on shape factor is removed. Changing the number of pixels constituting a hole, thus avoiding the counting of single, "white" pixels in the bubble perimeter as holes, may achieve these ends.

3. During the data alignment stage of the alternative process, the programme must be stopped and objects deleted if one of the 'extra objects' also contains holes. The alignment code can be adjusted to check cases where both the diameters and number of holes are not equal, to ensure that the data continues to align beyond this point.

6.2.2 Diameter Filter Manipulation

4. Analysing sets containing consistent bubble populations, but with fibres of various sizes may offer further validation of the variable minimum diameter method. The shift in distributions and mean values may then be evaluated as the potential error in the technique.

5. Characterisation of de-inking flotation machines may now be carried out.

6.2.3 Diameter Assignment Method

6. Further confirmation of the diameter assignment method, particularly for wide bubble size distributions, would allow for further investigation into the impact on volumetric error when assigning diameters. Systems containing very spherical as well as irregular bubbles would be particularly useful for these tests.

7. Investigate alternative diameters to better represent irregular bubbles, incorporating more than two radii, as judged by further reduction in volumetric error. Images of a single large bubble as it moves through the field of view (changing shape), may be used to evaluate the accuracy of the diameter assigned. Ideally, the assigned diameter would be the same no matter the shape of the bubble.

8. Automate diameter assignment into an MS Excel macro for easy application to all data sets.

6.2.4 Impact of Sample Tube Diameter

9. Establish that an ideal tube diameter exists by sampling a fine, narrow bubble size distribution with a variety of tube diameters, ranging from 0.25 in. to 1.0 in.. If an adequately fine distribution is used, the ideal sampling tube diameter may be reached, and a sampling tube diameter selection protocol developed.

10. An alternative to the telescopic sampling tube should be developed, allowing for uniform 1.0 in. sampling tube diameter, with the convenience of variable sampling

length. An external method of attaching tubes of equal diameter could be implemented, such that uniform diameter pieces could be combined until the desired length is reached.

11. Means of increasing the maximum sample tube diameter should be explored, including the addition of a cone at the tip of the sampling tube to increase the effective sampling diameter.

6.2.5 Characterisation of Jetting Spargers

As the ultimate purpose of extending the bubble viewer technique to wide distributions was the characterization of jetting spargers and probing their bubble production mechanism(s), jetting sparger operation should be revisited.

The effect of (at least) the following variables on the bubble distribution should be investigated:

1. Frother dosage
2. Air flow rate
3. Nozzle diameter
4. Addition of water to the air feed

Other characterisation recommendations are as follows:

1. Revisit prior tests to establish if trends previously concealed are revealed.

2. Establish mechanism(s) for bubble formation such that the mechanism producing small bubbles may be exploited, while that producing large bubbles minimised.

3. Conduct a comparison between jetting spargers, with particular attention to variation in the relative production of small and large bubbles.

4. Establish correlation with Reynolds number to facilitate data comparisons.

5. Establish the minimum frother concentration required to avoid coalescence.

6. Establish operation guidelines to minimise large bubble formation.

CHAPTER 7 – REFERENCES

Ahmed, N. and Jameson, G.J. (1985) "The Effect of Bubble Size on the Rate of Flotation of Fine Particles" *International Journal of Mineral Processing*, 14, 195-215.

Atkinson, C.M., and Clark, N.N. (1988) "Gas Sampling from Fluidized Beds – A Novel Probe System" *Powder Technology*, 54, 59-70.

Bakker, A., Smith, J.M., and Myers, K.J. (1994) "How to Disperse Gases in Liquids" *Chemical Engineering*, December 1994, 98-104.

Chen, F., Gomez, C.O., and Finch, J.A. (2001) "Technical Note: Bubble Size Measurement in Flotation Machines" *Minerals Engineering*, 14(4), 427-432.

de Rijk, J.H., van der Graff, J.M, and den Blanken, J.G. (1994) "Bubble Size in Flotation Thickening" *Wat. Res.*, 28(2), 465-473.

Deglon, D.A., Egya-Mensah, D., and Franzidis, J.P. (2000) "Review of Hydrodynamics and Gas Dispersion in Flotation Cells on South African Platinum Concentrators" *Minerals Engineering*, 13(3), 235-244.

Dobby, G.S. and Finch, J.A. (1991) "Column Flotation: A Selected Review, Part II" *Minerals Engineering*, 4(7-11), 911-923.

Finch, J.A. (1995) "Column Flotation: A Selected Review – Part IV: Novel Flotation Devices" *Minerals Engineering*, 8(6), 587-602.

Finch, J.A. and Hardie, C.A. (1999) "An Example of Innovation from the Waste Management Industry: Deinking Flotation Cells" *Minerals Engineering*, 12(5), 467-475.

Gomez, C.O., Hernandez-Aguilar, J.R., McSorley, G., Voigt, P., and Finch, J.A. (2003) "Plant Experiences in the Measurement and Interpretation of Bubble Size Distribution in Flotation Machines" In: Mineral Processing (C.O. Gomez and C.A. Barahona. eds). Proceedings of the Copper 2003-Cobre 2003, 5th International Conference – Volume III, Santiago, Chile, 225-240.

Gorain, B.K., Franzidis, J.-P., and Manlapig, E.V. (1995) "Studies on Impeller Type, Impeller Speed and Air Flow Rate in an Industrial Scale Flotation Cell – Part I: Effect on Bubble Size Distribution" *Minerals Engineering*, 8(6), 615-635.

Gorain, B.K., Franzidis, J.-P., and Manlapig, E.V. (1997) "Studies on Impeller Type, Impeller Speed and Air Flow Rate in an Industrial Scale Flotation Cell – Part 4: Effect of Bubble Surface Area Flux on Flotation Performance" *Minerals Engineering*, 10(4), 367-379.

Gorain, B.K., Napier-Munn, R.J., Franzidis, J.-P., and Manlapig, E.V. (1998) "Studies on Impeller Type, Impeller Speed and Air Flow Rate in an Industrial Scale Flotation Cell – Part 5: Validation of k-S_b Relationship and Effect of Froth Depth" *Minerals Engineering*, 11(7), 615-626.

Grau, R.A. and Heiskanen, K. (2002) "Visual Technique for Measuring Bubble Size in Flotation Machines" *Minerals Engineering*, 15, 507-513.

Hernandez-Aguilar, J.R. (2004) "A Technique for the Direct Measurement of Bubble Size Distributions and Applications in Flotation Systems" PhD Thesis in progress, McGill University, Montreal, Quebec.

Hernandez-Aguilar, J.R., Coleman, R.G., Gomez, C.O., and Finch, J.A. (2004) "A Comparison between Capillary and Imaging Techniques for Sizing Bubbles in Flotation Systems" *Minerals Engineering*, 17, 53-61.

Jameson, G.J., Nam, S., and Young, M.M (1977) "Physical Factors Affecting Recovery Rates in Flotation" *Minerals Science and Engineering*, 9(3), 103-118.

Leibson, I., Holcomb, E.G., Cacoso, A.G., and Jacmic, J.J. (1956) "Rate of Flow and Mechanics of Bubble Formation from Single Submerged Orifices" *A.I.Ch.E. Journal*, 2, 296-306.

Leifer, I., de Leeuw, G., Kunz, G., and Cohen, L.H. (2003) "Calibrating Optical Bubble Size by the Displaced-Mass Method" *Chemical Engineering Science*, 58, 5211-5216.

Lin, T.-J., and Fan, L.-S. (1999) "Heat Transfer and Bubble Characteristics from a Nozzle in High-Pressure Bubble Columns" *Chemical Engineering Science*, 54, 4853-4589.

Malysa, K., Ng, S., Cymbalisty, L., Czarnecki, J., and Masliyah, J. (1999) "A Method of Visualisation and Characterization of Aggregate Flow Inside a Separation Vessel, Part 1. Size, Shape and Rise Velocity of Aggregates" *International Journal of Mineral Processing*, 55, 171-188.

Polli, M., Di Stanislau, M., Bagatin, R., Bakr, E.A., and Masi, M. (2002) "Bubble Size Distribution in the Sparger Region of Bubble Columns" *Chemical Engineering Science*, 57, 197-205.

Rodrigues, R.T. and Rubio, J. (2003) "New Basis for Measuring the Size Distribution of Bubbles" *Minerals Engineering*, 16, 757-765.

Rowe, P.N., and Everett, D.J. (1972) "Fluidised Beds Viewed by X-rays. Part I: Experimental Details and the Interaction of Bubbles with Solid Surfaces" *Transactions of the Institute of Chemical Engineering*, 50, 42-48.

Schafer, R., Merten, C., and Eigenberger, G. (2002) "Bubble Size Distributions in a Bubble Column Reactor under Industrial Conditions" *Experimental Thermal and Fluid Science*, 26(6-7), 595-604.

Sung, J.S., and Burgess, J.M. (1987) "A Laser-Based Method for Bubble Parameter Measurement in Two-Dimensional fluidized Beds" *Powder Technology*, 49, 165-175.

Tucker, J.P., Deglon, D.A., Franzidis, J.-P., Harris, M.C., and O'Connor, C.T. (1994) "An Evaluation of a Direct Method of Bubble Size Distribution Measurement in a Laboratory Batch Flotation Cell" *Minerals Engineering*, 7(5-6), 667-680.

Unno, H. and Inoue, I. (1980) "Size Reduction of Bubbles by Orifice Mixer" *Chemical Engineering Science*, 35, 1571-1579.

van Krevelen, D.W., and Hoftijzer, P.J. (1950) "Studies of Gas-Bubble Formation: Calculation of Interfacial Area in Bubble Contactors" *Chemical Engineering Progress*, 46(1), 29-35.

Varley, J. (1995) "Submerged Gas-Liquid Jets: Bubble Size Prediction" *Chemical Engineering Science*, 50(5), 901-905.

Voigt, P.B. (2003) "Operation Manual Draft 2.0; Incline Bubble Viewer and Northern Eclipse Image Processing Software with use of a Digital Video Camera – January 2003", McGill University, Montreal.

Xu, M., Finch, J.A., and Uribe-Salas, A. (1991) "Maximum Gas and Bubble Surface Rates in Flotation Columns" *International Journal of Mineral Processing*, 32, 233-250.

Yianatos, J., Bergh, L., Condori, P., and Aguilera, J. (2001) "Hydrodynamic and Metallurgical Charaterization of Industrial Flotation Banks for Control Purposes" *Minerals Engineering*, 14(9), 1033-1046.

Zhang, L. and Shoji, M. (2001) "Aperiodic Bubble Formation from a Submerged Orifice" *Chemical Engineering Science*, 56, 5371-5381.

Zhou, Z.A., Egiebor, N.O., and Plitt, L.R. (1993) "Frother Effects on Bubble Size Estimation in a Flotation Column" *Minerals Engineering*, 6(1), 55-67.

APPENDIX A

McGILL UNIVERSITY BUBBLE SIZE ANALYSER OPERATING MANUAL

Inclined Bubble Viewer and Northern Eclipse Image Processing Software with use of a Digital Video Camera – February 2004

Adapted from Operation Manual Draft 2.0 (Voigt, unpublished work, 2003).

1.0 INTRODUCTION

This manual is based on the standard McGill University bubble size analyser ('bubble viewer') configuration and software, with images obtained by the Canon GL1 NTSC Digital Video Camcorder 3CCD. Alterations to this procedure may be required with changes to this general configuration.

The scope of this manual is the set-up and operation of the McGill bubble viewer with camera, and the subsequent capture and processing of bubble images. Instructions for the operation of the video camera are available at *http:\\www.canon.ca*. Guidance provided for the processing of images is for a general case, and as many special cases exist, care should be taken that output data is logical and not a result of inappropriate image processing techniques.

2.0 BUBBLE VIEWER AND CAMERA SETTINGS

2.1 Equipment List

Laboratory and plant bubble size measurement with the bubble viewer requires the following items:

Bubble Viewer	Standard McGill bubble viewer with sampling tube, stainless steel coupling and associated o-rings. For two-phase measurements, the sampling tube may have an in-line valve to control bubble flow. For measurements in three-phase systems, the valve may cause problems with sudden introduction of solids to the chamber as a result of frothing in the tube, therefore a rubber stopper at the end of the sampling tube should instead be used.
Disks of known Diameter	3mm diameter gold disks are placed in the camera field of view and may be used for camera focus and for calibration purposes in the absence of a ruler. The size of disks used must be validated with a microscope. Disks may be attached to either the inside or outside of the viewing pane, although the outside is preferable to prevent bubble adhesion. The location of the disk does not affect the measured disk size.
Set of Magnetic Cleaners	For two-phase applications, a pair of magnets with soft felt faces may be used to remove small bubbles from the viewing pane. Suitable magnets may be purchased at pet stores and are used for cleaning aquarium glass. Magnets should not be used on the back window as distortion of the light diffuser may result, nor in three-phase systems as the glass may become scratched.
Light diffuser	The light diffuser is made from translucent paper (typically 3 sheets) and mounted with a cardboard frame. The number of translucent sheets will depend on the intensity of the light. The diffuser gives even light distribution, preventing the appearance of bright areas during imaging. The diffuser is positioned on the outside of the back windowpane, before the incident backlighting is introduced.

Lamp	Positioned behind and parallel to the viewing chamber, the lamp provides backlight. The lamp is generally required to be of approximately 1000W, though bulbs as low as 500W have been successfully implemented. A reflective photographic light shield around the lamp is recommended. Ideally, the centre of the lamp should be in line with centre of the camera to ensure consistent light intensity across the field of view.
Windex	Used to clean windowpanes of moisture and dirt. Fog inhibiting Windex may be advantageous for plant conditions.
Lint-free cloths	Used to clean equipment and, if necessary, clean camera and camera outer lens.
Invisible tape	Used to attach light diffuser to rear windowpane of bubble viewing chamber.
Transparent ruler with square edge	Used for image calibration. The square edge is convenient for squaring the video camera with viewing windowpane.

Digital video camera	Canon GL1 NTSC Digital Video Camcorder 3CCD.
Blank video tape	For image recording.
Head cleaner tape	For maintaining recording and playback quality of video camera as well as maximising camera longevity. Cleaning tape should be used prior to inserting the tape for recording.

2.2 Equipment Set up

2.2.1 Bubble Viewer Set up

The bubble viewer and camera should be assembled such that the camera, viewing chamber, and light are on the same plane. The distance between the viewing chamber and the camera stand should be set to 18 cm. It should be noted that the spotlight is exposed, so care should be taken when filling the bubble viewer and during operation in humid conditions or where splashing may occur.

A disk of known diameter should be positioned on the viewing pane to aid in image processing. Disks should be positioned on the periphery of the camera field of view, preferably on the outside of the viewing pane, and may be carefully attached with transparent tape or clear drying glue. The field of view must be such that the bubbles are imaged after they have made contact with the inclined viewing pane and have spread into a single focal plane. The vertical placement of the field of view may be adjusted by moving the structural bar holding the camera along the main frame of the bubble viewer.

The translucent light diffuser must be attached to the rear window of the viewing chamber to diffuse incident light from the spotlight. Transparent tape is convenient for this purpose. The diffuser should be dry and free of markings and distortions.

The selection of the sampling tube is dependent on the specific application. The diameter of the tube may range from 1.3 cm (0.5 in.) to 2.5 cm (1.0 in.), with larger diameters being preferable to minimise sampling bias. For two-phase systems, the sampling tube may have an in-line ball valve, though a stopper may alternatively be used. For three-phase systems, an in-line valve is inappropriate as it may introduce a sudden influx of solids to the viewing chamber at the initiation of sampling due to froth effects in the tube. A stopper at the end of the sampling tube should be used, and may be attached by string to another tube for easy removal. Sampling tubes must be thoroughly cleaned to remove traces of machining lubricants and cleaning products, ensuring that frother performance is not compromised.

The viewing chamber must also be thoroughly cleaned. Although detergents may be used for a dirty chamber, it is advised that any use of cleaning surfactants is followed by thorough rinsing. Cleaning of both inner and outer glass surfaces may be finished with window cleaner.

The bubble viewer, with sampling tube attached, and sealed in cases requiring a rubber stopper, should now be placed into position with the base of the sampling tube at the desired location in the pulp. In cases with exceptional distance between the bubble viewer and desired location, a well-sealed telescopic tube may be used. If necessary, the bubble viewer may be physically secured to the supporting structure to ensure stability and safe operation. C-clamps are typically used for this purpose.

Aquarium magnets may be positioned on the viewing pane of the bubble viewer. During operation they should be positioned at the top or side of the viewing pane. If magnets remain at the bottom of the viewing pane distortions to bubble flow will occur. Bubbles must be removed from the back window by hand as the magnets can cause distortion of the light diffuser resulting in uneven light distribution. The use of magnets is not recommended for three-phase (mineral) applications as solids may become lodged on the magnet surface and scratch the window. Magnets have however been successfully applied for deinking applications.

The bubble viewer may now be filled with solution. In general, the viewing chamber must be filled with solution similar in chemistry and temperature to that in the flotation machine. For two-phase applications, the solution may be identical to that in the flotation machine. If this is not possible, a solution of similar temperature should be used to avoid the formation of small bubbles due to the temperature gradient. Continuity of frother concentration is also important. For three-phase applications, the use of flotation slurry is not realistic, so the emphasis is placed on using water of comparable temperature. Frother may also be added to the viewing chamber if required. In industrial settings process water is often desirable as some residual frother is present.

The screw cap (with o-ring) and ball valve on the bubble viewer may now be closed. Vacuum grease may be used both to ensure that the bubble viewer is sealed and to ease the movement of the lid while opening and closing.

After the bubble viewer has been filled and is prepared for operation, activate the backlight and test the light intensity to ensure adequate lighting will be available for optimal image processing. Note that upon introduction of bubbles to the chamber, the light intensity will be reduced due to increased scattering of the backlight.

Light intensity requirements varies between cameras. When using a different camera, initial trials should be conducted, varying the light intensity as necessary to achieve images adequate for processing. Low light intensity will result in darkly outlined bubbles on a grey background. High light intensity values will result in lightly outlined bubbles, loss of small bubbles, and a white background. Images with optimum lighting show well-defined small and large bubbles on a white or light grey background.

2.2.2 Video Camera Set up

This manual does not provide an instruction manual for the video camera. Individual camera user manuals must be consulted. Some understanding of the GL1 NTSC Canon Digital Video Camcorder is assumed.

Before attaching the video camera to the bubble viewer structure, operate the camera with the head-cleaning cassette on the record setting. This will ensure clean digital image capturing. For industrial applications where humidity and dust are factors, the camera should be wrapped in plastic for protection. Holes may be cut and taped around to allow operation of camera buttons.

A camera holder, screwing into the base of the camera, attaches the camera to the bubble viewer. Ensure the video camera lens is parallel to the viewing window by positioning the edge of the plastic ruler against the viewing window and squaring the video camera accordingly. Ensure the video camera is upright and aligned with the desired viewing area.

Selected magnification is dependent on the bubble populations to be imaged. Naturally, higher magnification is required for fine bubbles. For typical distributions, the +2 58mm lens should be attached to the front of the video camera, and the zoom adjusted to give an approximately 6 x 5 cm field of view. Further zooming and higher magnification lenses may be applied for fine bubble populations.

The camera should then be connected to a power source. The use of a battery pack is not recommended, as reliable and continuous operation cannot be ensured. A 110V power source is preferred.

Set the camera to 'Camera' mode on the toggle between 'Off', 'VCR' and 'Camera'.

Activate the backlight and select the following optical settings for the camera.

Shutter speed	(S)	2000
Focal depth	(F)	4.0
Gain	(dB)	12

It should be noted that the appropriate shutter speed is dependent on the system being studied. For the purposes of two-phase and pulp and paper systems, a setting of 2000 is appropriate. In typical three-phase systems, where light intensity is lost over the course of sampling due to fowling, a lower shutter speed (giving a brighter image) is recommended. The shutter speed should be a compromise between contrast at the beginning of the experiment and the experiment duration. The brighter the initial image, the longer experiment duration, but initial images must still feature closed bubbles. The current suggested shutter speed for three-phase systems is 1000. An initial test should be conducted for a given system in order to select the appropriate shutter settings. Other setting values doe not change between two-phase and three-phase systems. The light bar on the camera screen should be near the maximum level prior to the introduction of bubbles. Below the half mark images are too dark for processing, and the experiment stopped.

Camera settings are adjusted using the roller device near the front of the camera. The camera should be set to 'Manual Focus' and 'Black and White' modes using the digital effects menu. For further information please consult the camera user manual.

Adjust the camera to bring the disk into focus by adjustment of the manual focus dial. This focus is maintained by operating in manual focus mode. Fine focus adjustments may be made manually prior to the test by focussing on a ruler.

2.3 Calibration and Preparation

To track discrete measurements during a series of experiments, it is recommended that a piece of paper with experimental trial details such as date and operating parameters be recorded for several seconds to mark the beginning of each trial.

For all experiments, calibration for image processing must be conducted. Set the video camera to record and position the transparent ruler in the horizontal axis, ensuring its alignment in the field of view. The ruler may be held in place, but it is recommended that the transparent ruler be taped to the viewing window. Position the ruler in the vertical axis and record the ruler in this position for a few seconds. Some discrepancies between axes have been noted with this camera. As a means of resolving this issue has not been validated, tracking of the discrepancies by means of two calibration measurements is recommended.

The viewing pane may be prepared by cleaning outer glass surfaces with a window cleaner. Fog-reducing cleaner may be useful for humid plant conditions. The aquarium magnets positioned inside the bubble viewer may be used to remove small bubbles and impurities from the camera view.

2.4 Making Measurements

The introduction of a bubble stream into the viewing chamber is initiated according to the viewer set up, either by opening the in-line ball valve or by removing the rubber stopper from the end of the sampling tube.

Initial bubble flow into the bubble viewer is not representative of the true population and often contains slugs and small bubbles. Ideally, the system should be allowed to reach a quasi-steady state. Typically, 30 seconds is adequate, though the time varies with sample tube length. For the shorter tubes typically used in the lab, 15 seconds is often adequate. For industrial purposes, where tube lengths may exceed 2m, longer times are necessary. Given that at high gas flow rates the bubble viewer chamber empties quickly, and that in plant situations the chamber may be quick to foul, these times must be adjusted according to the particular situation. The trial should be recorded from the initial introduction of bubbles such that the appropriate time lapse may be selected upon review of the tape.

Labelling of experiments and calibration may be carried out prior to the introduction of bubbles. Any further camera movement or zoom adjustment requires recalibration. Just prior to the introduction of bubbles, the camera should be set to record for the sampling period. Prior to recording, it should be ensured that the field of view is free from condensation and debris.

The measurement session can be as long as required, though 4 minutes is usually adequate. The experiment is over when one of the following occurs:

- The liquid level in the bubble viewer enters the camera field of view.
- The camera is moved, bumped, or the zoom or any other settings are changed (recalibration required).
- The light intensity is no longer adequate for image quality (the light bar on the camera screen is below 50%).

When a measurement is complete, the recording is paused on the video camera (by pressing the record button again) and resumed when the next experiment is conducted. In the case of the in-line ball valve, bubbles may be stopped from entering the viewing chamber by closing the valve. For three-phase tests, the ball valve on the viewing chamber lid should be opened to release the vacuum and drain the remaining liquid.

The bubble viewer may now be prepared for the next experiment. In three-phase applications, the chamber should be thoroughly cleaned to avoid residual fowling. Video obtained from experimental trials requires processing to digitise and size bubbles.

3.0 IMAGE PROCESSING

The sizing process consists of image capture from the digital video, conversion of images to 8 bit grey scale, and image processing using Empix Northern Eclipse v6.0.

3.1 Image Capture

Image capture is currently conducted with one of two programs, ATI or Dazzle. Each program will be addressed separately. To date, ATI yields the better image capturing results, as the software comes with a dedicated video card. Dazzle yields poorer quality, however employs a USB interface making it convenient for application in the field.

Image capture may be achieved using either the camera in 'VCR' mode with an S-Video cable, or using a separate VCR. Assuming the dedicated video card and associated software has been installed in the local PC, a video interface device (small purple box) must be attached to the video card port. The video interface device may now be attached to the camera or VCR.

The head cleaner tape should be used on the play head to ensure playback free of digital interference.

3.1.1 ATI Image Capture Software

The ATI software comes as a package with various components. For capturing images, load the TV application within ATI from the 'Start' menu in MS Windows.

The program should load, showing the real time display of what the VCR is playing. The display consists of a screen and control panel. The 'Program Settings' button is located at the bottom of the control panel (rectangular box with a check mark). Select this button to configure the image capture.

Leave most settings as default. In the 'Stills Gallery' tab, select the check box, 'Capture to numbered file' only. Select 'Browse' to nominate the directory to which captured files will be stored. The image numbering may also be set at this time. Typically, if fewer than 1000 images will be captured '001' is the appropriate numbering style. Although different file types and resolutions can be selected, the program appears to default to 24 bit, 640 x 480. This is not a major problem, though it is preferable to capture images in the pixel resolution at which they were initially recorded.

In the 'Digital VCR' tab, select the check box, 'Capture High Resolution Stills'. The necessary options have now been selected and the 'TV-On-Demand' player set up box may be exited.

Please consult the ATI user manual for further information. However, there is limited technical support offered by ATI.

It is important during image capturing that sufficient space remains on the hard disk for the captured stills. Having approximately 1 gigabyte available on the local hard disk should be sufficient for a single run.

Occasionally, a video log is taken. While it increases image quality, problems with programme crashing and requirements for additional free space make its use rare. Check the local hard disk for file 'ATI_shift.vcr' after employing this option. This is the continuous log file and may be deleted after a capture session. Do not delete or move during capture, as the program will terminate.

To begin capturing images, press 'Play' on the camera. To capture an image, click the camera icon (to the left of the aspect ratio icon) or press Ctrl and Insert simultaneously. Ensure that at least one calibration image is captured for each of the axes.

The icon must be clicked continuously during the playing of the tape to capture images.

The program will begin to run statically, taking approximately one image per second. Keep pressing the camera icon for the duration of the sample period until the experiment has finished. Later excess images, such as those ATI continues to take after the end of the desired trial, may be deleted.

Images will not appear in the destination directory for a few seconds as they are transferred from the video RAM.

Once the experiment is finished, press 'Stop' on the video camera.

3.1.2 Dazzle Image Capture Software

The Dazzle interface unit is connected to the VCR via an S-Video cable. The Dazzle interface unit may then be plugged into an available USB port on the local PC. The USB device cannot simply be unplugged from the computer, as it will cause the computer to crash. To remove the USB devise safely, click the USB icon at the bottom right of the MS Windows operating system screen and disable. Further information is available from Dazzle and MS Windows user manuals.

Load the Dazzle Movie Star program from the 'Start' menu in MS Windows. In the far right of the program screen, click the camera icon to enter snapshot mode. Now the Dazzle display should show the view displayed on the video camera.

The program has five expandable menu tabs; two on the left side of the program screen and three on the bottom. The top tab, on the left contains image quality settings. Dazzle can be set to capture images at set intervals for a certain time period, removing the manual clicking required for ATI. Care should be taken when selecting the time interval, as bubbles must clear the field of view between images to avoid duplication. Images can also be captured by manually clicking.

In the 'Picture' tab, under the 'Frame' button, select either single (manual clicking), multiple, or periodic (automatic capturing). Set the picture resolution in the 'Size' button, it is recommended that 800 x 600 is used. Select 'Save Options' and 'Colour' as black and white. Similarly, select 'Format' as the desired file type. All other settings in this tab should remain as default settings. For more information consult the Dazzle user manual.

The second tab on the left hand side contains image saving destinations. In the 'Media' tab, delete all current images displayed by highlighting and pressing 'Delete'. Hold 'Shift' or 'Ctrl' while clicking images to make multiple selections. At the top right-hand side of this tab option is the 'Media Manager Properties' icon. Browse to select the save destination for stills files.

The program is now set for capturing images. Press 'Play' on the video player. Ensure that at least one calibration image is captured for each of the axes. If periodic capturing is requested, then click the camera icon next to the record button at the bottom of the Dazzle display. For manual capture, continually click the camera icon to capture images.

Once the experiment has finished, press 'Stop' on the video camera. Inspect the destination directory to ensure images have been captured. Again, it may take some time for images to be transferred from RAM to the hard disk.

3.2 Image Pre-Processing

By either ATI or Dazzle, destination directories should contain several hundred images (depending on the experiment duration).

Anomalies in the CCD chip in 'Off the shelf' video cameras (such as the camera detailed in this manual) result in dimensions in the X and Y being unequal. Ideally, this is avoided by capturing images of identical resolution to that of the video camera (in this case 600 x 450). As ATI defaults to 640 x 480, some distortion is present, though the magnitude varies between runs. In the absence of a universal correction method, it is advised that one axis is consistently used for calibration. The number of pixels in a given distance should be recorded for both axes, such that if necessary corrections may later be made.

Images also require conversion to 8-bit greyscale mode. Firegraphics XP is a useful programme for this purpose as it allows for batch conversion. To convert images, select all images to be converted, then select 8-bit grey scale in the 'Mode' menu option from the 'Image' menu. The converted images can replace original images or be saved under a different file name. Undesirable images may also easily be deleted in this programme by selecting and then pressing 'Delete'. The images are then deleted from the destination folder.

Once the images have been converted into 8-bit grey scale, and inappropriate images removed, Empix Northern Eclipse v6.0 is used for image processing. Please refer to the Northern Eclipse user manual for more information. Northern Eclipse requires a parallel port dongle key to be present for image processing. There are two types of keys. One has a red dot on the bottom. This may only be used for directly acquiring stills from a digital still camera to the local hard disk. It does not allow the processing features of Northern Eclipse to function. The other has a clear dot on the bottom. This may be used for both acquiring and processing images. It enables all functions.

Select and load the two best calibration images, one for each axis. Select the calibration option in the Northern Eclipse program. Make a calibration measurement in the *Y*-axis over at least 30mm on the ruler scale. Name and save this calibration, recording the number of pixels. The same process should then be carried out for the X-axis, though the calibration need not be saved, only the number of pixels over the same distance recorded.

3.3 Bubble Size Measurement

Northern Eclipse requires a Region of Interest (ROI) to be set, by way of applying a mask. Areas of the image inside the ROI will be analysed, while those outside will be ignored. The ROI is an ideal way to avoid the analysis of any systematic interference, including calibration disks. The mask should outline just inside the border of the image to avoid accidental inclusion of the thin black border around the image.

To create an image mask, a selection tool (circular, square, rectangle etc.) can be used to outline the desired ROI. If necessary, multiple areas may be selected. All objects inside the selected areas will be analysed. Selection of overlapping areas is not an issue as objects in these areas are only counted once. Once the ROI is selected, go to the 'Measure' menu, and 'Save Selection'. Save the mask using an arbitrary name, toher than 'Bubbles.msk'. To apply this particular mask during analysis, re-save the selection as 'Bubbles.msk'. This is the file that the subroutine uses to apply the mask filter.

Northern Eclipse comes preloaded with a Visual Basic subprogram, 'Bubbles', that automatically analyses a user-defined number of images. The subprogram will output data to an MS Excel file. MS Excel will be automatically started by the subroutine.

To begin image analysis, select 'Bubbles'. The number of images to be analysed must be entered. If a greater number is specified than are selected, an error message will appear after all selected images have been processed, and the sum and average values (constituting the last two lines of the MS Excel output) will not be calculated. This is an effective strategy if multiple data sets will be added together.

Next, filters can be applied. Values for maximum and minimum diameter must be entered, and specific values depend on the expected bubble size range. The default is 0.4mm to 2mm, but may be modified according to the anticipated bubble population. The parameter 'Max_Shape' refers to the shape factor and should remain at the default values of 0.7 to 1.2. However, if the system contains large, irregularly shaped bubbles with low shape factors, the values may be changed accordingly to include more bubbles. Care should be taken when modifying the shape factor criterion, as lowering values will include progressively more clusters of bubbles. When Eclipse analyses images, objects with either diameter or shape factor outside the specified ranges will not be counted and their dimensions will not appear in the MS Excel file. The 'Image Aspect' should remain at 1, and 'Fill Holes' should be selected.

The threshold is a setting that depends on the background lighting intensity. The selection of this parameter is discussed further in Section 3.4.

The term 'Experiment' may be replaced by an experiment name. This will appear at the top of the MS Excel file and is useful for keeping track of experimental results.

Now select the 'Process Images' button and select the batch of files for processing.

Once the file sequence has been selected, the program will automatically count bubbles in the selected images, and output the data to an MS Excel file.

3.4 Threshold Selection

Applying an image threshold polarises all shades of grey to either black or white, depending on the greyscale relative to the threshold.

The threshold setting is the most important setting in the overall accuracy of image processing and is a strong function of the background lighting during imaging. This is clearly a problem for three-phase measurements, as fouling will change the background intensity over time.

Although studies are underway to formalise the relationship between optimal threshold setting and background light intensity, selection of the appropriate threshold is still made by the operator. A threshold value is deemed appropriate if it allows the smallest bubbles to close with a complete perimeter, but does not cause significant distortion of larger bubbles. If the lighting is uneven, areas of the background may also be rendered black. These areas can be excluded by revising and resaving the image mask.

To set the threshold, open a series of images and select the 'Threshold' option. There are two slide bars for selecting the greyscale setting, 'From' and 'To'. Set the 'From' slide to zero. The other slide bar may be adjusted until an appropriate threshold level is found. The shape factor of small bubbles should be checked using the 'Measure' tool to ensure that their perimeters are complete, with low values indicating an incomplete perimeter. The threshold value should then be checked on several other images across the image set to ensure its suitability.

The threshold setting may be kept throughout image processing during the same experiment assuming the same light conditions.

3.4.1 Three-phase Threshold Settings

For three-phase, the changing background light intensity can cause problems during imaging. Depending on the system, light intensity may vary significantly over 1 to 2 minutes.

It is advised that threshold settings are revised as soon as a noticeable change in background light intensity is noted. Using Firegraphics XP, the images should be visually reviewed, and divided into subgroups with similar background intensity. The image sets should be processed separately, and if the MS Excel file is not altered between runs, the data will be added to the end of the previous set.

To set the threshold for an image set, open the first and last images. Find the appropriate threshold value for the last image. If all bubbles are coated in solids, the criterion of bubble closure cannot be used, and the disk diameter (measured as 3.099 ± 0.078 mm) should be used to set the threshold. Once this threshold is set, check the threshold with the first image in the set. If all bubbles are still closed, and the disk is reasonably close to its true diameter, this threshold value may be used for the given data set. If the threshold value is not suitable, the image set may be revised to include fewer images, and thus a smaller degree of variation between the beginning and end. Generally, if the bubbles are coated in solids and the ideal threshold level does not vary by more than 10 over the data set, then the threshold value is considered adequate and applied to the entire set.

4.0 DATA PROCESSING

4.1 Introduction

Data is output to an MS Excel file. The program will output the image file name, usually a number, and all the counted objects within that image. According to mask settings, the disk data will not be included.

Metrics are output as defined in the Northern Eclipse user manual. However, some metrics of note have been defined here.

Shape Factor – Based on the measurement of bubble perimeter, the "sphericity" of the bubble or disk is determined. A value of unity is a perfect circle. The value of shape factor is determined by the accuracy of the perimeter measurement, and thus the image resolution. The maximum shape factor that may be determined for a specified video camera on perfect circles (disks), and for this camera is approximately 0.9.

Diameter – Represents the longest chord across the object.

Equivalent Circle Diameter – Represents the diameter of a circle having the same area as the object.

Equivalent Volume Diameter – To determine this parameter, Eclipse finds the maximum and minimum radii of the object based on its centre of mass. These values then become the major and minor axes of an ellipsoid having an axis of symmetry along its minor axis. The output diameter is the diameter of a sphere having the same volume as this ellipsoid.

4.2 Preparation of Experimental Data

The output bubble size data must be corrected for hydrostatic pressure, atmospheric pressure and temperature such that comparisons between data sets may be made. The hydrostatic pressure is taken at the depth below the surface of the liquid where the measurement was made. Correction for temperature and pressure can be carried out in the typical fashion based on ambient conditions to correct the bubble size to a standard hydrostatic pressure and standard conditions. Such corrections are also required for complimentary mathematical models used to predict bubble size.

4.3 Selection of Output Equivalent Diameter

The three diameter output values each have specific instances where their application is appropriate.

The 'Diameter' output is the output that will accurately represent highly circular objects.

This is because the other equivalent diameters are based on less accurate auxiliary measurements such as perimeter and centre of mass coupled with mathematical approximation.

The 'Equivalent Circle Diameter' (ECD) is considered appropriate for relatively spherical bubbles, while the 'Equivalent Volume Diameter' (EVD) is thought to give the best equivalent diameter output for non-spherical bubbles.

A method of assigning the best equivalent diameter to individual bubbles is being developed based on knowledge of true bubble volume. The equivalent diameter that when converted into a spherical volume shows best agreement with this benchmark is considered appropriate.

4.4 Data Validation

Data validation is limited in cases where the bubbles being measured are of an unknown size as under plant conditions. In a laboratory situation, bubbles of known size may be generated from an orifice and verified using Tate's Law.

In both laboratory and plant conditions, the presence of the disks of known diameter in each shot provide an approximate indication of data integrity.

In both laboratory and plant situations, other parameters may be measured when dealing with bubble swarms such as superficial gas velocity (J_g) and gas holdup (ε_g). Both variables are input parameters to mathematical approximation models such as drift flux analysis.

As many validation checks as practical should be made.

4.5 Creation of a Histogram

A histogram can be created from experimental data using intrinsic MS Excel functions. Set a bin size by determining the bubble size range and the size increment (bin size) in the distribution. Typically, bin numeric increments of 0.1 mm are used, though geometric increments (either of the square or fourth root of two) may be advantageous for data. Continue this bin sequence to include the maximum bubble size. Highlight cells adjacent to values in the bin range. Go to the 'Insert' menu, then 'Function' and select to insert the 'Frequency' function.

As requested by the dialogue box, highlight the bin and data ranges. Once this is complete, press 'Ctrl' and 'Shift' and click 'OK' simultaneously for the calculation to apply to the entire set of highlighted cells. The output will be a number based distribution containing only integers.

The distribution can be converted to a volume-based distribution if desired. Find the equivalent sphere volume corresponding to the midpoint of each bin range. For example, for a bin increment of 0.1 mm, the 0.5 mm bin will contain bubbles with a diameter of 0.4 to 0.5 mm; the midpoint of this bin range is the diameter of 0.45 mm.

Multiply the equivalent volume by the corresponding counts in the frequency column. The output now is the distribution on a volume basis. The distribution can be normalised to a fraction. The normalised function may be plotted against the bin range to output a volume based bubble size distribution.

Distributions based on number, bubble surface area flux, and other parameters of interest may be obtained in a similar fashion.

APPENDIX B

VBA (MS EXCEL) CODE FOR Holesv8

```
Sub Holesv8()
'
' Macro to take process results with and without filled holes, line them up
'        based on matching diameters and holes, filter and and plot the resulting
distribution
' Upgraded by only counting objects with exactly one hole, removing the option of
zero holes,
'       and allowing for selected cases with more than one hole.  Additional filter
added
'     based of area ratios.
' Macro recorded 28/7/2003 by Marta Bailey


'copies data to file 'temp.xls'
   Range("A1").Select
   Range(Selection, ActiveCell.SpecialCells(xlLastCell)).Select
   Selection.Copy
   Workbooks.Add
   ActiveSheet.Paste
   Range("A1").Select
   Application.CutCopyMode = False
   ActiveWorkbook.SaveAs Filename:= _
      "C:\Documents and Settings\Marta\My Documents\temp.xls",
FileFormat:=xlNormal _
      , Password:="", WriteResPassword:="", ReadOnlyRecommended:=False, _
      CreateBackup:=False
   Range("A3").Select

'relabel the nofill column titles to add '1' at the end
   Range("C1").Select
   ActiveCell.FormulaR1C1 = "Object No1"
   Range("D1").Select
   ActiveCell.FormulaR1C1 = "Area1"
   Range("E1").Select
   ActiveCell.FormulaR1C1 = "EquivCircleDiam1"
```

```
    Range("F1").Select
    ActiveCell.FormulaR1C1 = "Shape(roundness)1"
    Range("G1").Select
    ActiveCell.FormulaR1C1 = "DiamCubed1"
    Range("H1").Select
    ActiveCell.FormulaR1C1 = "DiamSquared1"
    Range("I1").Select
    ActiveCell.FormulaR1C1 = "DiamRatio1"
    Range("J1").Select
    ActiveCell.FormulaR1C1 = "Holes1"
    Range("K1").Select
    ActiveCell.FormulaR1C1 = "MaxRadius1"
    Range("L1").Select
    ActiveCell.FormulaR1C1 = "MinRadius1"
    Range("M1").Select
    ActiveCell.FormulaR1C1 = "Diameter1"
    Range("N1").Select
    ActiveCell.FormulaR1C1 = "VolEquivDiam1"
    Range("O1").Select
    ActiveCell.FormulaR1C1 = "Perimeter1"
    Range("P3").Select
    Selection.EntireColumn.Insert
    Range("P3").Select
    ActiveCell.FormulaR1C1 = "HolesMatch"
    Range("Q3").Select
    ActiveCell.FormulaR1C1 = "DiaMatch"
    Range("P3").Select

'Delete cells that do not match (align data sets)
    Do
        ActiveCell.FormulaR1C1 = ("=RC[-6]=RC[11]") 'test if columns are equal
        ActiveCell.Activate
        ActiveCell.Offset(0, 1).Select
        ActiveCell.FormulaR1C1 = ("=RC[-4]=RC[13]")
        ActiveCell.Activate
        ActiveCell.Offset(0, -1).Select

        If (ActiveCell.Value) = (ActiveCell.Offset(0, 1).Value) Then 'if true scroll
down one
          ActiveCell.Offset(1, 0).Select

        ElseIf (ActiveCell.Value) > (ActiveCell.Offset(0, 1).Value) Then
            ActiveCell.Offset(1, 0).Select

        ElseIf (ActiveCell.Value) < (ActiveCell.Offset(0, 1).Value) Then
```

```
If (ActiveCell.Offset(0, 14).Value) = (ActiveCell.Offset(1, -3).Value) Then
    ActiveCell.Offset(0, -15).Select   'select over
    ActiveCell.Range("A1:O1").Select   'select cells to delete (relative
address)
    ActiveCell.Activate
    Selection.Delete Shift:=xlUp  'delete cells and shift cells up
    ActiveCell.Offset(0, 15).Select 'select back to original true/false column
    ActiveCell.FormulaR1C1 = ("=RC[-6]=RC[11]") 'test if columns are
equal
    ActiveCell.Activate
    ActiveCell.Offset(0, 1).Select
    ActiveCell.FormulaR1C1 = ("=RC[-4]=RC[13]")
    ActiveCell.Activate
    ActiveCell.Offset(0, -1).Select

 ElseIf (ActiveCell.Offset(1, 14).Value) = (ActiveCell.Offset(2, -3).Value)
Then
    ActiveCell.Offset(0, -15).Select   'select over
    ActiveCell.Range("A1:O1").Select   'select cells to delete (relative
address)
    ActiveCell.Activate
    Selection.Delete Shift:=xlUp 'delete cells and shift cells up
    ActiveCell.Offset(0, 15).Select 'select back to original true/false column
    ActiveCell.FormulaR1C1 = ("=RC[-6]=RC[11]") 'test if columns are
equal
    ActiveCell.Activate
    ActiveCell.Offset(0, 1).Select
    ActiveCell.FormulaR1C1 = ("=RC[-4]=RC[13]")
    ActiveCell.Activate
    ActiveCell.Offset(0, -1).Select

 ElseIf (ActiveCell.Offset(0, -3).Value) = (ActiveCell.Offset(1, 14).Value)
Then
    ActiveCell.Offset(0, 2).Select
    ActiveCell.Range("A1:O1").Select
    ActiveCell.Activate
    Selection.Delete Shift:=xlUp
    ActiveCell.Offset(0, -2).Select
    ActiveCell.FormulaR1C1 = ("=RC[-6]=RC[11]") 'test if columns are
equal
    ActiveCell.Activate
    ActiveCell.Offset(0, 1).Select
    ActiveCell.FormulaR1C1 = ("=RC[-4]=RC[13]")
    ActiveCell.Activate
    ActiveCell.Offset(0, -1).Select
```

```
        ElseIf (ActiveCell.Offset(1, -3).Value) = (ActiveCell.Offset(2, 14).Value)
Then
            ActiveCell.Offset(0, 2).Select
            ActiveCell.Range("A1:O1").Select
            ActiveCell.Activate
            Selection.Delete Shift:=xlUp
            ActiveCell.Offset(0, -2).Select
            ActiveCell.FormulaR1C1 = ("=RC[-6]=RC[11]") 'test if columns are
equal
            ActiveCell.Activate
            ActiveCell.Offset(0, 1).Select
            ActiveCell.FormulaR1C1 = ("=RC[-4]=RC[13]")
            ActiveCell.Activate
            ActiveCell.Offset(0, -1).Select

        ElseIf (ActiveCell.Offset(2, 14).Value) = (ActiveCell.Offset(3, -3).Value)
Then
            ActiveCell.Offset(0, -15).Select   'select over
            ActiveCell.Range("A1:O1").Select   'select cells to delete (relative
address)
            ActiveCell.Activate
            Selection.Delete Shift:=xlUp  'delete cells and shift cells up
            ActiveCell.Offset(0, 15).Select 'select back to original true/false column
            ActiveCell.FormulaR1C1 = ("=RC[-6]=RC[11]") 'test if columns are
equal
            ActiveCell.Activate
            ActiveCell.Offset(0, 1).Select
            ActiveCell.FormulaR1C1 = ("=RC[-4]=RC[13]")
            ActiveCell.Activate
            ActiveCell.Offset(0, -1).Select

        ElseIf (ActiveCell.Offset(0, 14).Value) = (ActiveCell.Offset(2, -3).Value)
Then
            ActiveCell.Offset(0, -15).Select   'select over
            ActiveCell.Range("A1:O1").Select   'select cells to delete (relative
address)
            ActiveCell.Activate
            Selection.Delete Shift:=xlUp  'delete cells and shift cells up
            ActiveCell.Offset(0, 15).Select 'select back to original true/false column
            ActiveCell.FormulaR1C1 = ("=RC[-6]=RC[11]") 'test if columns are
equal
            ActiveCell.Activate
            ActiveCell.Offset(0, 1).Select
            ActiveCell.FormulaR1C1 = ("=RC[-4]=RC[13]")
            ActiveCell.Activate
```

```
            ActiveCell.Offset(0, -1).Select
          ElseIf (ActiveCell.Offset(1, 14).Value) = (ActiveCell.Offset(3, -3).Value)
Then
            ActiveCell.Offset(0, -15).Select   'select over
            ActiveCell.Range("A1:O1").Select   'select cells to delete (relative
address)
            ActiveCell.Activate
            Selection.Delete Shift:=xlUp  'delete cells and shift cells up
            ActiveCell.Offset(0, 15).Select 'select back to original true/false column
            ActiveCell.FormulaR1C1 = ("=RC[-6]=RC[11]") 'test if columns are
equal
            ActiveCell.Activate
            ActiveCell.Offset(0, 1).Select
            ActiveCell.FormulaR1C1 = ("=RC[-4]=RC[13]")
            ActiveCell.Activate
            ActiveCell.Offset(0, -1).Select
            '
          ElseIf (ActiveCell.Offset(3, 14).Value) = (ActiveCell.Offset(4, -3).Value)
Then
            ActiveCell.Offset(0, -15).Select   'select over
            ActiveCell.Range("A1:O1").Select   'select cells to delete (relative
address)
            ActiveCell.Activate
            Selection.Delete Shift:=xlUp  'delete cells and shift cells up
            ActiveCell.Offset(0, 15).Select 'select back to original true/false column
            ActiveCell.FormulaR1C1 = ("=RC[-6]=RC[11]") 'test if columns are
equal
            ActiveCell.Activate
            ActiveCell.Offset(0, 1).Select
            ActiveCell.FormulaR1C1 = ("=RC[-4]=RC[13]")
            ActiveCell.Activate
            ActiveCell.Offset(0, -1).Select
          ElseIf (ActiveCell.Offset(4, 14).Value) = (ActiveCell.Offset(5, -3).Value)
Then
            ActiveCell.Offset(0, -15).Select   'select over
            ActiveCell.Range("A1:O1").Select   'select cells to delete (relative
address)
            ActiveCell.Activate
            Selection.Delete Shift:=xlUp  'delete cells and shift cells up
            ActiveCell.Offset(0, 15).Select 'select back to original true/false column
            ActiveCell.FormulaR1C1 = ("=RC[-6]=RC[11]") 'test if columns are
equal
            ActiveCell.Activate
            ActiveCell.Offset(0, 1).Select
            ActiveCell.FormulaR1C1 = ("=RC[-4]=RC[13]")
```

```
      ActiveCell.Activate
      ActiveCell.Offset(0, -1).Select
    '
    ElseIf (ActiveCell.Offset(2, -3).Value) = (ActiveCell.Offset(3, 14).Value)
Then
      ActiveCell.Offset(0, 2).Select
      ActiveCell.Range("A1:O1").Select
      ActiveCell.Activate
      Selection.Delete Shift:=xlUp
      ActiveCell.Offset(0, -2).Select
      ActiveCell.FormulaR1C1 = ("=RC[-6]=RC[11]") 'test if columns are
equal
      ActiveCell.Activate
      ActiveCell.Offset(0, 1).Select
      ActiveCell.FormulaR1C1 = ("=RC[-4]=RC[13]")
      ActiveCell.Activate
      ActiveCell.Offset(0, -1).Select
    ElseIf (ActiveCell.Offset(3, -3).Value) = (ActiveCell.Offset(4, 14).Value)
Then
      ActiveCell.Offset(0, 2).Select
      ActiveCell.Range("A1:O1").Select
      ActiveCell.Activate
      Selection.Delete Shift:=xlUp
      ActiveCell.Offset(0, -2).Select
      ActiveCell.FormulaR1C1 = ("=RC[-6]=RC[11]") 'test if columns are
equal
      ActiveCell.Activate
      ActiveCell.Offset(0, 1).Select
      ActiveCell.FormulaR1C1 = ("=RC[-4]=RC[13]")
      ActiveCell.Activate
      ActiveCell.Offset(0, -1).Select
    ElseIf (ActiveCell.Offset(4, -3).Value) = (ActiveCell.Offset(5, 14).Value)
Then
      ActiveCell.Offset(0, 2).Select
      ActiveCell.Range("A1:O1").Select
      ActiveCell.Activate
      Selection.Delete Shift:=xlUp
      ActiveCell.Offset(0, -2).Select
      ActiveCell.FormulaR1C1 = ("=RC[-6]=RC[11]") 'test if columns are
equal
      ActiveCell.Activate
      ActiveCell.Offset(0, 1).Select
      ActiveCell.FormulaR1C1 = ("=RC[-4]=RC[13]")
      ActiveCell.Activate
      ActiveCell.Offset(0, -1).Select
```

```
        Else
          ActiveCell.Offset(0, -15).Select   'select over
          ActiveCell.Range("A1:O1").Select    'select cells to delete (relative
address)
          ActiveCell.Activate
          Selection.Delete Shift:=xlUp  'delete cells and shift cells up
          ActiveCell.Offset(0, 15).Select 'select back to original true/false column
          ActiveCell.FormulaR1C1 = ("=RC[-6]=RC[11]") 'test if columns are
equal
          ActiveCell.Activate
          ActiveCell.Offset(0, 1).Select
          ActiveCell.FormulaR1C1 = ("=RC[-4]=RC[13]")
          ActiveCell.Activate
          ActiveCell.Offset(0, -1).Select

        End If

      End If
   ' Continue this loop until the cell A(n) is empty
   Loop Until IsEmpty(ActiveCell.Offset(0, -14))

   ActiveCell.Activate  'delete the remaining useless cells
   Range(Selection, ActiveCell.SpecialCells(xlLastCell)).Select
   Selection.ClearContents
   Range("A1").Select


'Set up advanced filter on Sheet 3
   Sheets("Sheet3").Select
   Range("A1").Select
   ActiveCell.FormulaR1C1 = "Holes1"
   Range("B1").Select
   ActiveCell.FormulaR1C1 = "VolEquivDiam"
   Range("C1").Select
   ActiveCell.FormulaR1C1 = "Shape(roundness)"
   Range("A2").Select
   ActiveCell.FormulaR1C1 = "=1"
   Range("A3").Select
   ActiveCell.FormulaR1C1 = ">1"
   Range("B2").Select
   ActiveCell.FormulaR1C1 = ">0.1"
   Range("B3").Select
   ActiveCell.FormulaR1C1 = ">0.1"
   Range("C3").Select
   ActiveCell.FormulaR1C1 = ">0.8"
```

```
' Filter ensures that: (Holes=1, EVD>0.2), OR, (Holes>1, EVD>0.2, SF>0.8)


'Select Sheet 2 and execute Advanced Filter
  Sheets("Sheet2").Select
  Sheets("Sheet1").Range("A1:AE32768").AdvancedFilter  Action:=xlFilterCopy,
_
     CriteriaRange:=Sheets("Sheet3").Range("A1:AE3"),
CopyToRange:=Range("A1"), _
     Unique:=False
  ActiveWindow.ScrollColumn = 17
  ActiveWindow.SmallScroll ToRight:=1

'Secondary filter, see p23 of lab book 2 for reasoning
  Sheets("Sheet2").Select
  Range("AF1").Select
  ActiveCell.FormulaR1C1 = "Ratio"
  Range("AF2").Select
  ActiveCell.FormulaR1C1 = "=RC[-11]/(PI()*RC[-4]^2)"
  Range("AF2").Select
  Selection.Copy
  Range(Selection, Selection.End(xlDown)).Select
  ActiveSheet.Paste
  Sheets.Add
  Sheets("Sheet3").Select
  Range("A1").Select
  Range(Selection, ActiveCell.SpecialCells(xlLastCell)).Select
  Selection.ClearContents
  Range("A1").Select
  ActiveCell.FormulaR1C1 = "Ratio"
  Range("A2").Select
  ActiveCell.FormulaR1C1 = ">0.5"
  Sheets("Sheet4").Select
  Sheets("Sheet2").Range("A1:AF32768").AdvancedFilter  Action:=xlFilterCopy,
_
     CriteriaRange:=Sheets("Sheet3").Range("A1:AF2"),
CopyToRange:=Range("A1"), _
     Unique:=False
  ActiveWindow.ScrollColumn = 17
  ActiveWindow.SmallScroll ToRight:=1


'Delete data from no holes filled
  Sheets("Sheet4").Range("A1:P32768").Select
```

```
    ActiveCell.Activate
    Selection.ClearContents
    Range("Q1:AF32768").Select
    Selection.Cut
    Range("A1").Select
    ActiveSheet.Paste
    Range("A1").Select
    Sheets("Sheet1").Select
    Range("A2").Select  'copies run name to cell A1 revised data
    ActiveCell.Copy
    Sheets("Sheet4").Select
    Range("A1").Select
    ActiveSheet.Paste


'Copy relevant data and paste in new workbook
    Range(Selection, ActiveCell.SpecialCells(xlLastCell)).Select
    Selection.Copy
    Workbooks.Add
    Range("A1").Select
    ActiveSheet.Paste
    Range("A1").Select


'Save file as experiment name
    SaveName = Format$(Range("A1").Value)
    ActiveWorkbook.SaveAs (SaveName)


'Close temp.xls
    Windows("temp.xls").Activate
    ActiveWorkbook.Save
    ActiveWindow.Close
    Kill ("C:\Documents and Settings\Marta\My Documents\temp.xls")


'Set up max value and bin
   Range("R1").Select
    ActiveCell.Formula = "=MAX(E:E)+0.1"
    Max = ActiveCell.Value

    Range("Q1").Select
    ActiveCell.FormulaR1C1 = "bin"

    'Thank you Jorge!!!
```

```
    j = 2
    For i = 0 To Max Step 0.1
    j = j + 1

    Range("Q" & j).Select
    ActiveCell.Formula = "=" & i

    Next i


'Get frequency of Equiv Circle Diameter
    Columns("R:R").Select
    ActiveCell.FormulaR1C1 = "=FREQUENCY(C[-12],C[-1])"
    Selection.FormulaArray = "=FREQUENCY(C[-12],C[-1])"
    Range("R1").Select


'Get rid of #N/A's
    Range(Selection, ActiveCell.SpecialCells(xlLastCell)).Select
    Selection.Copy
    Range("T1").Select
    Selection.PasteSpecial Paste:=xlValues, Operation:=xlNone, SkipBlanks:= _
        False, Transpose:=False
    Application.CutCopyMode = False
    Selection.Cut
    Range("R1").Select
    ActiveSheet.Paste
    Range("R1").Select
    Cells.Find(What:="#N/A", After:=ActiveCell, LookIn:=xlValues, LookAt:= _
        xlPart, SearchOrder:=xlByRows, SearchDirection:=xlNext,
MatchCase:=False) _
        .Activate
    Range(Selection, ActiveCell.SpecialCells(xlLastCell)).Select
    Selection.Delete
    Range("R1").Select
    ActiveCell.Activate
    Range(Selection, Selection.End(xlDown)).Select
    Selection.Cut
    Range("R3").Select
    ActiveSheet.Paste
    Range("R1").Select
    ActiveCell.FormulaR1C1 = "frequency"


'Normalise
```

```
    Range("S1").Select
    ActiveCell.FormulaR1C1 = "norm"
    Range("Q3").Select
    Range(Selection, Selection.End(xlDown)).Select
    Selection.Copy
    Range("S3").Select
    ActiveSheet.Paste
    Range("S3").Select
    Application.CutCopyMode = False
    ActiveCell.FormulaR1C1 = "=RC[-1]/SUM(C[-1])"
    Range("S3").Select
    Selection.Copy
    Range("S3").Select
    Range(Selection, Selection.End(xlDown)).Select
    ActiveSheet.Paste
    Range("U3").Select


'Plot
    Range("Q3").Select
    Range(Selection, Selection.End(xlDown)).Select
    Range("Q3:Q103,S3").Select
    Range("S3").Activate
    Range(Selection, Selection.End(xlDown)).Select
    Charts.Add
    ActiveChart.ChartType = xlXYScatterSmooth
    ActiveChart.SetSourceData
Source:=Sheets("Sheet1").Range("Q3:Q200,S3:S200"), _
        PlotBy:=xlColumns
    ActiveChart.Location Where:=xlLocationAsObject, Name:="Sheet1"
    With ActiveChart
        .HasTitle = True
        .ChartTitle.Characters.Text = "Frequency Distribution"
        .Axes(xlCategory, xlPrimary).HasTitle = True
        .Axes(xlCategory, xlPrimary).AxisTitle.Characters.Text = _
        "Bubble Diameter (mm)"
        .Axes(xlValue, xlPrimary).HasTitle = True
        .Axes(xlValue, xlPrimary).AxisTitle.Characters.Text = _
        "Fractional Frequency"
    End With
    ActiveChart.HasLegend = False
    ActiveChart.Axes(xlValue).Select
    With ActiveChart.Axes(xlValue)
        .MinimumScale = 0
        .MaximumScaleIsAuto = True
```

```
        .MinorUnitIsAuto = True
        .MajorUnitIsAuto = True
        .Crosses = xlAutomatic
        .ReversePlotOrder = False
        .ScaleType = xlLinear
        .DisplayUnit = xlNone
    End With
    ActiveChart.PlotArea.Select
    With Selection.Border
        .ColorIndex = 16
        .Weight = xlThin
        .LineStyle = xlContinuous
    End With
    With Selection.Interior
        .ColorIndex = 2
        .PatternColorIndex = 1
        .Pattern = xlSolid
    End With


End Sub
```